TENSILE DEFORMATION OF METASTABLE AUSTENITIC STAINLESS STEEL AT CRYOGENIC TEMPERATURE.

A THESIS WORK SUBMITTED IN PARTIAL FULFILMENT REQUIREMENT FOR THE AWARD OF THE DEGREE OF

MASTER OF ENGINEERING IN METALLURGICAL ENGINEERING
FACULTY OF ENGINEERING AND TECHNOLOGY

DEPARTMENT OF METALLURGICAL AND MATERIAL ENGINEERING
JADAVPUR UNIVERSITY

KOLKATA-700032
SESSION: 2017-2019
BY

AMIT MAITY
REGISTRATION. NO. 140892 OF 2017-2018
EXAMINATION ROLL NO. M4MET19003

UNDER THE GUIDANCE
OF
PROF. PRAVASH CHANDRA CHAKRABORTI
DEPARTMENT OF METALLURGICAL AND MATERIAL ENGINEERING
FACULTY OF ENGINEERING AND TECHNOLOGY
JADAVPUR UNIVERSITY
KOLKATA: 700032

FACULTY OF ENGINEERING & TECHNOLOGY METALLURGICAL AND MATERIAL ENGINEEERING DEPARTMENT JADAVPUR UNIVERSITY

RECOMMENDATION CERTIFICATE

This is to certify that we have examined the thesis entitled **"Tensile Deformation of Metastable Austenitic Stainless Steel at Cryogenic Temperature**" submitted by Amit Maity (Registration no-140892 of 2017-2018 and Examination roll no-M4MET19003) and accepted in partial fulfillment of the requirement for the degree of Master of engineering in Metallurgical Engineering. It is bonafide work carried out by him under our guidance.

PROF. P.C. CHAKRABORTI
Supervisor
Metallurgical and Material
Engineering Department
Jadavpur University

PROF. A.K. PRAMANICK
H.O.D
Metallurgical and Material
Engineering Department
Jadavpur University

PROF. CHARANJIB BHATTACHARJEE
Dean,
Faculty of Engineering and Technology, Jadavpur University

FACULTY OF ENGINEERING & TECHNOLOGY
METALLURGICAL AND MATERIAL ENGINEEERING DEPARTMENT
JADAVPUR UNIVERSITY

CERTIFICATE OF APPROVAL

This is to certify that I have examined the thesis entitled **"Tensile Deformation of Metastable Austenitic Stainless Steel at Cryogenic Temperature"** submitted by Amit Maity and here by accord my approval of it as a study carried out and presented in a manner required for its acceptance in the field of Metallurgical and Material Engineering.

Committee of ----------

Final Examination for

Evaluation of the thesis ----------

FACULTY OF ENGINEERING & TECHNOLOGY
METALLURGICAL AND MATERIAL ENGINEEERING DEPARTMENT
JADAVPUR UNIVERSITY

DECLARATION

I do hereby solemnly declare that the research work embodied in this thesis **"Tensile Deformation of Metastable Austenitic Stainless Steel at Cryogenic Temperature"** is the original investigation carried out independently by me under the supervision of **Prof. Pravash Ch. Chakraborti**, Dept. of Metallurgical & Materials Engineering, Jadavpur University, Kolkata, India for the award of the degree of Master of Engineering in Metallurgical Engineering of Jadavpur University. To the best of my knowledge and belief, this work has not been presented for any degree or distinction under any other university.

Amit Maity
Department of Metallurgical &
Material Engineering
Jadavpur University, Kolkata

Date-

ACKNOWLEDGEMENT

I owe a deep debt of gratitude to my project supervisor **Prof. Pravash Ch. Chakraborti,** Department of Metallurgical and Material Engineering, Jadavpur University for his invaluable and untiring guidance, encouragement and supervision, throughout this research work.

My special thanks goes to **Dr. Amrita Kundu**, Department of Metallurgical and Material Engineering, Jadavpur University for her encouragement and valuable suggestion.

I am also thankful to the librarian and technical staffs of Metallurgical and Material Engineering Department, specially **Mr. Sudhir Ghosh** and **Mr. Jayanta Bhattachariya**, Jadavpur University for their cordial assistance.

Special thanks to **Mr. Rahul Kumar**, **Mr. Manish Kumar Patel**, **Mr. Sayan Kalyan Chandra**, **Mr.Jayanta Kumar Mahato**, **Mr.Chadesham Pravakar**, **Mr. Ujjwal Mandal**, and **Mr. Utpal Maity** for their support and encouragement during this research work. I thankfully acknowledge the support of all those people, who some time or the other directly or indirectly rendered their help at different stages of this work.

I express my heartiest thanks to my friends and classmates, specially **Mr.Sourjadeep Dasgupta , Nishant Kumar Singh** and **Mr. Rakesh Kundu** for their useful assistance, co-operation and support. Last but not the least, special thanks to my beloved parents, as they always stood by me, caring least the prevalent situation.

CONTENTS

LIST OF FIGURES

LIST OF TABLES

ABSTRACT

Stainless steels are highly corrosion resistant in a variety of environments under ambient conditions. The predominant alloying element for corrosion resistance property is chromium and at least 11 wt.% is required for corrosion resistance purpose. Nickel and molybdenum addition also enhance the corrosion resistance. Chromium reacts with oxygen in the air and form a thin passive layer of chromium oxide on the surface. It is seen that low alloyed austenitic stainless steels are close to the martensite region and these grades are called metastable austenitic stainless steels, since they are susceptible to deformation induced martensitic transformation. The metastable grade, such as AISI 304 stainless steel is extremely ductile and is used in applications requiring good formability. Moreover, it has an extremely high strain hardening characteristics. This results in high strength in cold rolled condition. The martensitic transformation for metastable austenitic stainless steel is governed mainly by temperature and deformation.

.As AISI 304 stainless steel used in the application involving liquid natural gas(LNG) and also in nuclear facilities. The present study have been made to understand the tensile behaviour of AISI 304 austenitic stainless steel under cryogenic temperatures facilities.

It is found out that the ultimate tensile strength and yield strength both increases with decreasing temperature in cryogenic temperature range. Also the ductility decreases between - 20 ^{o}C to

-100^{o}C.

Also, the strain-hardening behaviour is non-linear and occurs in multi-stage due to the effect of α'-martensite formation. The second stage hardening increases rapidly as temperature falls further from -40 to -100^{o} C.

CHAPTER-1

INTRODUCTION

Stainless steel is the name given to a family of corrosion and heat resistant steels containing a minimum of 10.5% chromium. Just as there is a range of structural and engineering carbon steels meeting different requirements of strength, weldability and toughness, so there is a wide range of stainless steels with progressively higher levels of corrosion resistance and strength. This results from the controlled addition of alloying elements, each offering specific attributes in respect of strength and ability to resist different environments. Austenitic stainless steels have many advantages from a metallurgical point of view. They can be made soft enough (i.e., with a yield strength about 200 MPa) to be easily formed by the same tools that work with carbon steel, but they can also be made incredibly strong by cold work, up to yield strengths of over 2000 MPa (290 ksi). Their austenitic (fcc, face-centered cubic) structure is very tough and ductile down to absolute zero. They also do not lose their strength at elevated temperatures as rapidly as ferritic (bcc, body-centered cubic) iron base alloys. The least corrosion-resistant versions can withstand the normal corrosive attack of the everyday environment that people experience, while the most corrosion-resistant grades can even withstand boiling seawater.

It is well known that 300 series austenitic stainless steel provides high resistance to corrosion, oxidation, retains high strength and excellent ductility over a wide temperature range. These properties make the 300 series highly desirable for applications in liquid natural gas (LNG) storage and nuclear facilities, specifically, LNG cargo barriers and valves.

Since LNG is stored under cryogenic temperatures of 110 K, its transportation and storage system must be protected from low temperature embrittlement and high pressure. While AISI 304 and 316 are widely used in industry because of their distinct toughness and ductility under cryogenic temperatures.

In this study, AISI 304 austenitic stainless steel was selected to test their cryogenic performances. Factors such as low temperature brittleness (cold shortness) were also considered.

CHAPTER-2

LITERATURE REVIEW

2.1 Stainless Steel

Stainless steels are highly corrosion resistant in a variety of environments under ambient conditions. The predominant alloying element for corrosion resistance property is chromium and at least 11 wt.% is required for corrosion resistance purpose. Nickel and molybdenum addition also enhance the corrosion resistance. Chromium reacts with oxygen in the air and form a thin passive layer of chromium oxide on the surface. The formation of this passive layer is responsible for high oxidation resistance of stainless steels in an oxidizing atmosphere. The passive layer has the ability to self-heal, which means that if the surface is scratched, new chromium oxide will form in the scratch, and protect the steel from corrosion.

There are many different grades of stainless steels with a variety of properties. They are often divided in five different types, named after their structure: (a) ferritic,(b) martensitic, (c) austenitic, (d) duplex (austenitic and ferritic) and (e) precipitation hardened.

2.2 Phase stability

One commonly used diagram to determine the phase present at room temperature from the chemical composition is the Schaeffler-DeLong diagram (shown in Figure 2.1) [1].

In the diagram, it is seen that low alloyed austenitic stainless steels are approaching the lower left corner. They are, therefore, close to the martensite region and these grades are called metastable austenitic stainless steels, since they are susceptible to deformation induced martensitic transformation. Highly alloyed austenitic steels are more stable and will not transform to martensite during deformation. The metastable grade, such as AISI 304 stainless steel is extremely ductile and is used in applications requiring good formability. Moreover, it has an extremely high strain hardening characteristics. This results in high strength in cold rolled condition. The nominal compositions for different grades of stainless steels are found from Figure 2.1

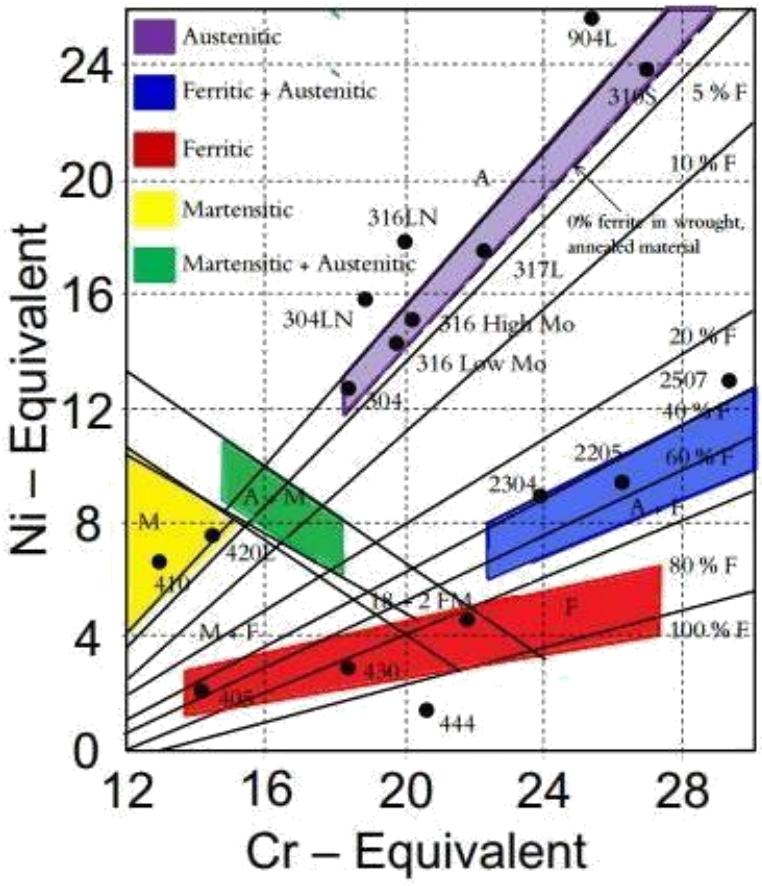

Figure 2.1: The Schaeffler-DeLong diagram depicting the phases as a function of nickel and chromium equivalents [1]

2.3 Tensile deformation behavior of ASS

Tensile flow and work hardening behavior attract continued scientific and technological interest in view of improving the appropriate conditions for material processing and ensuring safe performance during service. The tensile deformation behavior of the austenitic stainless steel depends upon several factors such as material chemistry, temperature, grain size, stress state, strain and strain rate. It is known that the monotonic deformation behavior of FCC metal is greatly affected by strain rate of deformation and temperature at which it exposed.

2.3.1 Stages of tensile flow behaviour

Tensile flow of single crystal FCC metals occurs in the three different stages. In stage I easy glide occurs where the material undergoes little strain hardening. During this stage, the dislocations are able to move over large distances without encountering the barriers. In this stage slip always occurs on one slip system and thus it is known as laminar flow. In

stage II strain hardening increases rapidly with straining the material. In this stage slip occurs in more than one set of slip system. Here, Lomer-Cottrell barrier increases and dislocation tangles begins to develop and thus eventually results in the formation of distinct cell structure of high dislocation density. In stage III the strain hardening rate decreases with strain due to dynamic recovery. In this stage the stress is enough so that the dislocations can take part in process that is suppressed at lower stress. Cross slip is believed to occur and hence reduce the internal stress field.in this stress the flow stress is strongly dependent on temperature. These three stage tensile flow behaviour is mainly dependent on the purity of the metal, testing temperature and strain rate of deformation.

2.3.2 Effect of strain rate

It is known that the stress required continuing deformation increases with increase in strain rate. This is usually referred to as strain rate effect. Many investigators reported the effect of strain rate on the flow behaviour of the material. Sastry et al. [2] have reported that the tensile flow stress of Fe-Al alloy strongly dependent on the strain rate of deformation and testing temperature. Lindholm [3] examined the strain rate effect in FCC metals by using Hopkinson bar test and explained the results by using dislocation theories. He proposed that the possible cause of strain rate effects were dislocation glide and dislocation interaction among themselves. The effect of strain rate on the flow behaviour can be described by the strain rate sensitivity. The strain rate sensitivity can be defined as the increase in stress required causing a certain increase in plastic strain rate at a particular strain and temperature [4]. The strain rate sensitivity (SRS) of a material depends on the testing temperature; at room temperature it is lower and increases with increase in testing temperature.

The strain rate sensitivity of different material has been investigated by several researcher, like Kundu and chakraborti [5] for 304 ASS, Dao et al. [6] for copper, Picu et al. [7] for commercial Al alloy. Kundu and chakraborti [8] reported that the strain rate sensitivity decreases linearly with strain.

2.4 Work hardening behaviour

The increase in stress required to cause slip because of the previous plastic deformation is known as work- hardening or strain hardening [4]. Work hardening of metals/alloys occurs during plastic deformation caused by dislocation movement, whereas movement of dislocation becomes more restricted when strain increases due to the dislocation-dislocation interaction and piling up dislocation. There are several work hardening model available to analyse the response of the material during plastic deformation [9-12]. In this section few work hardening models are analysed.

2.4.1 Hollomon relationship

The work hardening behaviour of most metals are usually analysed by the relationship proposed by Hollomon [10].

$$\sigma = K.(\varepsilon_p)^n$$

Where σ is true stress, is true plastic strain; K is strain hardening co-efficient and n is strain hardening exponents. According to the Hollomon relationship [Eq. 7] true stress (σ)-true plastic strain ( ) on double logarithmic scale is supposed to yield a straight line. and the intercept (= 0) of the resulting plot on double logarithmic scale are the strain hardening exponent (n) and strain hardening co-efficient (K) respectively.

Many investigators [13-15] reported that the tensile deformation of different austenitic stainless steels occurs in a number of stages. It was reported that the transition strain i.e. from one stage to another stage, largely depends on strain rate of deformation and the minimum work hardening parameter (1) decreases with increasing strain rate, indicating that multiple slip/ cross slip activity set in to accommodate higher strain rate [10].

2.4.2 Ludwik Analysis

The strain hardening behaviour of the materials can be analyzed by the relationship proposed by Ludwik [12]. Mathematically it is represented as

$$\sigma = \sigma_0 + \acute{K}(\varepsilon_p)^{\acute{n}}$$

Where, true yield stress and **Ḱ, ń** are strain hardening co-efficient and strain hardening exponent respectively. After taking logarithmic on both sides [Eq. 8] following expression can be obtained.

$$\ln(\sigma - \sigma_0) = \ln(\acute{K}) + \acute{n}.ln(\varepsilon_p)$$

Like Hollomon relationship the plot of (− 0) vs. on double logarithmic scale should yield a single straight line. Jadav et al. [16] found two stage behaviour in Nimonic C-263 alloy at 300 °C and 650 °C. They suggested that planer slip is the dominant mechanism over cross slip in the lower strain range and vice versa.

2.4.3 Differential Crussard–Jaoul (C-J) Analysis

The differential C-J analysis of work hardening can be represented mathematically by the following expression [9]

$$\sigma = \sigma_0 + \acute{K}(\varepsilon_p)^{\acute{n}}$$

Where,**, Ќ, ń** are material constants. The logarithmic form of equation [10], after differentiating with respect to is

$$\ln\left(\frac{d\sigma}{d\varepsilon_p}\right) = \ln(\acute{n}.\acute{K}) + (\acute{n} - 1)\ln(\varepsilon_p)$$

Like the Hollomon and Ludwik analysis, the plot of the plot of ln(/d) vs. ln( ) should yield a straight line.

2.4.4 Kocks-Mecking (K-M) Analysis

Following K–M approach, the work hardening behaviour in metals and alloys is conveniently described using the variations of instantaneous work hardening rate(=d /) with the flow stresses.

However, Kocks and Mecking [11] pointed out that different work hardening stages can be better understood by multiplying true stress with work hardening rate (θ). Choudhary et al. [17] reported that P9 steel exhibited two-stage work hardening behaviour characterised by rapid decrease in instantaneous work hardening rate at low stresses (TS) followed by a gradual decrease at high stresses. Similar observation was found by Palaparti et al. [18] in 9Cr–1Mo ferritic steel.

2.5 Cryogenic Temperature effect on ASS

Most of the material shows different tensile and fracture behavior at cryogenic temperature compared to room temperature. Following studies has been made by the researcher to disclose the reason behind these behavior at cryogenic temperature.

2.5.1Effect on Tensile behavior

Thomas **S.** DeSisto and Frank L. Carr [19] found that the tensile strengths of the 300 series stainless steels generally increase with decreasing temperature, figure 2.2 . This increase is fairly linear to -320 F, but at -452 F the strengths of types 302,

303 and 304 are lower than would be expected by extrapolating from the higher temperatures. This might be taken to indicate a slight degree of embrittlement at -452 F .[19].

The ductility of the stainless steels tested generally decrease with decreasing temperature. An exception is Type 316 which increases from room temperature ton -105 F, remains constant to -320 F and drops at -452 F. The least ductile of these materials is Type 303, which has the highest tensile strength.[19]

At the higher strains, the flow Stress increases (figure 2.3) with decreasing temperature. At the lower strains, the nature of the curves are different. In the vicinity of 0.15 to 0.17 strain, the flow stress of Types 302, 303, and 304 is lower at -452 F than at -320 F. Over the same range of strain, the stress of Type 347 at -452 F is coincident to the flow stress curve at - 320 F. It is also noted that, at -105 F and below, there is a concave upward trend in the curve in this strain range.

Tis increased rate of et al, strain hardening has the been explained by Powell, to be caused by strain-induced transformation of retained austenite to martensite.

True stress at maximum load for the 300 series stainless steels increases with decreasing temperature to -320 F and then increases more markedly. This marked increase at -452 F is attributed to the deformation process, which results in a higher strain at maximum load. The fracture stress, shown in Figure 9, also increases with decreasing temperature. An exception is Type 304 which shows a slight decrease below -320 F[19].

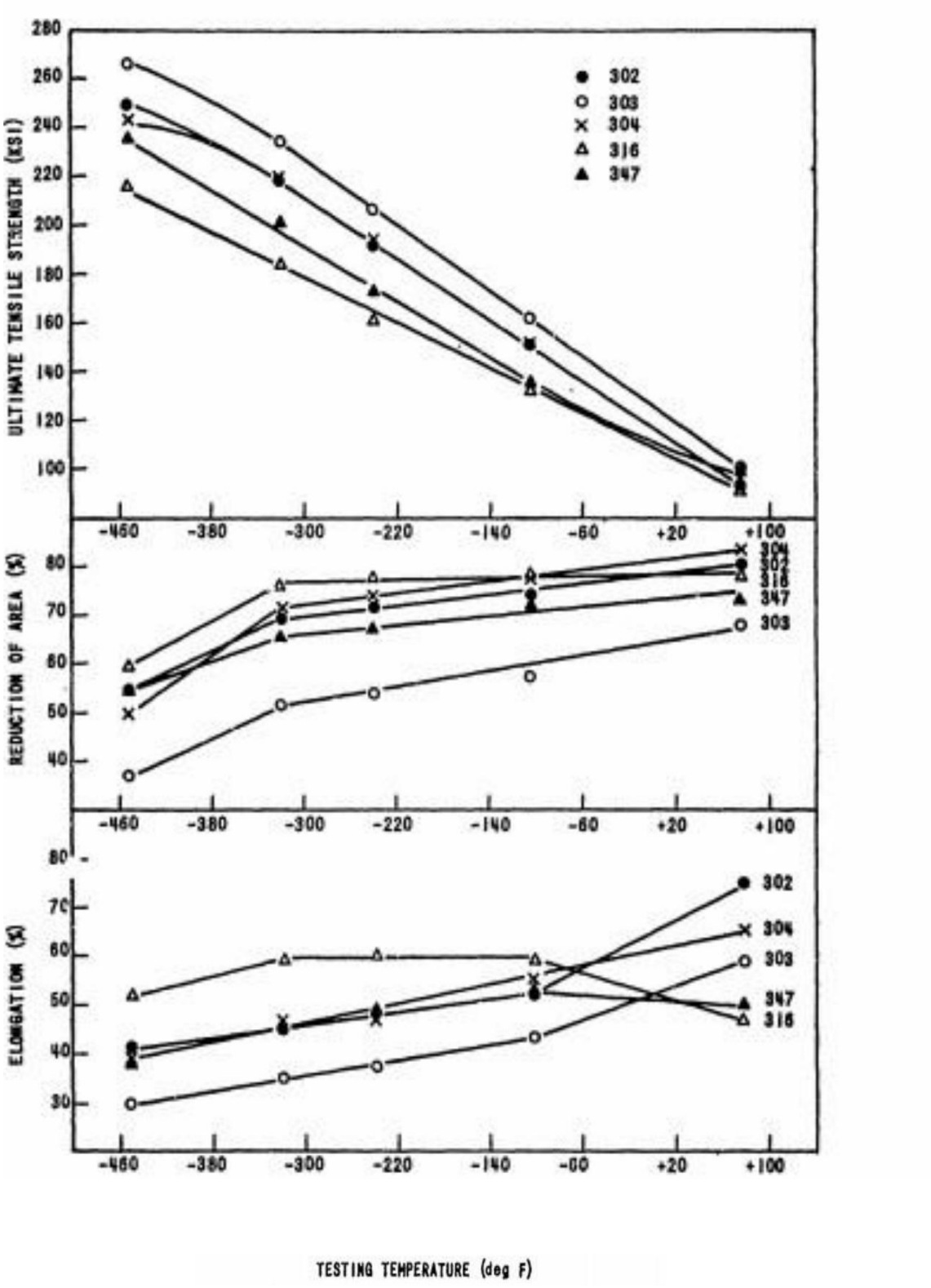

Figure-2.2 [19] Engineering tensile properties of 300 series stainless steels at various tempatures.

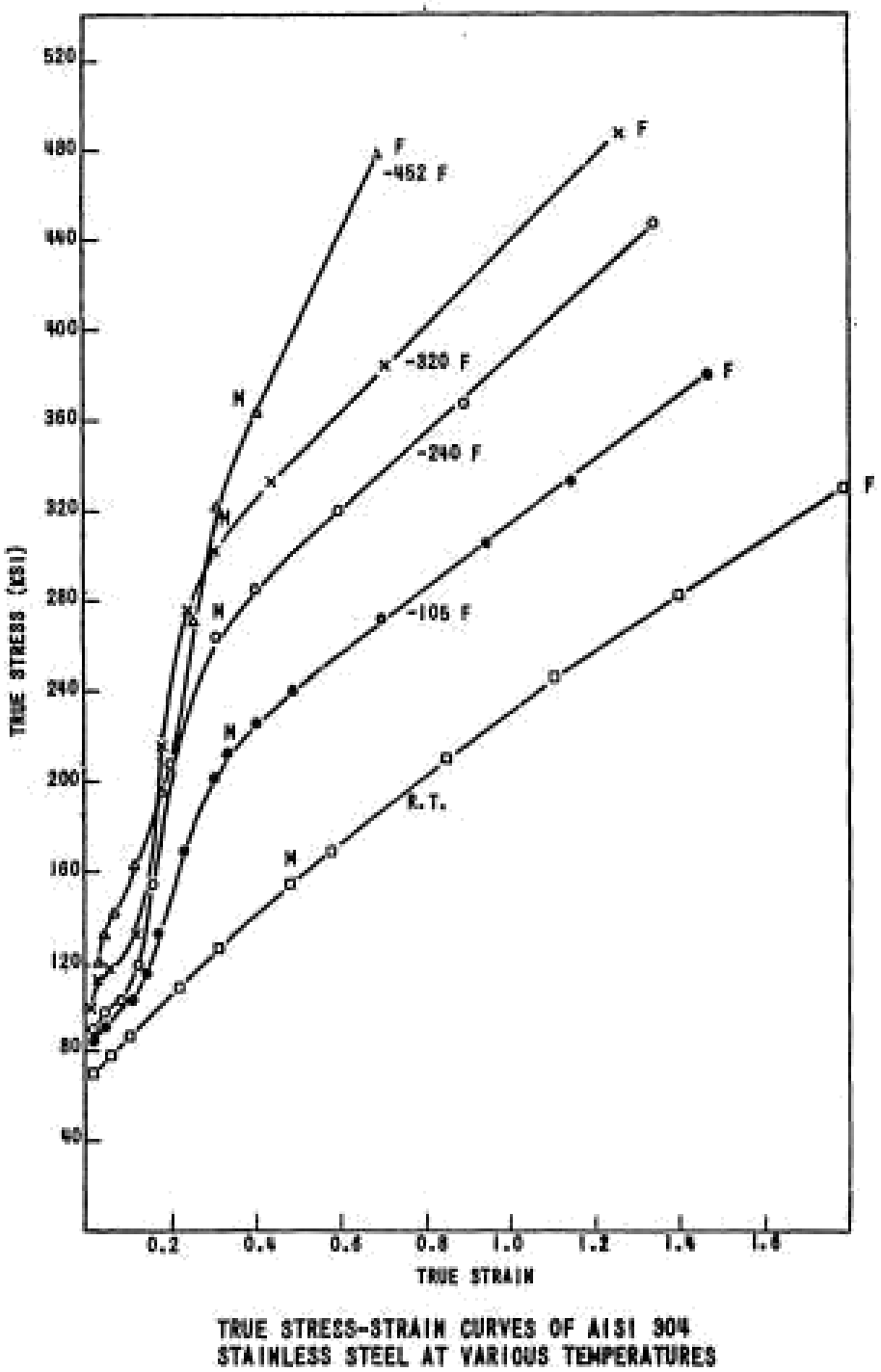

TRUE STRESS-STRAIN CURVES OF AISI 304 STAINLESS STEEL AT VARIOUS TEMPERATURES

Figure2.3 True stress –strain curves of aisi 304 stainless steel at various Tempereature.[19]

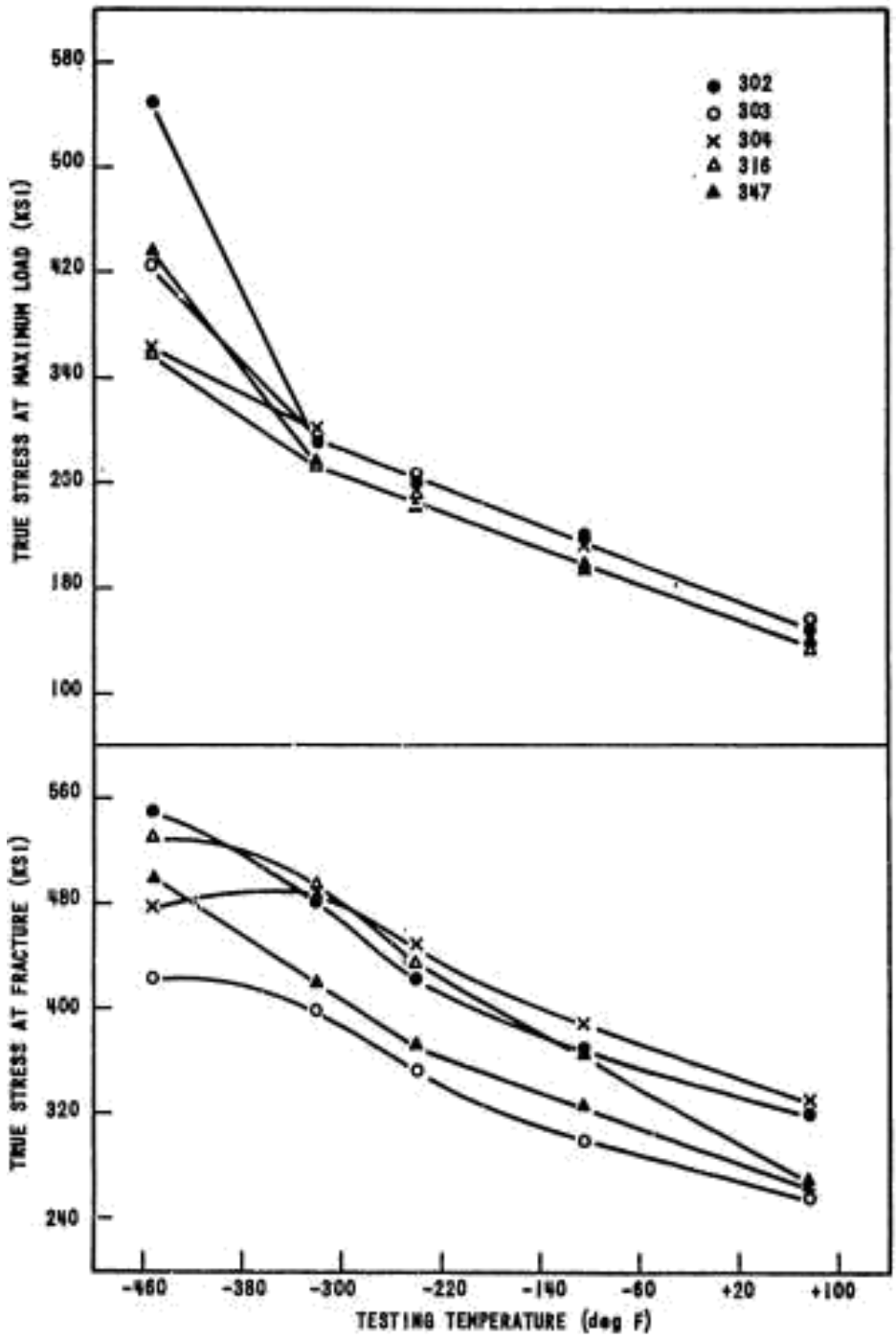

Figure 2.4- Effect of temperature at Fracture and at maximum Load.[19]

Eiji fukushima, akira goto, Mitsuzo fushimi [20] carried tensile test on 18-8 stainless steel and found that the rate of strain hardening increases in general decrease in temperature and has a tendency to decrease at the end of deformation between room temperature and -245^{o} c. But the rate of strain hardening does not decrease even at the end of deformation at -269^{o} c and -271^{o}c.

18-8 stainless steel yields at 3 to 4 % of plastic deformation before the yield point below -100^{o}c. This phenomenon has close relationship with the formation of martensite at the beginning of deformation.[20].

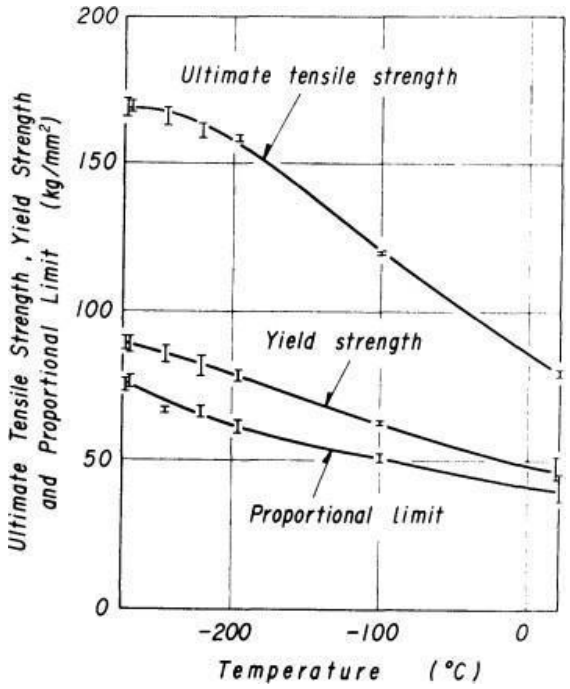

Figure 2.5-ultimate tensile strength , yield strength , and proportional limit in variation with ttemperature of 18-8 stainless steel.[20]

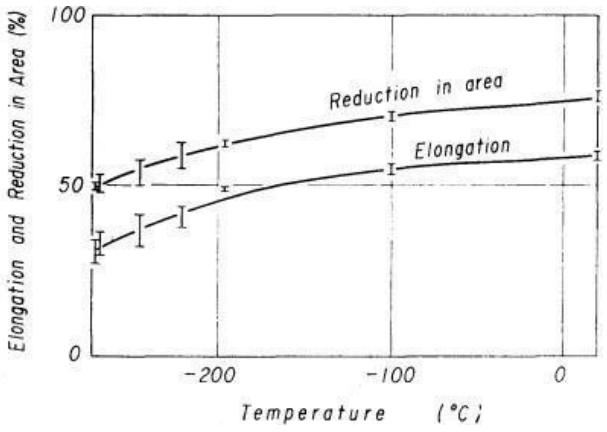

Figure-2.6 variation of elongation and reduction in area with temperature [20].

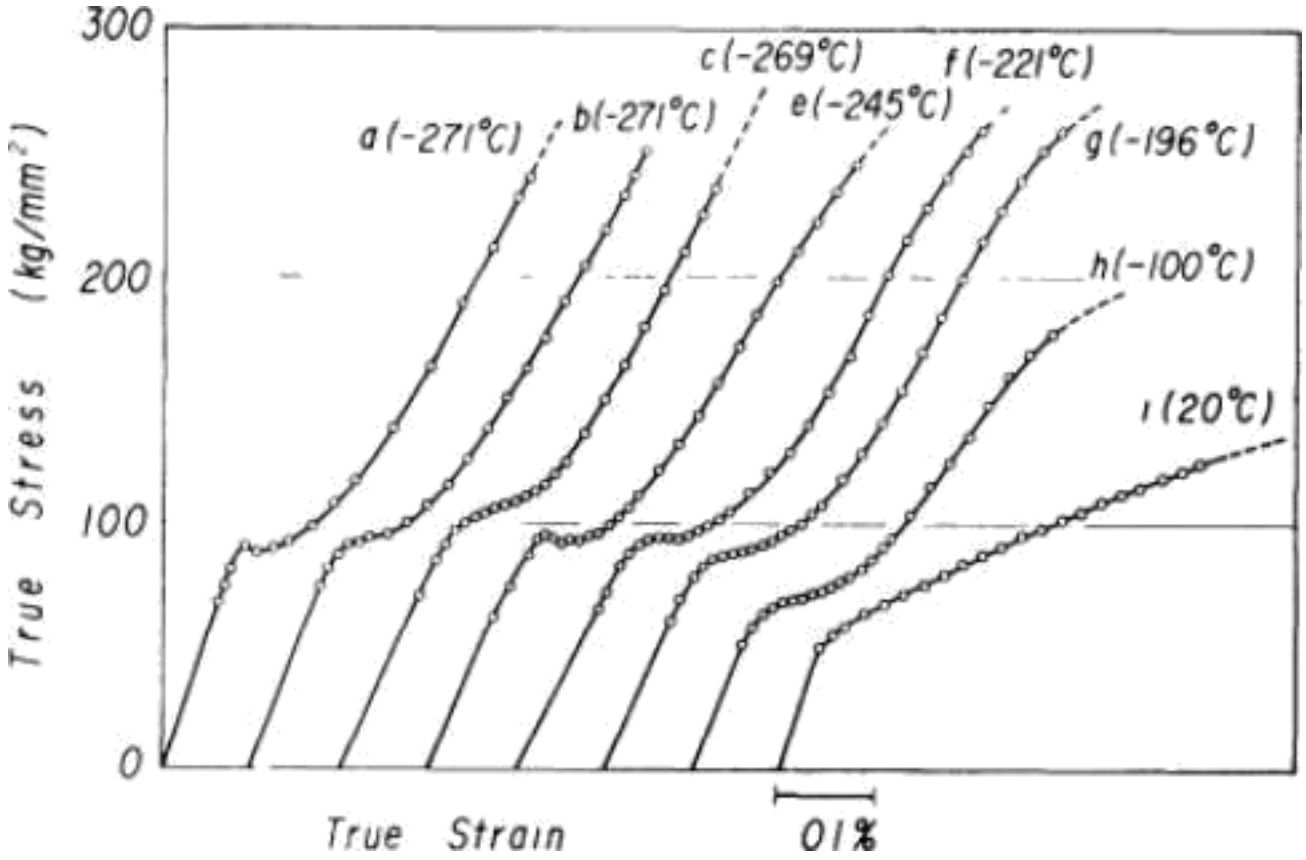

Figure 2.7- variation of true stress –true strain at different temperature.[20].

2.5.2 Effect on Work-Hardening Behavior

Woong Sup Park, Seong Won Yoo, Myung Hyun Kim, Jae Myung Lee [21] has shown in Fig.2.8, at below 223 K temperatures, the austenitic stainless steel shows two-stage sigmoidal deformation which is non-linear hardening behavior that is dependent on temperature. In general, the steels possess metallic properties at room temperature, but as strain-rates increased, the ultimate tensile strength and yield strength also increased. By contrast, under low temperature, as strain-rate increased, yield strength increased (σy1 to σy2), but the ultimate tensile strength decreased (σt1 to σt2).

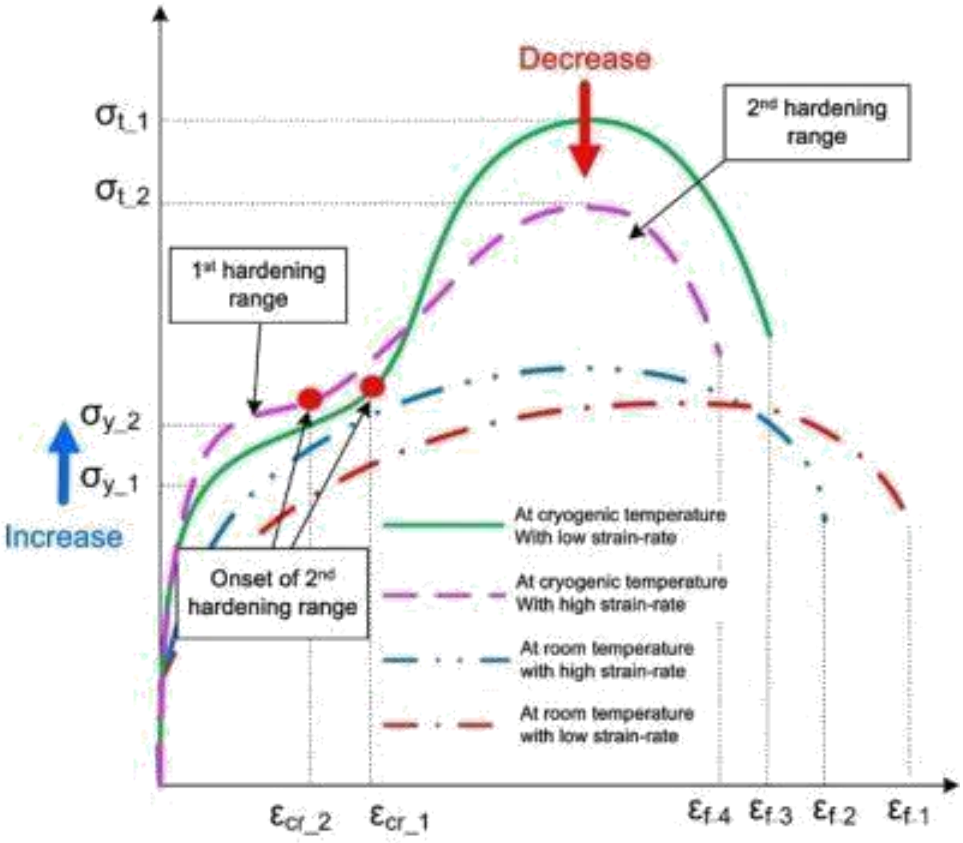

Figure- 2.8 The engineering stress–strain curves of test specimens deformed at temperatures ranging from 110 K to 293 K and strain-rates ranging from 1.6E4 s^{-1} to 1.0E2 s1, respectively[21].

According to the Olson–Cohen analysis, internal thermal lift, which is caused by adiabatic heating, lowered the chemical driving force of the γ α'transformation, therefore increasing the SFE, work-hardening rate, ultimate tensile strength and decreasing the ductility of materials. These characteristic and plastic (Transformation Induced Plasticity (TRIP)) phenomena were observed in this study.

Figs-2.8 show the engineering stress–strain curves of test specimens deformed at temperatures ranging from 110 K to 293 K and strain-rates ranging from 1.6E4 s^{-1} to 1.0E2 s^{-1}, respectively.

The 2nd hardening phenomenon, one of the main characteristics of austenite steels at low temperatures, was observed and a strong temperature dependency was observed in all cases. As expected, the yield strength and ultimate tensile strength increased as the test temperature decreased

Dieter has reported that yield strength is slightly influenced by strain-rate and temperature, but ultimate tensile strength is affected significantly during cryogenic tensile tests.

the threshold strain (or critical strain), which is the inflection position between the 1st and 2nd hardening curve and is defined as the onset of 2nd plastic hardening, was observed at temperatures of below 223 K in all materials. The threshold strain is an important parameter to analyze the non-linear behavior of austenitic steel numerically under cryogenic conditions.[21].

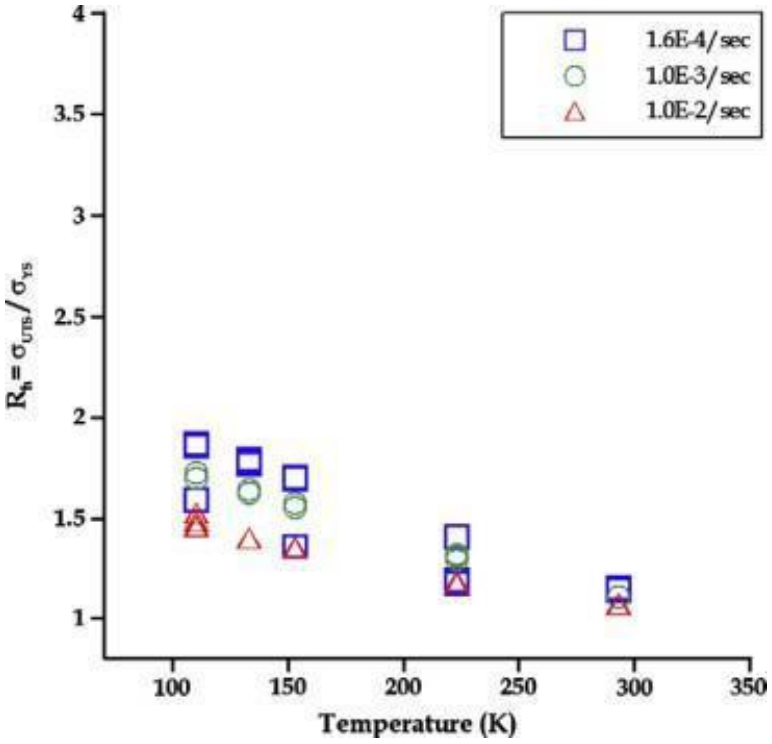

Figure- 2.9 Second hardening ratio of AISI 304L[21]

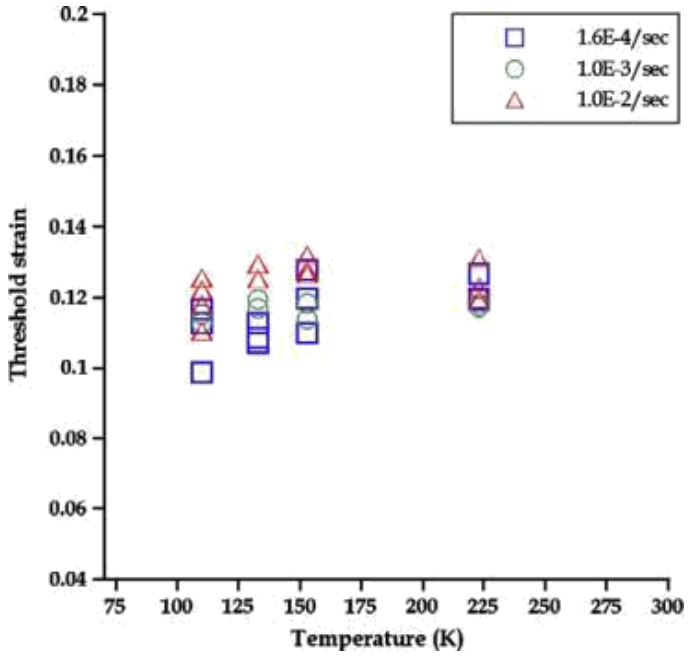

Figure 2.10 Threshold strain of AISI 304L.[21]

As reported in the previous research [22], austenitic stainless steel generally exhibits very clear second hardening phenomenon in the low-temperature range. Fig. 2. 11 shows the graphs depicting the relationship between the true strain and SHR for all amounts of pre-strain. Because of the nonlinear TRIP behaviors, all of the θ - ε_{true} curves are nonlinear (parabolic) [22].

We found that there is an increase in the SHR of the specimens pre-strained at ambient temperature (AL test) as the amount of pre-strain increases, while the strain range remains almost constant. On the contrary, we found that there is a significant decrease in the SHR of the specimens pre-strained at a low temperature (LL test) as the amount of pre-strain increases (see Fig. 12(B)), while the strain decreases. Since the SHR indicates the level of hardening (especially TRIP as second hardening), the non-TRIP behavior observed in the case of the LL tests can be explained by the decrease in SHR with the amount of pre-strain.

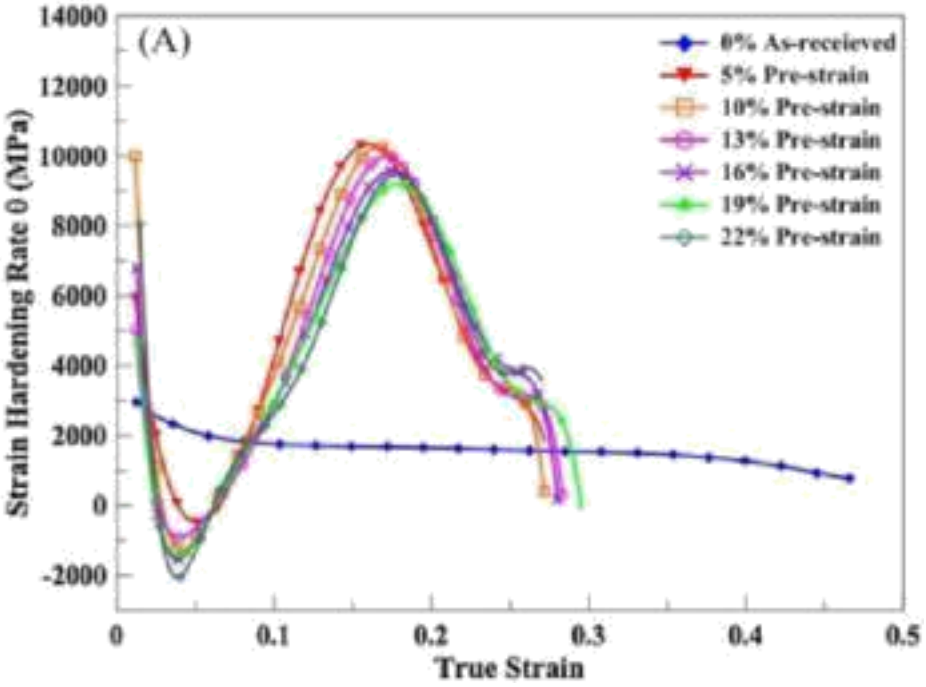

Figure-2.11 θ-ε_p graph of 304L stainless steel at different pre-strain depicting the non-linear trip effect.[22].

2.5.3 Effect on Fracture Surface

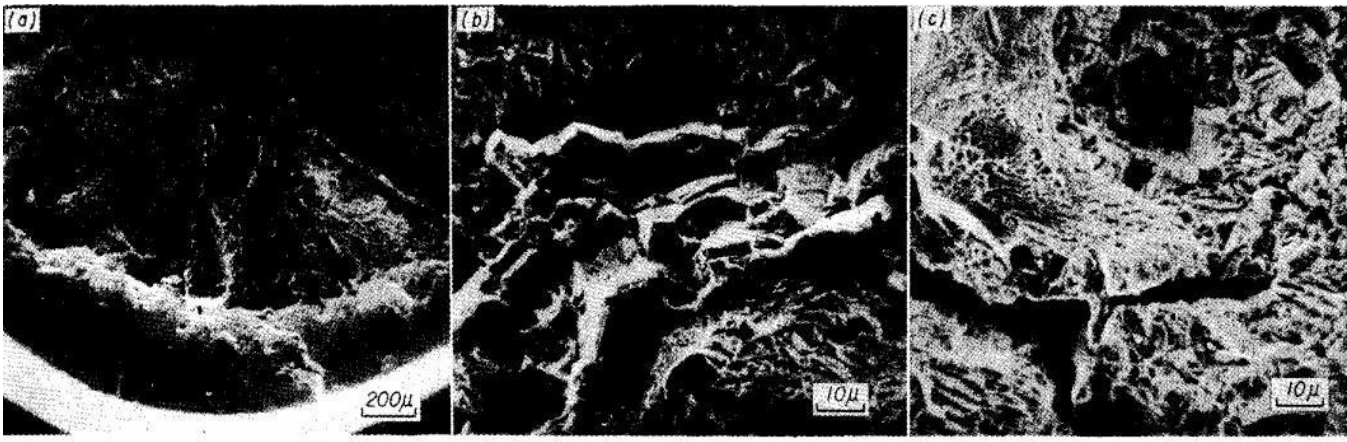

Photo.1 Micro-fractographs of a specimen fractured at −271°C (whose load-extension curve is a in Fig.4)
(a) From the center to the rim of the fracture surface
(b) The center of the fracture surface
(c) Cracked part of the fracture surface

Figure – 2.12 Fracture surface of 18-8 stainless steel at -271^{o}c.[20]

The threshold strain decreased with decreasing temperature at a constant strain-rate. This was attributed to a reduction in ductility. Talonen and Ogata's research [Z], internal thermal lift from adiabatic heating after reaching the yield point of deformation accompanying phase transformation to ε and α' martensite phase. Significant fibrous zones and shear lips were found in the form of Cup-and-Cone fractures at the ductile fracture location of the tested materials[21].

2.6 Deformation behaviour of materials

Deformation behaviour of polycrystalline materials is different from that of single crystals. Because of the random crystallographic orientations of the numerous grains, the slip direction varies from one grain to another [23]. For each, disloca-tion motion occurs along the slip system that has the most favourable orientation. Gross plastic deformation of a polycrystalline material results from deformation of the individual grains by means of slip. During deformation, continuity of the grains is maintained along the grain boundaries and hence the grain boundaries usually do not open up or overlap. As a consequence, each individual grain is constrained, to some degree, in the shape it may assume by its neighbouring grains. Polycrystalline metals are stronger than their single-crystal equivalents, which mean that greater stresses are required to initiate slip and the attendant yielding. This is, to a large degree, also a result of geometrical constraints that are imposed on the grains during deformation. Even though a single grain may be favourably oriented with the applied stress for slip, it cannot deform until the adjacent and less favourably oriented grains are capable for slip also; this requires a higher applied stress level [23].

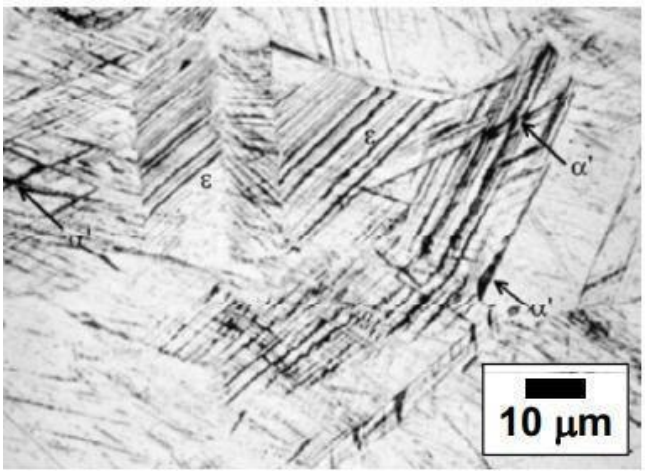

Figure 2.13: Microstructure of the coarse-grained 304 austenitic stainless steel sample strained 10% at -50∝C, indicating both the (hcp) and ′ (bcc) martensites.The sample was etched in a solution of 10% HCl and 0.25% sodium metabisulfite [24]

In metallic systems, the two basic modes of deformation are *slip* and *twinning* and the most significant parameter with respect to the choice of deformation mode is the value of the SFE [25]. In metals with low SFE, the difficulty of cross slip reduces the ability of the material to change its shape during plastic deformation by slip alone, and, therefore, deformation twinning may occur. The combination of the slip plane and slip direction is termed as *slip system* [26]. The slip system depends on crystal structure of the metal and is such that the atomic distortion that accompanies the motion of a dislocation is a minimum. For a particular crystal structure, the slip plane is that plane having the most dense atomic packing, that is, the greatest planer density. The slip direction corresponds to the direction, in this plane, that is, most closely packed with atoms, that is, the highest linear density. The possible slip systems for *bcc*, *fcc* and *hcp* crystal structures are listed in Table 2.1. For these structures, slip is possible on more than one family of planes. Metals with *fcc* or *bcc* crystal structures have a relatively large number of slip systems. These metals are quite ductile because extensive plastic deformation is normally possible along the various systems. Conversely, *hcp* metals, having few active slip systems, are normally quite brittle.

Table 2.1: Twin planes and twin directions [23].

Crystal structure	Twinning plane	Twin direction
bcc	$\{112\}$	$[111]$
hcp	$\{10\bar{1}2\}$	$[\bar{1}011]$
fcc	$\{111\}$	$[112]$

The second important mechanism by which metals deform is the process known as *twinning*. Twinning results when a portion of the crystal takes up an orientation that is related to the orientation of the rest of the untwinned lattice in a definite, symmetrical way. The twinned portion of the crystal is a mirror image of the parent crystal. The plane of symmetry between the two portions is called the *twinning* plane.

It is noted that twinning differs from slip in several specific respects. In slip, the orientation of the crystal above and below the slip plane is the same after deformation as before, while twinning results in an orientation difference across the twin plane. Slip is usually considered to occur in discrete multiples of the atomic spacing, while in twinning the atom movements are much less than an atomic distance.

Slip occurs on relatively widely spread planes, but in the twinned region of a crystal, every atomic plane is involved in the deformation.

Twins may be produced by mechanical deformation or as the result of annealing following plastic deformation. The first type are known as \mechanical twins"; the latter are called “annealing twins". Mechanical twins are producedin *bcc* or *hcp* metals under conditions of rapid rate of loading (shock loading) and decreased temperature. Face centered cubic metals are not ordinarily considered to deform by mechanical twinning.

2.7 Crystallography of Martensitic Transformation

2.7.1 Martensitic transformation

Martensite remains as the greatest technological importance in steels where it can confer an outstanding combination of strength (as high as 3500 MPa) and toughness (as high as 200 MPa $^{1/2}$) [91]. Many materials other than steel are now known to exhibit the same type of solid-state phase transformation, known as a martensitic transformation, frequently also called a shear or displacive transformation. Martensite occurs in, for example, nonferrous alloys, pure metals, ceramics, minerals, inorganic compounds, solidified gases and polymers (Table 2.2).

Table 2.2: The temperature *MS* at which martensite first forms on cooling, and the approximate Vickers hardness of the resulting martensite for a number of materials [27].

Composition	M_s / K	Hardness HV
ZrO_2	1200	1000
Fe–31Ni–0.23C wt%	83	300
Fe–34Ni–0.22C wt%	≤ 4	250
Fe–3Mn–2Si–0.4C wt%	493	600
Cu–15Al	253	200
Ar–40N_2	30	-

Martensitic transformations are *diffusion less*. It can form at very low temperatures, where diffusion, even of interstitial atoms, is not conceivable within the time period of the experiment. Table 2.3 gives values of the highest temperature at which martensite forms in a variety of materials; this temperature is known as the martensite-start, or temperature. However, a low transformation temperature is not a sufficient evidence for diffusionless character of martensitic transformation [28]. Martensite plates can grow at speed which approaches that of sound in the metal. In steel, this can be as high as 1100 *ms*-1,

in comparison to fastest recorded solidifications front velocity of about 80 *ms*-1 in pure nickel. Such large speeds are inconsistent with diffusion during transformation. It is to be noted that martensite need not grow so rapidly. For example, in shape-memory alloys or in single-interface transformations, the interface velocity is small enough to observe. The chemical composition of martensite in steel can be measured and shown to be identical to that of the parent austenite. The totality of these observations demonstrates convincingly that martensitic transformations are diffusion less [28].

The *fcc* microstructure of most austenitic stainless steels is not thermodynamically stable around room temperature. Therefore, applied stress or plastic deformation may induce martensitic transformation, by which the metastable austenite phase is transformed to the thermodynamically more stable martensite phase.

Table 2.3: Equation to determine temperature of stainless steels. First equation is given by Eichelman et *al*[29] and second equation is given by Pickering[30].

Equation
M_S (°C) = 1302 - 42Cr - 61Ni - 33Mn - 28Si - 1667(C + N)
M_s (°C) = 775 - 810C - 1230N - 13Mn - 30Ni - 12Cr - 54Cu - 46Mo

Two types of martensite can form in stainless steels: ferromagnetic, body-centred cubic (BCC) α'-martensite and non-ferromagnetic, hexagonal closed-packed (HCP) ε-martensite. α'-martensite in steels generally has a BCC or body-centred tetragonal (BCT) structure but in case of stainless steels due to the relatively low content of interstitials, it is normally referred to as BCC rather than BCT.

The lattice parameters are typically: a' = 0.2872 nm, and $a\epsilon$ = 0.2532 nm; $c\epsilon$ = 0.4114 nm. Assuming $a\gamma$ = 0.3585 nm [31], one can calculate that the (fcc) → ′ (bcc) transformation causes a volume increase of 2.57%, while the (fcc) → (hcp) transformation causes a volume decrease of 0.81%

[32]. The formation of DIM transformations has a pronounced influence on the mechanical properties of metastable austenitic stainless steels [33].

In the FCC crystal structure an intrinsic stacking fault changes the regular staking sequence of the {111} planes from ABCABCABC to, for instance, ABCACABCA. Therefore even a single stacking fault has a thin layer of HCP phase (CACA) which can be regarded as a nucleus of ε-martensite [10]. The perfect ε-martensite grows if intrinsic stacking faults overlap regularly on every second {111} plane [34-36]. If two intrinsic stacking fault overlap on the successive {111} planes, an extrinsic stacking fault

with ABCACBCAB sequence will form which can be regarded as a twin nucleus. The growth of the mechanical twin takes place by proceeding the overlapping of intrinsic stacking faults on successive {111}. Irregular overlapping causes a stacking fault bundle which may be regarded as either faulted ε-martensite or faulted austenite. Therefore it is difficult to distinguish between microstructure features originating from the formation and overlapping of stacking faults in austenitic stainless steels and a collective term "shear bands" is often used for the planar defects including bundles of overlapping stacking faults, ε-martensite and mechanical twins.

The crystallography of the martensite transformation is usually described by the habit plane and orientation relationships between the martensite and the parent austenite phase. The habit plane for martensite changes with chemical composition; nevertheless, steels of vastly different composition can have identical habit plan and other crystallographic characteristics. It has been reported that steels with low amount of carbon have a {557} habit plane, which is similar to a {111} plane; whereas high-carbon steels have habit planes of {259} or {225}.

The diffusion less transformation involves the coordinated movement of atoms. Therefore, the parent and product lattices will be closely related. The orientation relationship describes an existing parallelism between planes in the parent and the product phase [37].

The orientation relationship between the austenitic matrix phase and ε-martensite is often reported as: [38]

(1) $\{111\}_\gamma \| \{0001\}_\varepsilon$

$\langle 1\bar{1}0\rangle_\gamma \| \langle 1\bar{2}10\rangle_\varepsilon$

Whereas the orientation relationship for α'-martensite and parent phase is mostly reported to follow the Kurdjumov-Sachs (K-S) criteria: [39]

(2) $\{111\}_\gamma \| \{011\}_{\alpha'}$

$\langle 1\bar{1}0\rangle_\gamma \| \langle 1\bar{1}1\rangle_{\alpha'}$

However broad distribution around the ideal orientations of expected variants or deviation towards Nishayama-Wassermann (N-W) is observed in low carbon and alloy steels [40-42].

According to K-S orientation relationship, due to the symmetry in cubic systems, 24 equivalent crystallographic variants in α'-martensite can be developed from an austenite single crystal. Table 2.4 shows 24 orientation variants which satisfy the KS

relationship and the 10 different misorientation angles that can be formed between the variants [40].

Table 2.4-The 24 K-S orientation variants and misorientation angle from V1.

Variant no.	Plane parallel	Direction parallel	Misorientation angle from V1 (°)	CSL*
V1	$(111)_\gamma \| (011)_{\alpha'}$	$[\bar{1}01]_\gamma \| [\bar{1}\bar{1}1]_{\alpha'}$	-	-
V2		$[\bar{1}01]_\gamma \| [\bar{1}1\bar{1}]_{\alpha'}$	60.00	Σ3
V3		$[01\bar{1}]_\gamma \| [\bar{1}\bar{1}1]_{\alpha'}$	60.00	-
V4		$[01\bar{1}]_\gamma \| [\bar{1}1\bar{1}]_{\alpha'}$	10.53	Σ1
V5		$[1\bar{1}0]_\gamma \| [\bar{1}\bar{1}1]_{\alpha'}$	60.00	-
V6		$[1\bar{1}0]_\gamma \| [\bar{1}1\bar{1}]_{\alpha'}$	49.47	Σ11
V7	$(1\bar{1}1)_\gamma \| (011)_{\alpha'}$	$[10\bar{1}]_\gamma \| [\bar{1}\bar{1}1]_{\alpha'}$	49.47	Σ19b
V8		$[10\bar{1}]_\gamma \| [\bar{1}1\bar{1}]_{\alpha'}$	10.53	Σ1
V9		$[\bar{1}\bar{1}0]_\gamma \| [\bar{1}\bar{1}1]_{\alpha'}$	50.51	-
V10		$[\bar{1}\bar{1}0]_\gamma \| [\bar{1}1\bar{1}]_{\alpha'}$	50.51	-
V11		$[011]_\gamma \| [\bar{1}\bar{1}1]_{\alpha'}$	14.88	Σ1
V12		$[011]_\gamma \| [\bar{1}1\bar{1}]_{\alpha'}$	57.21	-
V13	$(\bar{1}11)_\gamma \| (011)_{\alpha'}$	$[0\bar{1}1]_\gamma \| [\bar{1}\bar{1}1]_{\alpha'}$	14.88	Σ1
V14		$[0\bar{1}1]_\gamma \| [\bar{1}1\bar{1}]_{\alpha'}$	50.51	-
V15		$[\bar{1}0\bar{1}]_\gamma \| [\bar{1}\bar{1}1]_{\alpha'}$	57.21	-
V16		$[\bar{1}0\bar{1}]_\gamma \| [\bar{1}1\bar{1}]_{\alpha'}$	20.61	-
V17		$[110]_\gamma \| [\bar{1}\bar{1}1]_{\alpha'}$	51.73	-
V18		$[110]_\gamma \| [\bar{1}1\bar{1}]_{\alpha'}$	47.11	-
V19	$(11\bar{1})_\gamma \| (011)_{\alpha'}$	$[\bar{1}10]_\gamma \| [\bar{1}\bar{1}1]_{\alpha'}$	50.51	-
V20		$[\bar{1}10]_\gamma \| [\bar{1}1\bar{1}]_{\alpha'}$	57.21	-
V21		$[0\bar{1}\bar{1}]_\gamma \| [\bar{1}\bar{1}1]_{\alpha'}$	20.61	-
V22		$[0\bar{1}\bar{1}]_\gamma \| [\bar{1}1\bar{1}]_{\alpha'}$	47.11	-
V23		$[101]_\gamma \| [\bar{1}\bar{1}1]_{\alpha'}$	57.21	-
V24		$[101]_\gamma \| [\bar{1}1\bar{1}]_{\alpha'}$	21.06	-

* Coincidence site lattice is indicated when Brandon's criterion [43] is satisfied.

2.7.2 Morphology

The mechanical properties and formability of austenitic stainless steels is remarkably affected by martensitic transformation and its morphology during straining [44, 45]. A variety of martensite morphologies has been observed in ferrous alloys including lath, butterfly, lenticular and thin plate [45, 46], but in case of stainless steels,

due to low carbon content, lath martensite appears more frequently. The morphology and crystallography of the lath martensite has been greatly investigated by optical microscopy and transmission electron microscopy (TEM) [47-51].

Although the small size of martensite laths makes the clear observation of individual laths in optical micrographs very difficult, the lath martensite shows a characteristic microstructure at a coarse scale, since they have a tendency to align themselves parallel to one another in the large area of the parent grain.

The martensite lath is a single crystal of martensite with a high density of lattice defects. General view is that an austenite grain breaks down to several packets (the group of laths with the same habit plane) each containing parallel blocks (the group of narrow, ruler shaped [50] laths of the same orientation or variant) [52, 23]. Figure 2.14 illustrates a typical lath martensite structure with laths, blocks and packets within a single grain of austenite [40].

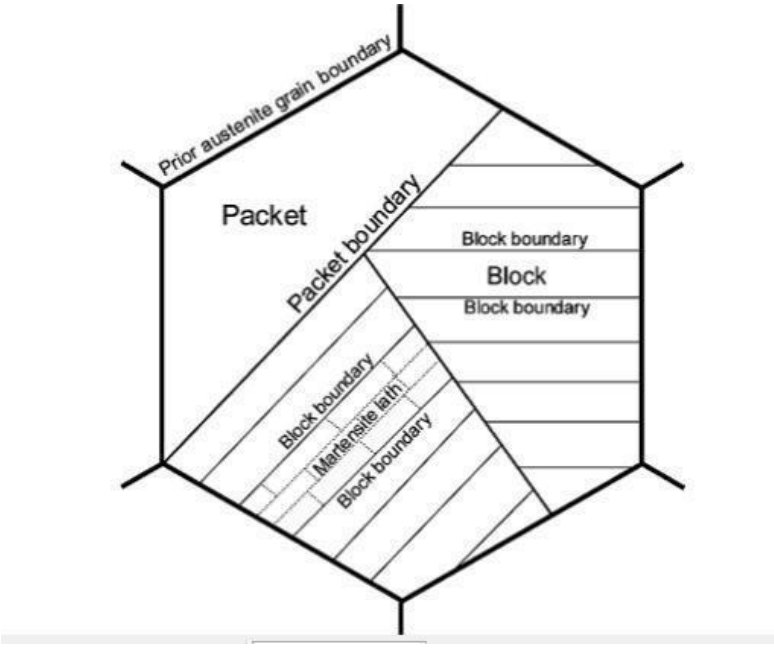

Figure 2.14-The three-level hierarchy in lath martensite morphology [40].

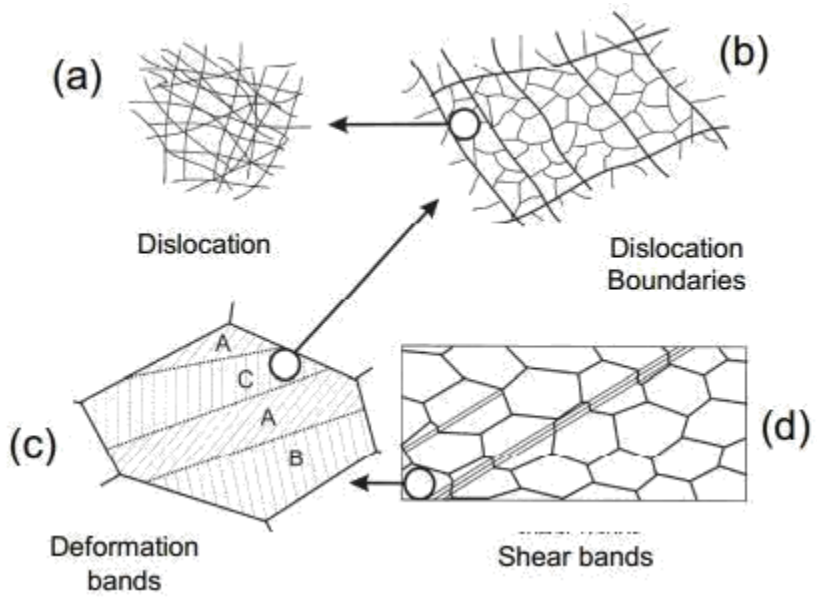

Figure 2.15: The hierarchy of microstructure in a polycrystalline metal deforming by slip. The various features are shown at increasing scale: (a) Dislocations, (b) Dislocation boundaries, (c) Deformation and transition bands within a grain, (d) Specimen and grain-scale shear bands [54]

According to Table 2.4, most of the misorientations at the packet and block boundaries that satisfy the K-S orientation relationship exceed 15°, which is generally the criterion between the low and high angle boundaries. Even the minimum misorientation, 10.53°, is relatively large, whereas the misorientations along the individual laths are low angle boundaries within a range of few degrees.

The laths in a single packet have similar habit plane and different crystallographic orientations. Orientation relationship between an identical (111) austenite plane and six K-S Variants (V1-V6) in a given packet is showed in Figure 2.16.

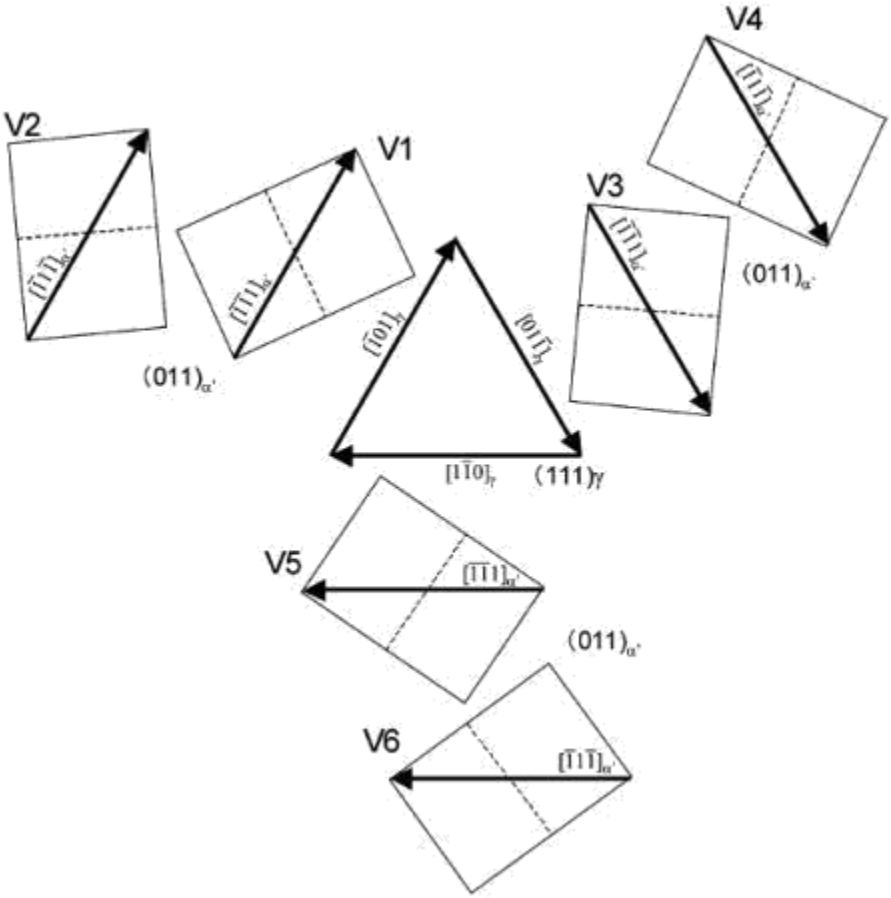

Figure 2.16-Schematic illustration of six crystallographic variants for the K-S orientation relationship in a packet [42].

K-S orientation relationship gives four separate groups of α'-martensite variant pairs (in a given packet) with different misorientation angles (Table 2.4), whereas the variants with the same habit plane in N-W OR are related by [011]/60° rotation.

Table 2.5-Misorientation between variant pairs in a given packet [42].

Group	Variant pair	Misorientation axis/angle
1	V1-V4, V3-V6, V5-V2	[011]/10.5°
2	V1-V6, V3-V2, V5-V4	[011]/49.5 °
3	V1-V3, V3-V5, V5-V1, V2-V4, V4-V6, V6-V2	[011]/60.0 °
4	V1-V2, V3-V4, V5-V6	[111]/60.0 ° twin related =[011]/70.5 ° (Σ3)

2.7.3 *Ms* Temperature

The *MS* temperature is a very useful parameter for estimating the stability of austenite against martensitic transformation and is affected by a number of
factors, such as chemistry of the steel, grain size, structural defects, stress state, deformation temperature, existence of pre{existing martensite, etc. Among these factors, the influence exerted by steel chemistry has received considerable interest. The martensite start temperature, *MS*, is defined as the highest temperature at which austenite transforms to martensite. Over the past few years, a number of authors have focused attention on developing models of wider applicability. Two categories of techniques have prevailed, those based on thermodynamics [55-59] and others fully empirical [60, 61]. Table 2.4 shows the relationships for *MS* with chemical composition of austenite commonly used by many researchers.

Table 2.6: Equation to determine *Ms* temperature of stainless steels.

Scientists	Year	Equation
Eichelman et *al.* [54]	1953	M_S (°C) = 1302 - 42Cr - 61Ni - 33Mn - 28Si - 1667(C + N)
Pickering [55]	1985	M_s (°C) = 775 - 810C - 1230N - 13Mn - 30Ni - 12Cr - 54Cu - 46Mo

2.7.4 Nucleation of *ε* (hcp) martensite

Hsu and Zuyao [62] found that the SFE plays an important role in the determination of the critical driving force, *Gc* for DIM transformation:

γ (fcc)→ ε (hcp) in ternary Fe-Mn-Si alloys. Δ( )→ (*h*) increases with the amount of the substitutional alloying element, Mn and decreases with Si. However, the effect of the interstitial elements on the thermodynamics of *γ* (fcc) → *ε* (hcp) transformation has not yet been properly understood.

Datta et *al.* [63] extensively examined the role of *ε* (hcp) martensite during strain-induced transformations in metastable austenitic stainless steels at low temperature. In their work, they have explained the nucleation micro- mechanisms of *ε* (hcp) martensite. If intrinsic stacking faults overlap regularly on every second *{*111*}* plane, then a perfect *ε* (hcp) martensite phase with perfect *hcp* crystal structure is formed. Overlapping on successive

*{*111*}* planes produces a mechanical twin. If the overlapping is irregular, then a planar defect referred to as a stacking fault bundle is formed. A stacking fault bundle may be regarded as either faulted austenite or faulted ε (hcp) martensite. In metastable austenitic stainless steels, it is well established that intersections of shear bands formed by ε (hcp) martensite platelets, or twins, or slip bands, can be very effective DIM nucleation sites [63].

Fundamental studies, including the *in-situ* observations of the formation of DIM in stainless steel were carried out in the late 1970s by Brooks et *al.* [64, 65]. It was shown that ε (hcp) martensite occurs in regions where appropriately, but usually irregularly, spaced stacking faults are formed, while α (bcc) martensite nucleation is associated with dislocation pile{ups on the activated slip plane. Stacking faults in stainless steel have been shown to have the supplementary displacement, in addition to the expected 1/3 <111>, which has the same sense and direction as the change in interplanar spacing of the close packed planes which occurs in γ (fcc) $\rightarrow\varepsilon$ (hcp) transformation. The nucleation and growth of ε (hcp) martensite is correlated with the defects in the structure.

Venables [66] studied the nucleation of the low temperature ε (hcp) and α' (bcc) martensites produced under deformation in a AISI 304 stainless steel through their extensive TEM analysis. Yuan et *al.* [67] observed by optical microscopy and SEM that the γ (fcc) $\rightarrow$ (hcp) transformation takes place due to the temperature cycling and stress concentration, whereas nitrogen can stabilize the austenitic microstructures extensively. Petit et *al.* [68] distinguished between the ε (hcp) and α' (bcc) martensites in tensile deformed austenitic stainless steel. According to them, the amount of ε (hcp) martensite at the initial stage of straining is almost as large as the amount of α'' (bcc) martensite. It reaches a maximum at 10% strain and finally decreases to zero for strains higher than 30%. In fact, ε (hcp) martensite transforms to α' (bcc) martensite whose amount continuously increases with the strain.

Jun and Choi [69] have discussed the change in the *Ms* temperature of γ(fcc) $\rightarrow\varepsilon$ (hcp) transformation as a function of austenite grain size correlating to the SFE in a Fe-18%Mn alloy. With the increase in the austenite grain size, the *MS* temperature increases rapidly up to 35 μm and gradually increases in larger grains. They have found a good linear relationship between the *MS* temperature and the inverse of SFE, and concluded that the variation in *Ms* temperature with austenite grain size depends strongly on the change in SFE. Yang and Wayman [70, 71] carried out the crystallographic analysis on the secondary variants formed at

intersections of ε (hcp) martensite variants. Formation mechanisms of these variants were proposed based on the intersecting shears associated with intersecting initial variants.

2.7.5 Formation of stacking faults

The atomic arrangement on the *{*111*}* plane of an *fcc* structure and the {0001*}* plane of an *hcp* structure could be obtained by the stacking of closed packed planes of spheres. For the *fcc* structure, the stacking sequence of the planes of atoms is given by *ABC ABC ABC*. For the *hcp* structure, the stacking sequence is given by *AB AB AB*. Errors, or faults, in the sequence can be produced in most metals by plastic deformation [72]. There are two kinds of stacking faults: intrinsic and extrinsic.

Intrinsic stacking faults form in the *fcc* crystal lattice as a consequence of the dissociation of a/2 <110> perfect dislocations into two a/6 <211> partial dislocations,
referred to as Shockley partial dislocations. An intrinsic stacking fault is formed between the partials, and consequently, the stacking sequence of the *{*111*}* planes are changed from the regular *ABCABCABC* to, for instance, *ABCACABCA*.

If two intrinsic stacking faults overlap on the successive *{*111*}* planes, the resulting stacking sequence will be *ABCACBCAB*, which has one excess plane with the *C* stacking. Such a fault is referred to as an extrinsic stacking fault or twins. Thus stacking faults in *fcc* metals can also be considered as sub{microscopic twins of nearly atomic thickness. The reason why mechanical twins of microscopically resolvable width are not formed readily when *fcc* metals are deformed is that the formation of stacking faults is very much energetically
favourable. Consequently, it is difficult to distinguish between single stacking fault, bundle of overlapping stacking faults, and faulted or perfect ε (hcp) martensite. Therefore, a collective term “shear band" [73] has often been used to designate the microstructural features originating from the formation and overlapping of stacking faults in austenitic stainless steels.

The differences in the deformation behaviour of *fcc* metals are due to the differences in stacking fault behaviour. SFE is very sensitive to chemical composition and temperature. A recent research by Byun et *al.* [74] has established that, besides SFE, deformation structures in AISI 316LN stainless steel can also be classified very well by equivalent stress levels, which may be affected by strain, defects, temperature etc. Several authors have reported that the SFE of austenitic stainless steels increases with increasing temperature [33, 75]. The influence of temperature and SFE on the deformation characteristics of austenitic steels has been schematically shown in Figure 2.6 [75]. The twinning was found to be an intermediate mode of deformation between the formations of

ε (hcp) martensite and dislocation cells, corresponding to the SFEs of 10-40 *mJ/m*2. Austenitic Co-Ni-Cr-Mo alloys were found to show essentially equivalent behaviour [75].

Table 2.7 Different equations for calculation of SFE in stainless steels.

Scientists	Year	Equation
Schramm et *al.* [72]	1975	SFE (mJ/m^2) = - 53 + 6.2Ni + 0.7Cr + 3.2Mn + 9.3Mo
Rhodes et *al.* [73]	1977	SFE (mJ/m^2) = 1.2 + 1.4Ni + 0.6Cr + 7.7Mn - 44.7Si
Brofman et *al.* [74]	1978	SFE (mJ/m^2) = 16.7 + 2.1Ni - 0.9Cr + 26C
Pickering [55]	1985	SFE (mJ/m^2) = - 25.7 + 2Ni + 410C - 0.9Cr - 77N - 13Si - 1.2Mn
Dai et *al.* [75]	2002	γ^{300} (mJ/m^2) = γ^0 + 1.59Ni - 1.34Mn + 0.06Mn^2 - 1.75Cr + 0.01Cr^2 + 15.12 Mo - 5.59Si - 60.69 $(C + 1.2N)^{0.5}$ + 26.27 (C + 1.2N) $(Cr + Mn + Mo)^{0.5}$ + 0.61 $[Ni(Cr + Mn)]^{0.5}$ (where γ^{300} is the value of SFE at room temperature and γ^0 is the value of SFE of pure austenitic iron at room temperature.)

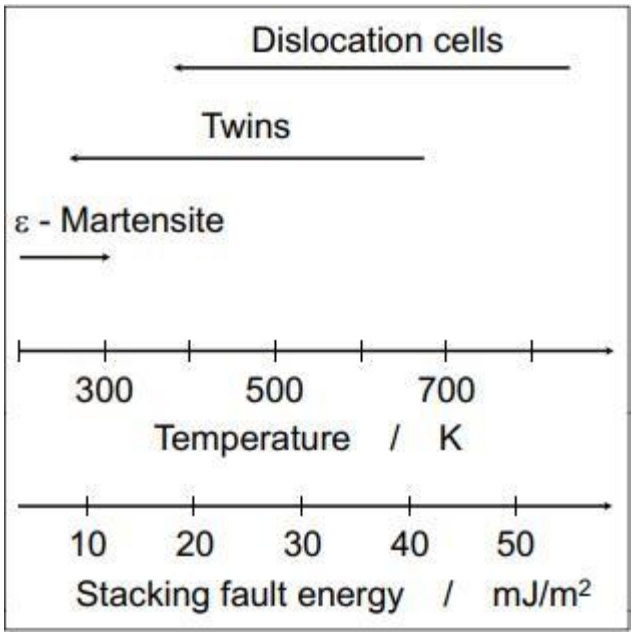

Figure 2.17: Effect of temperature and SFE on the deformation microstructures of austenitic Fe-Mn-Cr-C alloys [75].

2.7.6 Nucleation of α' (bcc) martensite

Volumes of reports are available on the topic of nucleation micro-mechanisms of α' (bcc) martensite in different kinds of austenitic steels under various deformation modes. In the following paragraphs, the findings of some pioneer studies have been reviewed and discussed.

It is well established that the α' (bcc) martensite nucleates at the intersections of micro shear bands [64-66, 76]. Recently Bracke et *al.* [77] found that, during DIM formation in an austenitic stainless steel, α' (bcc) martensite nucleated at the intersection of two ε (hcp) martensite laths. Some investigators also found that α' (bcc) martensite nucleation took place within single shear band [78, 79]. Narutani et *al.* [80, 81] and Lichtenfeld et *al.* [82] have reported that the α' (bcc) martensite transformation occured without the presence of ε (hcp) martensite. Venables [10] has reported that in stainless steel deformed by tension at 77 K, α'(bcc) martensites are always associated with ε(hcp) martensites.

The orientation between the γ (fcc) austenite and α' (bcc) martensite phases has been shown to obey the Kurdjumov-Sachs orientation relationship, i.e., [83, 66, 76, , 84]: $(111)_\gamma // (110)_{\alpha'}$ and $[110]_\gamma // [111]\alpha'$. Mangonon and Thomas
[115] found that initially the relationship was that of Nishiyama, i.e.,: $(111)_\gamma // (211)_{\alpha'}$ and $[110]\gamma // [111]\alpha'$ and changed to the Kurdjumov-Sachs as the transformation proceeded. Bowkett et *al.* [85], however, claimed that it is not possible to distinguish between these two relationships based on the selected area diffraction pattern (SADP) technique.

In general, the α' (bcc) martensite nucleation involves a process by which an array of Shockley partial dislocations, i.e., another shear band, can penetrate through the other shear band. Olson and Cohen [3, 71] discussed the nucleation of α' (bcc) martensite based on the work of Bogers and Burgers [86]. They suggested that the *bcc* structure can be generated from *fcc* by two successive shears, the first involving a 1/3 *FCC* twinning shear of austenite and the other a 1/2 *FCC* twinning shear, referred to as T/3 and T/2, respectively. Olson and Cohen [87, 88] rationalised the T/3 shear by the spreading of an array of a/6
<112> Shockley partial dislocations on every third (111) plane and the T/2 by the spreading of the Shockley partial dislocations on every second (111) plane. As the movement of the Shockley partial dislocations on every second (111) plane produces perfect α'(bcc) martensite; Olson and Cohen [87, 88] suggested that an α' (bcc) martensite nucleus is formed by the passage of a T/3 shear through an ε(hcp) martensite platelet. Since a significant amount of chemical driving force

is available, the process transforms the stacking of the atoms from *fcc* to *bcc*, and enables the partial dislocations to penetrate through the ε (hcp) platelet.

2.7.7 Nucleation of deformation twin

Another important mechanism by which plastic deformation of metals occurs is known as twinning. Deformation of austenitic stainless steels may involve deformation twinning micro-mechanisms. A mechanical twin is formed by overlapping of the intrinsic stacking faults, i.e., by the glide of Shockley partials of the same sign on successive (111) planes [89, 90]. The theory of deformation twinning merits attention both because of their intrinsic importance as a mode of plastic deformation in many crystalline solids and because of its close association to the theory of martensitic transformation.

Christian and Mahajan [91] have demonstrated all the probable aspects of twinning micro{mechanisms in their pioneer studies. Karaman et *al.* [92] studied the stress{strain behaviour of nitrogen containing AISI 316L stainless steel single crystals with different crystallographic orientation, and suggested that the overall stress-strain response was strongly dependent on the crystallographic orientation, and nitrogen addition suppressed deformation twinning, although planar slip was evident, stemming from the non monotonous change in SFE with nitrogen content as well as the role of short range atomic ordering. Lecroisey and Pineau [89] investigated that in 16/11, 16/13 and 18/12 type of austenitic stainless steels, deformation twins occurred along with ε (hcp) martensite. They observed that with increasing temperature and strain, the number of the twins increased, and attributed this to the increase in the SFE with increasing temperature.

Ferreira et *al.* [93] found that high strain rate promoted the deformation twinning in AISI 304 stainless steel, and also increased the number of twin variants from one to two. Deformation twinning has been found to be a preferred mechanism of plastic deformation in nitrogen alloyed austenitic stainless steels at high strains and stress levels. Venable [66] suggested that the prismatic glide sources could dissociate into a Frank{type pole dislocation and Shockley type twinning partial, and rotating twinning partial caused the generation of jogs, resulting in the formation of deformation twinning. Mahajan and Chin [94] proposed that two coplanar glide dislocations with different Burgers vectors dissociated into Shockley partials and finally evolved into the dislocation configuration of three layer twins in *fcc* materials. Mechanical twinning subdivides the austenitic grains and, therefore, increases the barriers to slip and leads to an increase in the flow stress.

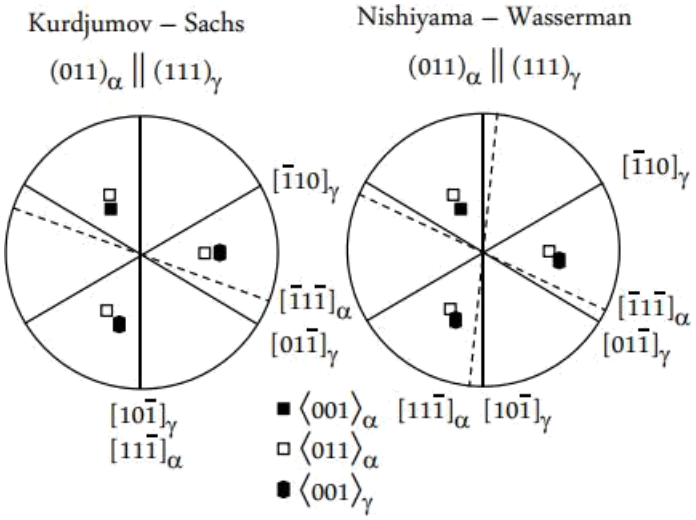

Figure-2.18 Stereographic representation of the Kurdjumov{Sachs and Nishiyama{Wasserman orientation relationships [28].

2.7.8 Orientation relationship

The formation of martensite involves the coordinated movement of atoms. It follows that the austenite and martensite lattices will be intimately related. All martensitic transformations, therefore, lead to a reproducible orientation relationship between the parent and product lattices. It is frequently the case that a pair of corresponding close-packed planes in the ferrite and austenite are parallel or nearly parallel, and it is usually the case that corresponding close packed directions within these planes are roughly parallel (Figure 2.18). Kurdjumov-Sachs orientation relationships are:

$$\{111\}_\gamma \parallel \{011\}_\alpha,\ \langle 10\bar{1}\rangle_\gamma \parallel \langle 11\bar{1}\rangle_\alpha;$$

Nishiyama-Wasserman orientation relationships is:

$$\{111\}_\gamma \parallel \{011\}_\alpha,\ \langle 10\bar{1}\rangle_\gamma,$$

about 5.3° *from* <1̶1̶1>α *towards* ~~*<111>α*~~ *and Greninger-Troiano orientation relationships are: {111}α about 0:2° from {011}α, <101>γ about 2:7° from <111>α towards <111>α*

It is to be noted that these relationships have been stated approximately: the true relations are irrational, meaning that the indices of the parallel planes and directions cannot be expressed using rational numbers [28].

2.7.9 Athermal nature of transformation

In the vast majority of cases, the extent of reaction is found to be virtually independent of time:

$$1 - V_{\alpha'} = EXP\{\beta(M_S - T)\} \qquad \text{…….2.2.9(1)}$$

where β = { 0.011, $V_{\alpha'}$ = is the fraction of martensite and T is a temperature below Ms. This is the Koistinen and Marburger equation [95]; the time parameter does not feature in this relation (Equation 2.2.9(1)). Hence the fraction of martensite depends only on the undercooling below the martensite-start temperature. This transformation character is a consequence of very rapid nucleation and growth, so rapid that the time taken can in normal circumstances be neglected. Isothermal martensite is possible when nucleation is hindered, although the growth rate of individual plates of martensite can still be rapid [28].

2.7.10 The shape deformation

The passage of a slip dislocation through a crystal causes the formation of a step where the glide plane intersects the free surface (Figure 2.19). The
passage of many such dislocations on parallel slip planes causes macroscopic shear (Figure 2.8). Slip causes a change in shape but not a change in the crystal structure, because the Burgers vectors of the dislocations are also lattice vectors[28].

During martensitic transformation, the pattern in which the atoms in the parent crystal are arranged is *deformed* into that appropriate for martensite. Hence, there must be a corresponding change in the macroscopic shape of the crystal undergoing transformation. The dislocations responsible for the deformation are in the α'/γ interface, with Burgers vectors such that in addition to deformation they also cause the change in crystal structure. The deformation is such that aninitially flat surface becomes uniformly tilted about the line formed by the intersection of the interface plane with the free surface. Any scratch traversing the transformed region is similarly deflected through the scratch remains connected at the α'/γ interface. These observations, and others, confirm that the measured shape deformation is an invariant{plane strain (Figure 2.18 (e, g)) with a large shear component (≈ 0.22) and a small dilatational strain (≈ 0.22) directed normal to the habit plane.

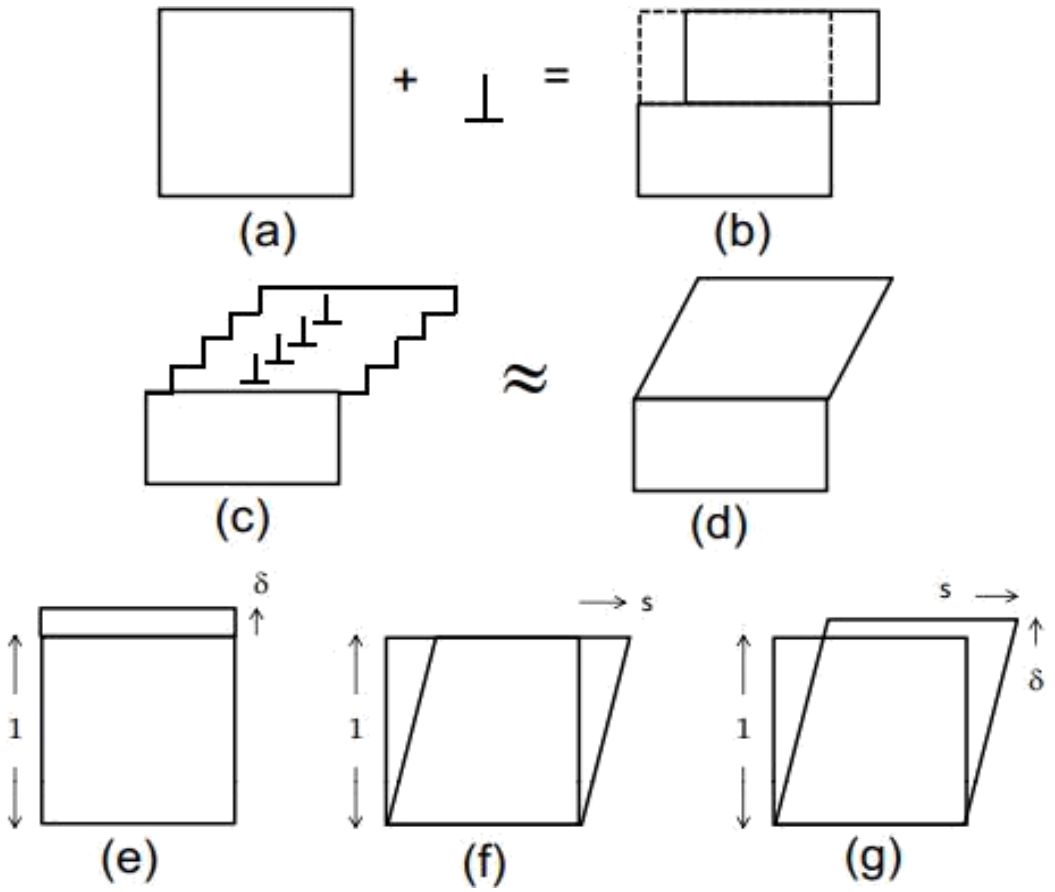

Figure 2.19: (a, b) Step caused by the passage of a slip dislocation. (c, d) Many slip dislocation, causing a macroscopic shear. (e) An invariant-plane strain with uniaxial dilatation. (f) An invariant-plane which is a simple shear. (g) An invariant-plane strain which is the combined effect of a uniaxial dilatation and a simple shear [28].

2.8 Thermodynamics

Several attempts have been made to associate the temperature to the chemical composition by empirical equations. The Eichelmann and Hull's equation is one of the most commonly used: [31].

$$M_s(°C) = 1302 - 42(\%Cr) - 61(\%Ni) - 33(\%Mn) - 28(\%Si) - 1667(\%[C+N]) \dots\dots \quad (3)$$

As this equations shows, many stable and metastable austenitic steels will partially transform to α'-martensite when cooled to a cryogenic temperature. The impoverishment of chromium, carbon and other alloying elements close to the grain boundaries due to precipitation of 23 6 increases the the temperature. Consequently, the sensitization enhances the ability of α'-martensite formation adjacent to grain boundaries during cooling [97].

The martensitic transformation in stable austenitic grades happens only during cooling to cryogenic temperatures whereas the strain induced martensite is more frequently seen at room temperature in less stable grades. This transformation and the amount of α' and ε-martensite is affected by e.g. temperature, chemical composition, stacking fault energy (SFE) of austenite, deformation degree, deformation rate, and also stress state during deformation [98].

Thermodynamics of strain induced martensite are illustrated in Figure 2.3 [99], which schematically shows that if adequate mechanical driving force (U') is applied on the austenite, the martensitic transformation can take place at a temperature (1) higher than . Whereas the spontaneous transformation occurs only at when the chemical driving force reaches the critical value $(\Delta G_{M_s}^{\gamma\rightarrow\alpha'})$:

$$\Delta G_{T_1}^{\gamma\rightarrow\alpha'} + U' = \Delta G_{M_s}^{\gamma\rightarrow\alpha'} \quad (4)$$

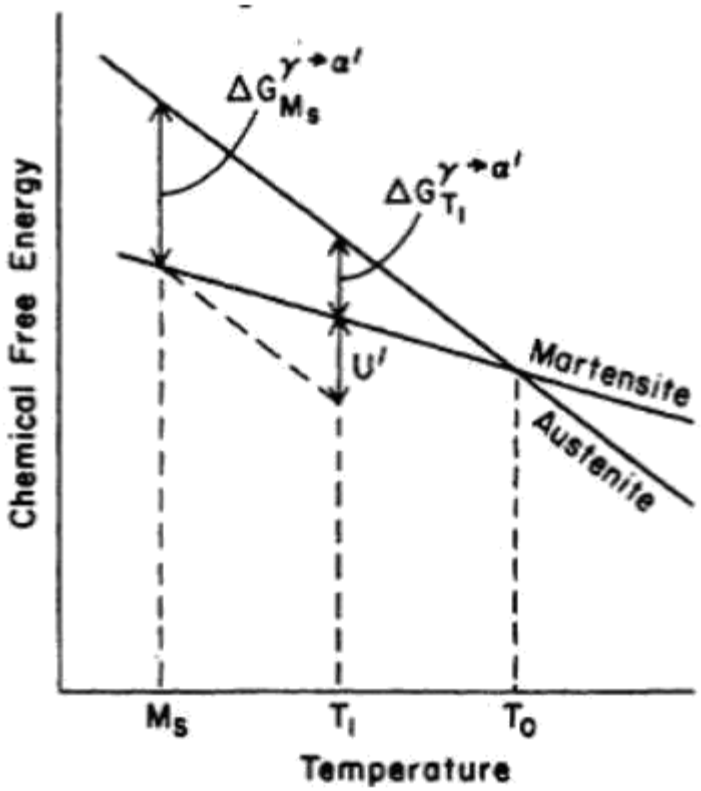

Figure 2.21-Schematic illustration of chemical free energies of austenite and martensite phases as a function of temperature [99].

It has been shown that the mechanical driving force results from the applied stress which aids the chemical driving force. Patel and Cohen [100] suggested that the mechanical driving force can be calculated using the crystallographic theory of martensitic transformation as function of stress and orientation. Thus, according to Fig.
2.22 the corresponding stress level increases linearly with temperature. This linear relation is believed to be valid until the stress level reaches the austenite yield strength.

In 1970 Bolling and Richman defined the as the temperature below which the yielding can take place by martensite transformation, whereas at temperatures above the transformation takes place after the plastic deformation of austenite. The idea of *stress-assisted* and *strain-induced* martensitic transformation was later established in 1972 by Olson and Cohen [101] in order to clarify the transformation mechanism below and above

the . They defined the temperature as the maximum temperature at which, the

stress-assisted martensitic transformation takes place by means of the “elastic” stress and

the critical stress to initiate the transformation within this range increases linearly with temperature.

At temperatures above when the martensitic transformation takes place after plastic flow of the austenite, the transformation is referred to as strain-induced transformation. Olson and Cohen suggested that the plastic strain of the austenite contributes to the transformation by the generation of energetically favorable nucleation sites through shear band intersections. In this temperature regime the transformation critical stress decreases significantly, and the temperature is defined as the upper limit for strain-induced transformation to reflect the stability of austenitic phase. The discussion presented above is illustrated in Figure 2.22.

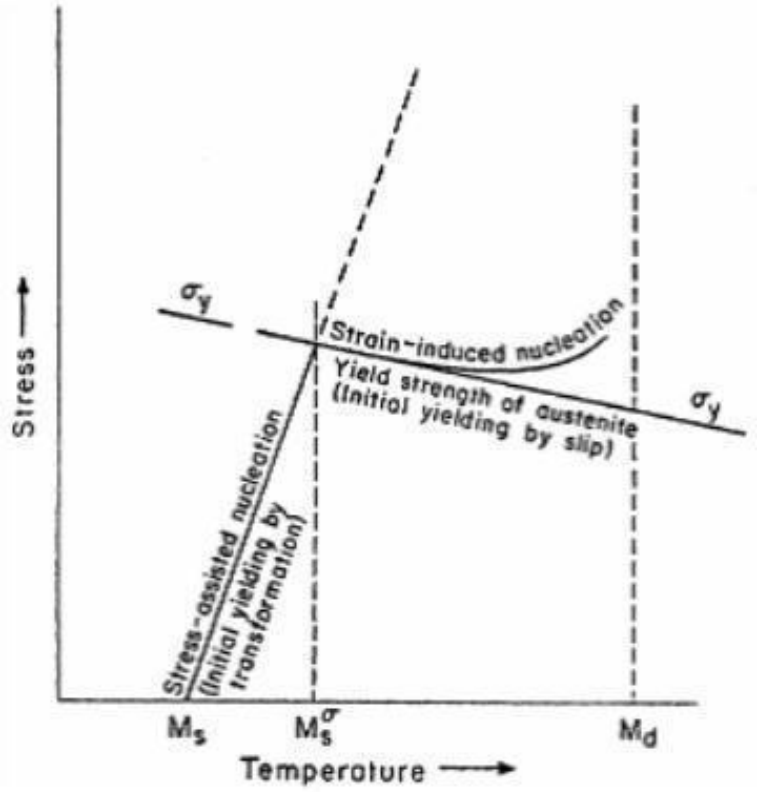

Figure 2.22-Schematic illustration of the critical stress to initiate martensite transformation as function of temperature [101].

It is well established that the austenite stability and the extent of the strain-induced α'-martensite transformation, is significantly affected by chemical composition, temperature and strain rate.

Numerous studies have been made to relate the temperature to chemical composition in which one of the most used formulas is attributed to Angel [102],

$$M_d(30/50)(°C) = 413 - 13.7(\%Cr) - 9.5(\%Ni) - 8.1(\%Mn) - 18.5(\%Mo) - 9.2(\%Si) - 462(\%[C+N]) \ldots\ldots \quad (5)$$

where (30/50) (°C) the temperature at which 50 vol. % α'-martensite is formed after a true tensile strain of 30 %.

Another most often used equation is due to Nohara et al. [10]. They conducted the following equation by modifying Angel's equation and including the effect of grain size:

$$M_d(30/50)(°C) = 551 - 13.7(\%Cr) - 29(\%[Ni+Cu]) - 8.1(\%Mn) - 18.5(\%Mo) - 9.2(\%Si) - 462(\%[C+N]) - 68(\%Nb) - 1.42(GS-8) \quad (6)$$

Where GS is the grain size according to ASTM.

Normally, in solution-treated condition, the temperature is below room temperature for most of the austenitic grades, but temperature is usually above room temperature.

The austenite stability and the extent of the strain-induced α'-martensite transformation has been explained in terms of the variation in the chemical free energy difference between the austenite and α'-martensite phases, referred to as the chemical driving force. However, the stacking fault energy play also an important role in determining the austenite stability, since it controls the generation of energetically favorable nucleation sites for the α'-martensite through formation of the shear bands. Several authors have shown that the SFE is strongly dependent on the chemical composition [104–106] and temperature [107-109].

Although there is no empirical equation for ε-martensite formation like that for α'-martensite, it is generally accepted that the decrease in stacking fault energy of the austenite increases the ε-martensite formation, whereas an increase of the stacking fault energy changes the dominant deformation mode from the formation of ε- martensite to twinning, and then to slip. This is illustrated in figure 2.23 as the schematic diagram defined for an austenitic Fe-Mn-Cr-C alloy by Remy and Pineau 1977) [110].

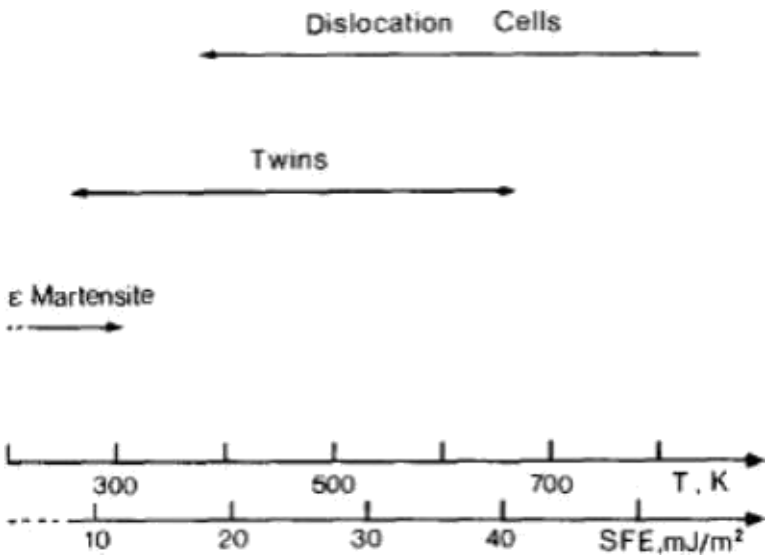

Figure 2.23-Deformation structure of an austenitic Fe-Mn-Cr-C alloy as a function of both temperature and stacking fault energy [110].

The α' and ε-martensite form almost simultaneously which makes investigation of their formation mechanism rather difficult. According to Mangonon and Thomas
[38] the amount of ε-martensite formed during deformation of an AISI304 reaches a maximum and decreases afterwards, while the amount of α'-martensite continuously increases with deformation. Seetharaman and Krishnan [111] also showed that ε-martensite formation precedes the formation of α'-martensite during deformation of AISI316 steel at low temperatures. Therefore it has been suggested that ε-martensite is formed from austenite and it is then transformed to α'-martensite. It is also found that α'-martensite can be directly formed from austenite.

The deformation induced martensite in stainless steels may revert to austenite during annealing at lower temperatures and shorter times than those required for the recrystallization of deformed stainless steels without the formation of martensite [112]. Burstein et al. [113] found that it is possible to remove the strain induced martensite in AISI304L by proper electrochemical treatment in aqueous solutions at much lower temperatures than conventional annealing heat treatments.

2.9 Influencing parameters of martensitic transformation

The extent of deformation induced martensitic transformation is significantly affected by several factors, including chemical composition, temperature, stress, stain, strain rate, stress state, strain state, strain path, grain size and initial crystallographic micro texture of the austenite phase. The variation of the extent of martensite has been shown to have substantial influence on the mechanical response of metastable austenitic stainless steels. Thus, thorough understanding of the role of each factor is essential when using these steels in engineering applications.

2.9.1 Chemistry

Since the transformation occurs above M_S, the metastability of austenitic stainless steel cannot be properly indexed by M_S temperature. The stability of these steels is instead rated by other parameters. The M_d temperature is the limit for deformation induced martensitic transformation, and no martensite can form above this. Alloying makes austenitic stainless steels more stable against the deformation induced transformation. This is a consequence of the alteration of the SFE and the chemical driving force, $G_{\gamma \rightarrow \alpha'}$.

However, this temperature is hard to measure and hence another parameter, M_{d30}, was established by Angel [114]. M_{d30} is the temperature where 50% of martensite has formed at 30% true strain. This temperature is a good measure of the stability of the metastable austenitic stainless steels. Several empirical formulae (Table 2.8) have been proposed in the literatures [114, 115] to describe the influence of chemical composition on the tendency to martensitic transformation.

Table 2.8: Empirical formula for determining M_{d30} temperature.

Scientists	Year	Equation
Angel [98]	1954	M_{d30} (°C) = 413 - 462 (C + N) - 9.2Si - 8.1Mn - 13.7Cr - 9.5Ni - 18.5Mo
Nohara et *al.* [99]	1977	M_{d30} (°C) = 551 - 462 (C + N) - 9.2Si - 8.1Mn - 13.7Cr - 29 (Ni + Cu) - 18.5Mo - 68Nb - 1.42(*GS - 8) (*GS = ASTM grain size number.)

2.9.2 Stress/strain

The thermodynamics of martensitic transformation is well established. At temperatures above M_S , martensitic transformation takes place when the summation of the mechanical interaction energy due to the externally applied stress and the chemical driving force exceeds a critical value [33]. Deformation can stimulate the kinetics of solid state phase transformations through both the pure thermodynamic effect of applied stress and through the generation of new catalyzing defects by employing plastic strain.

For the case of martensitic phase transformations, these interactions can be described by the very well known schematic stress-temperature diagram as shown in Figure 2.24 [116]. The spontaneous displacive transformation is triggered by the pre existing nucleation sites of DIM on cooling to the $M_{s\sigma}$ temperature of the alloy. Stress assisted nucleation on the same sites will; therefore, occur as the applied stress denoted by the solid line shown in the figure. At the temperature designated, M_S^{σ} , this stress reaches the yield point, σy for the slip in the parent austenite phase. Above the M^{σ}_s , temperature, the new potent nucleation sites of DIM introduced by the plastic strain trigger strain induced martensite nucleation. The temperature, M_S^{σ} thus dictates the approximate boundary between the temperature regimes where the two modes of nucleation mechanisms dominates, near the M_s^{σ} both modes operate.

Due to the transformation induced plasticity, the observed yield stress follows the stress for the stress assisted martensite transformation below the M_s^{σ} temperature. A reversal of the temperature dependence of the flow stress of the material thus provides a convenient determination of the M_s^{σ} temperature. The M_s^{σ} *temperature* characterizes the stability of the parent austenite phase against DIM transformation. M_d is the maximum temperature above which the DIM transformation cannot be induced by deformation.

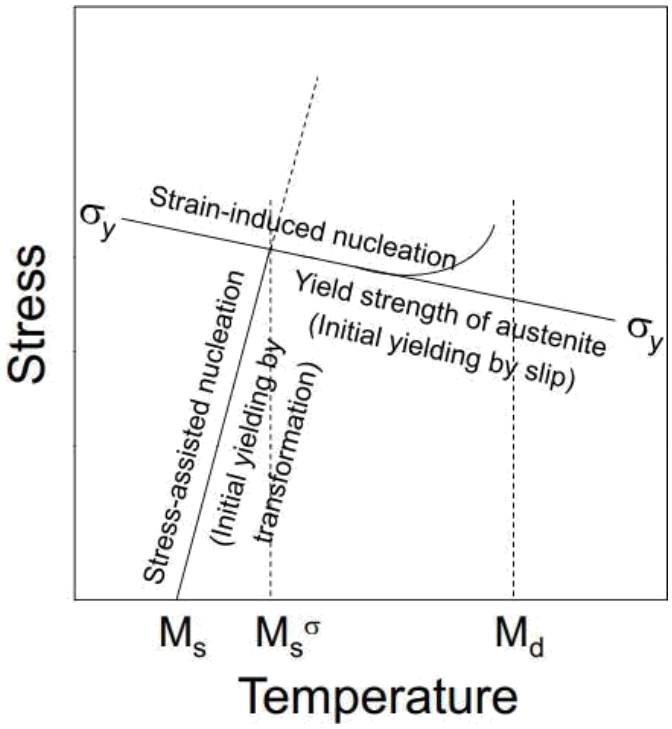

Figure 2.24: Schematic illustration of the influence of temperature and applied stress on martensite transformation mechanisms. Solid line indicates the critical stress required to initiate martensite transformation at temperatures above *MS* [149].

2.9.3 Grain size

The influence of austenite grain size on martensitic transformation has been studied extensively by many investigators [115, 117-121]. Lee et *al.* [122] found

that *Ms* temperature increases with increasing austenite grain size for low alloy steels. According to Iwamoto et *al.* [118], volume fraction of martensite increases with increase of austenite grain size in case of TRIP steels. Also Varma et *al.* [119] found that large grain size promoted the α' (bcc) martensite formation during tensile and cold rolling deformation of AISI 304and 316 stainless steels. In contrast, Shrinivas et *al.* [120] found that the formation of α' (bcc) martensite during cold rolling increased with decreasing grain size in AISI 304 steel and was grain size independent in AISI 316 stainless steel. Recently Yang et *al.* [121] investigated that the volume fraction of martensite formed in the early stages of transformation is proportional to the cube of the austenite grain size. Thus the fraction of transformation needed to detect *Ms* is reached at a smaller undercooling when the austenite grain size is large (Figure 2.25) [121].

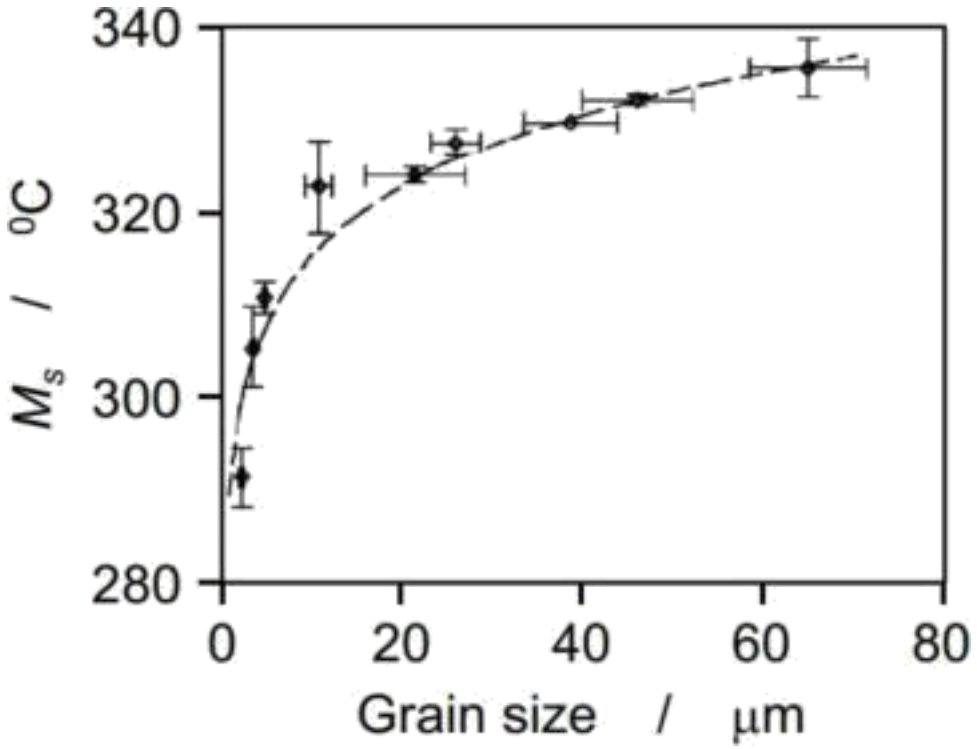

Figure 2.25: Measured variation in the martensite{start temperature determined from dilatometric data using the offset method of Fe-0.13C-5Ni-2.27Mn alloy [121].

2.9.4 Temperature

It is well known that deformation induced martensitic transformation is suppressed with increasing temperature [31, 114]. An example of the temperature dependence found by Angel [114] is shown in Figure 2.26. It is clear that a stabilizing effect is operative during the later stages of transformation and also that there is a stimulating effect in the beginning, The behaviour is normally attributed to the decrease in the chemical driving force, $G_\gamma \rightarrow \alpha$ with increasing temperature, as indicated in Figure 2.25 [114].

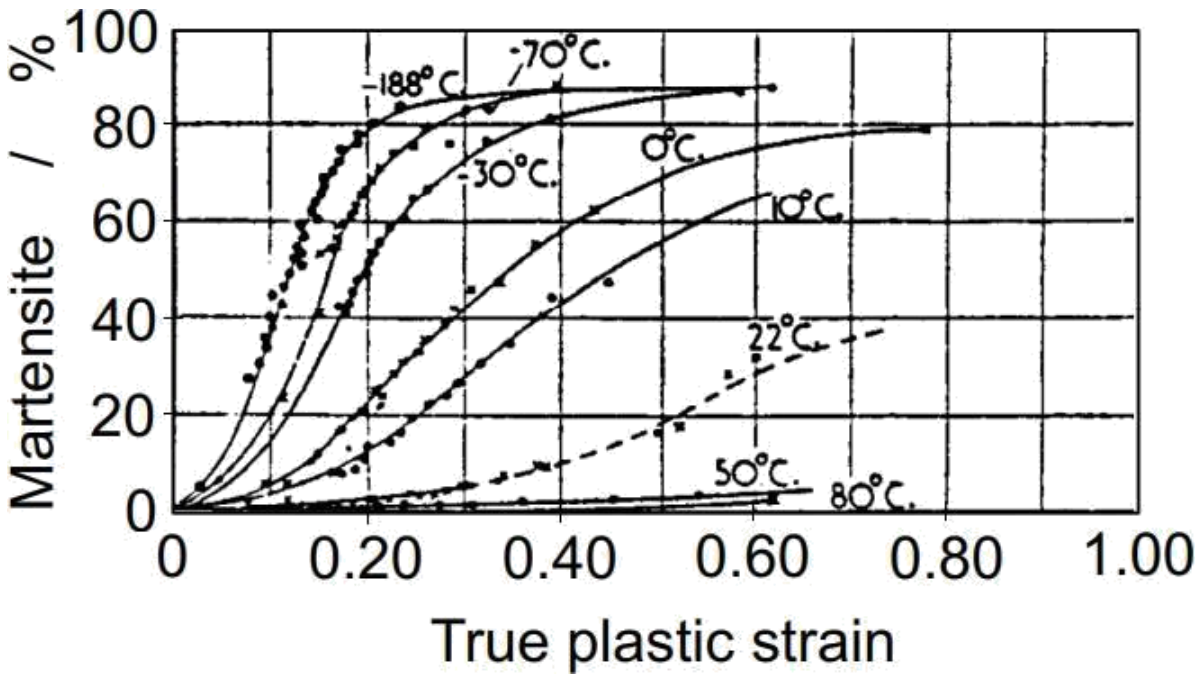

Figure 2.26: Formation of martensite by plastic tensile strain at various deformation temperatures for 18/8 stainless steels [114].

2.9.5 Modelling of martensitic transformation

The best known model to predict the kinetics of the strain-induced α' martensite transformation has been developed by Olson and Cohen [73]. They presumed that the α' martensite is nucleated at the shear band intersections, and that the nucleation and growth process of α' martensite is controlled by two parameters, α'_{oc} and β_{oc}.. As a result, the following equation for the α' martensite volume fraction, $f^{\alpha'}$ as a function of true plastic strain ε is obtained.

The parameter α_{oc} controls the rate of the shear band formation. It was assumed to be dependent on the SFE and strain rate. The parameter β_{oc} is proportional to the probability that the α' martensite is nucleated at a shear band
intersection, and it is dependent on the chemical driving force and temperature. The exponent n describes the rate of the formation of shear band intersections,
and it was found to have the constant value of 4.5. The model predicts a sigmoidal $f^{\alpha'}$ vs. ε curve, and it has been shown to agree well with the experimental data.

2.9.6 Effect of martensitic transformation on mechanical properties

The influence of microstructural evolution on the mechanical properties of austenitic stainless steels has been a subject of numerous investigations since 1950's. Although the high work{hardening capacity of austenitic stainless steels has been related to the low SFE and to the consequent slip planarity, the formation of stacking faults, deformation twins and α' martensite [90] undoubtedly play a key role in the mechanical behaviour of metastable austenitic stainless steels. According to Spencer et *al.* [123], DIM in austenitic stainless steels acts as a reinforcing phase in two ways. Firstly, it acts as an elastic reinforcing phase and secondly it co-deforms with the austenite, but the flow stress of the DIM has higher temperature dependence than that of the austenite. Thus at low temperatures, DIM is expected to make a more significant contribution to flow stress of the composite, as the flow stress in *bcc* materials increases rapidly with decreasing temperature, relative to that of *fcc* materials.

2.10 Monotonic Deformation

Zackay et *al.* [124] suggested that the steels, whose mechanical properties are characterized by the enhancement of strength and ductility by the strain-induced α' martensite transformation, could be referred to as TRIP (Transformation Induced Plasticity) steels. At present, the term TRIP effect is widely used to denote the strain-induced α' martensite transformation itself and its influence on the mechanical behaviour.

The strain-induced α' martensite transformation is associated with a strong increase in the work-hardening rate [74, 89, 125-129]. Consequently, the formation of the stress-strain induced α' martensite increases the tensile strength. When the work-hardening rate of metastable steel exhibiting the transformation is plotted as a function of strain, the curve has been found to show first a minimum and then a subsequent maximum [127, 128]. Examples of the work-hardening curves of AISI 304L steel at different temperatures are shown in Figure 2.25 [128].

The behaviour is often referred to as the abnormal work hardening or as the work hardening abnormality, since it differs from the behaviour of the most metals and alloys showing

continuously decreasing work{hardening rate. The work{hardening peak has been related to the formation of the α' martensite phase. As the extent of the α' martensite transformation is temperature- dependent, the work-hardening rate also exhibits a pronounced variation with temperature, as illustrated in Figure 2.27. Another characteristic of the work-hardening behaviour of metastable steel grades is the minimum that is reached before the maximum.

The work-hardening minimum has been attributed to the formation of α' martensite [79, 130]. Some researchers have explained the enhanced ductility in terms of the excessive formation of deformation twins and stacking faults, the most widely accepted view is that the α' martensite transformation governs the ductility. Furthermore, it has been shown that it is not the total amount but the rate and the point at which the α' martensite transformation takes place, which is important [131, 126, 127, 132-135].

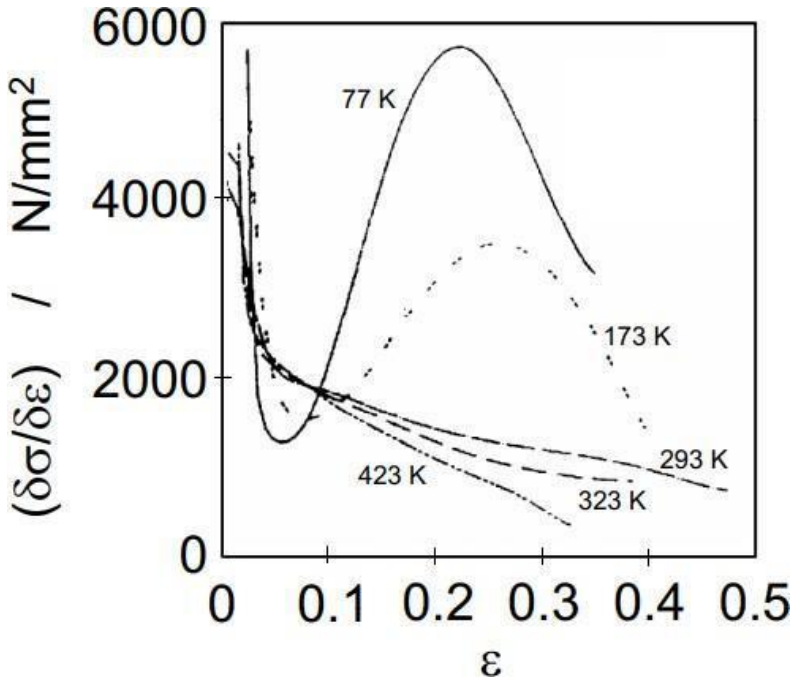

Figure 2.27: Effect of deformation temperature on the work-hardening rate of austenitic stainless steel AISI 304L as a function of true strain [128].

Consequently, when the uniform or total elongation of a metastable austenitic stainless steel is plotted as a function of the deformation temperature, the curve exhibits a peak value, as shown in Figure 2.28 [133]. Uniform elongation is reached when the highest α' martensite transformation rate and the associated work-hardening peak occur at high strain levels [136, 127, 137-139].

On the right hand side of the elongation peak, the temperature is such that the transformation is prevented, and as a consequence, the elongation is reduced. At the lower temperatures, i.e., on the left side of the elongation peak, the *α'* martensite transformation occurs rapidly, resulting in rapid work hardening at low strains and consequent premature fracture.

Bhadeshia [140] showed with a simple theoretical study that if austenitic steel is fully transformed to martensite, the maximum elongation due to the transformation strain can only be 15%.

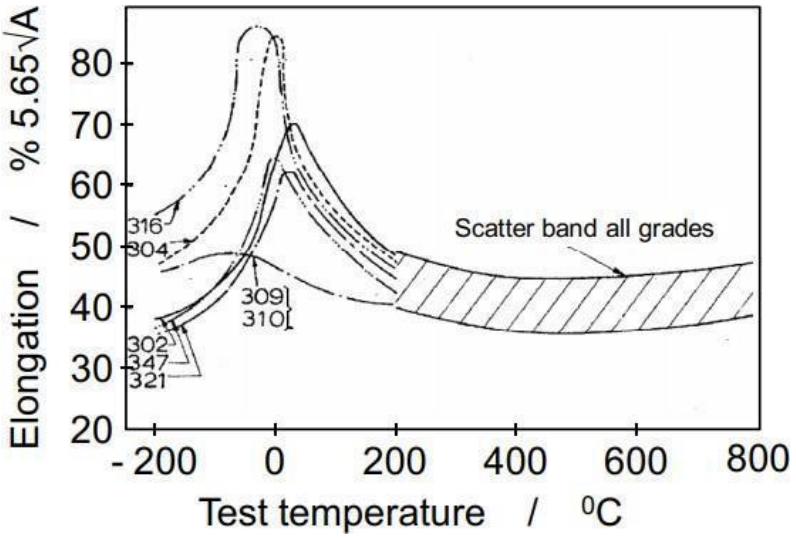

Figure 2.28: Influence of deformation temperature on the elongation to fracture of various austenitic steel grades [133].

2.11 Quantitative Measurement Methods

The are various Various techniques have been used for quantitative measurements of α'-martensite, in which X-ray diffraction and techniques based on the ferromagnetism of α'-martensite phase are the most common methods. Density measurements are also used for quantitative phase analysis of α'-martensite [69]. EBSD diffraction pattern, TEM analysis are very advanced nowadays to give a proper microstructural view.

2.12 XRD Analysis

Various techniques have been used for quantitative measurements of α'-martensite, in which X-ray diffraction and techniques based on the ferromagnetism of α'-martensite phase are the most common methods. Density measurements are also used for quantitative phase analysis of α'-martensite [141].

X- ray diffraction method is based on the difference between the crystal structures of the austenite and α'-martensite. The texture in the sheet materials, especially after plastic deformation, decreases the accuracy of X-ray diffraction. However this

effect can be reduced by averaging intensities of several diffraction peaks [142]. The X-ray diffraction is also expensive and time consuming.

According to [143], the integrated intensities of the martensite and austenite diffraction lines, ^{h} and , are given in terms of the volume fractions VM and VA (= 1 − VM) of each phase by,

$$I_{\mathrm{M}}^{hkl} = \frac{C V_{\mathrm{M}} m_{hkl} \mathrm{LP}(\theta_{\mathrm{M}}) F_{\mathrm{M}}^2 e^{-B_{\mathrm{M}}/2d_{\mathrm{M}}^2}}{v_{\mathrm{M}}^2}$$

$$I_{\mathrm{A}}^{HKL} = \frac{C V_{\mathrm{A}} m_{HKL} \mathrm{LP}(\theta_{\mathrm{A}}) F_{\mathrm{A}}^2 e^{-B_{\mathrm{A}}/2d_{\mathrm{A}}^2}}{v_{\mathrm{A}}^2}$$

where, C is a constant embodying the dimensions of the diffractometer, the incident beam power and the attenuation coefficient of the sample (it is as-sumed that μM = μA), ^{h} and the multiplicity factors, and are the cell volumes, and are the d spacings in martensite and austenite, respectively, FM and FA are the structure factors for the hkl and HKL lines respectively, and are the Debye-Waller factors for each phase, LP ( ) and LP ( ) are the Lorentz-Polarization factors which, for the diffractometer used in this work, are given by LP(θ) = (1+cos2 2θ cos2 2θmono)/ sin 2θ cos θ where is the Bragg angle of the graphite diffracted beam monochromator (i.e. = 13.3◦).

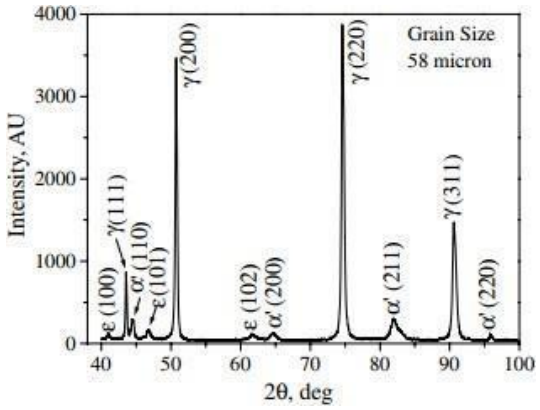

Fig. 2.29 X-ray diffraction scan using Cu Ka radiation of a 304 SS sample strained 15% at -50 C showing the presence of -hcp, ′- martensite and austenite phases.[144].

SUMMARY OF LITERATURE REVIEW

1. It is seen that low alloyed austenitic stainless steels are close to the martensite region and these grades are called metastable austenitic stainless steels, since they are susceptible to deformation induced martensitic transformation.

2. Tensile flow of single crystal FCC metals occurs in the three different stages. In stage I easy glide occurs where the material undergoes little strain hardening. During this stage, the dislocations are able to move over large distances without encountering the barriers. In stage II strain hardening increases rapidly with straining the material. In this stage slip occurs in more than one set of slip system. Here, Lomer-Cottrell barrier increases and dislocation tangles begins to develop. . In stage III the strain hardening rate decreases with strain due to dynamic recovery.

3. Eiji fukushima, akira goto, Mitsuzo fushimi [20]carried tensile test on 18-8 stainless steel and found that the rate of strain hardening increases in general decrease in temperature and has a tendency to decrease at the end of deformation between room temperature and -245^{o} c But the rate of strain hardening does not decrease even at the end of deformation at -269^{o} c and -271^{o}c.

4. According to the Olson–Cohen analysis, internal thermal lift, which is caused by adiabatic heating, lowered the chemical driving force of the γ α'transformation, therefore increasing the SFE, work-hardening rate, ultimate tensile strength and decreasing the ductility of materials.

5. the threshold strain (or critical strain), which is the inflection position between the 1st and 2nd hardening curve and is defined as the onset of 2nd plastic hardening, was observed at temperatures of below 223 K in all materials. The threshold strain is an important parameter to analyze the non-linear behavior of austenitic steel numerically under cryogenic conditions

6. Zackay et *al.* [124] suggested that the steels, whose mechanical properties are characterized by the enhancement of strength and ductility by the strain-induced *α'* martensite transformation, could be referred to as TRIP (Transformation Induced Plasticity) steels. At present, the term TRIP effect is widely used to denote the strain-induced *α'* martensite transformation itself and its influence on the mechanical behaviour.

7. The strain-induced α' martensite transformation is associated with a strong increase in the work-hardening rate [74, 89, 125-129]. Consequently, the formation of the stress-strain induced α' martensite increases the tensile strength

8. The work-hardening behaviour is often referred to as the abnormal work hardening or as the work hardening abnormality, since it differs from the behaviour of the most metals and alloys showing continuously decreasing work-hardening rate. The work-hardening peak has been related to the formation of the α' martensite phase. As the extent of the α' martensite transformation is temperature- dependent, the work-hardening rate also exhibits a pronounced variation with temperature.

9. The work-hardening minimum has been attributed to the formation of α' martensite [125, 129]. Some researchers have explained the enhanced ductility in terms of the excessive formation of deformation twins and stacking faults, the most widely accepted view is that the α' martensite transformation governs the ductility.

CHAPTER-3

EXPERIMENTAL DETAILS

3.1 Materials

The received material was AISI 304 austenitic stainless steel sheet of thickness 2.14 mm. Which was cold rolled and the rolling direction was there marked on the sheet. The micro hardness of received material was 191.4 HV and after room temperature tensile deformation the hardness value was 254.5 HV.

3.2 Chemical composition

The chemical composition of the AISI 304 austenitic stainless steel used for the present study is given in table 3.1.

Table 3.1: Chemical composition of the 304 stainless steel.

Grade	C	Si	Mn	P	S	N	Cr	Mo	Ni
304	0.048	0.290	1.78	0.031	0.010	0.073	18.21	0.191	8.07

Table 3.2: Md30/50(oC), MS(oc) and SFE(mj/m2) temperature of the 304 stainless steel.

$M_{d30/50}(^oC)$	10.34	Eichelman[31]
	-38.07	Nohara[37]
$Ms(^oc)$	-223.65	Angel[9]
$SFE(mj/m^2)$	-17.79	Pickering[55]

3.3 Optical microscopy

For microstructural observation, the specimens were obtained from as-received 304 AISI stainless steel sheet by using Struers make slow speed abrasive cutter, Secotom-10. These small specimens were mounted by Bakelite. The Bakelite mounted specimens were first hand polished using successively finer grades of silica carbide based abrasive papers followed by cloth polishing to make the specimen completely scratch free. Diamond paste of grit size 6 μm, 3 μm, and 1 μm used successively for cloth polishing. After metallographic polishing the specimen was etched with 1:1 HCL + HNO3 for 10 to 12s etching time and observed in an optical microscope, Leica DM 2500M.

3.4 Hardness measurement

Average hardness of received specimen as well as the deformed specimen after the room temperature tensile deformation was determined using 100g load and a dweel time of 15 second in a Vickers micro hardness tester (Matsuzawa). For the hardness test, sample is very finely polished on the emery paper up to grade of 2500. 15 to 20 indentation is used to calculate the average hardness.

3.5 Xrd Analysis

X-ray diffraction (XRD) analysis was used for the identification and quantification of retained austenite and the formed martensite in 304 austenitic stainless steel after room as well as cryogenic deformation. For the XRD test the sample were cut from the gauge length of the specimens which are deformed up to 30%true strain at different cryogenic temperature. These experiments were carried out in Rigaku Ultima-III using Cu target. Scanning was carried out with a 0.05 deg step size and allowing 2 seconds for each step over a 2θ range from 35 to 100 deg. The machine was operated at 30 mA and 40KV settings.

3.6 Tensile Test

The specimen geometry used for tensile tests in shown in figure 3.1. The specimens have been fabricated from as-received steel sheets for both rolling and transverse direction.

Tensile tests have been done in a computer controlled servohydraulic universal testing machine, Instron 8501 (Instron, High Wycombe, U.K.) of ± 100 KN load capacity at room temperature [~298K (25 ^{O} C)].

For the cryogenic test a cryogenic chamber is installed and liquid nitrogen is used to achieve the cryogenic temperature. The strain was fixed at 0.001 s^{-1} for every tensile test ranging from room temperature to -4^{o}C , -20 ^{o}C, -40 ^{o}C, -60 ^{o}C ,-80 ^{o}C , -100 ^{o}C. For fractography the specimen were deformed upto fracture at various above mension cryogenic temperature. For xrd analysis the specimens were deformed upto 30% true strain at various temperature.

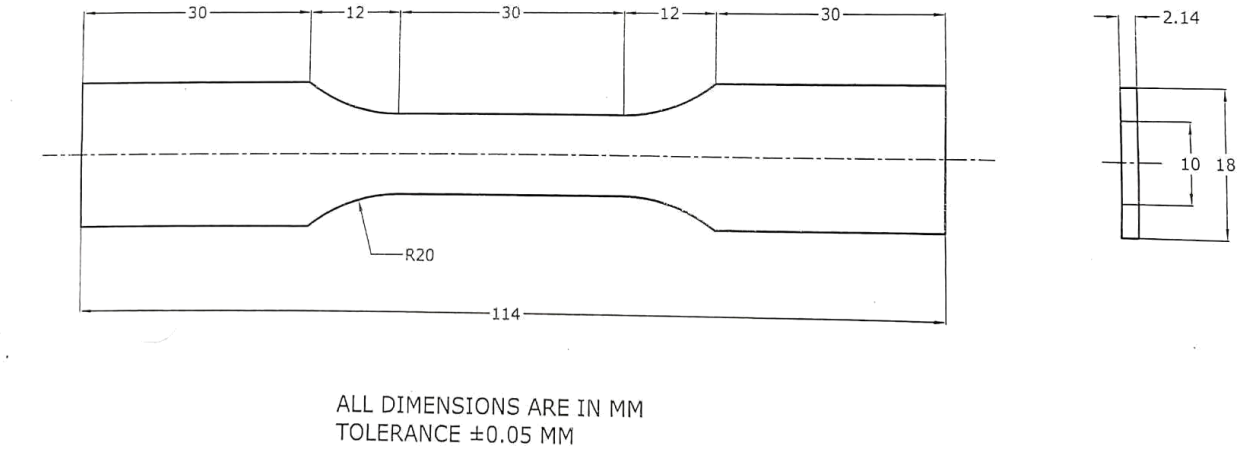

Fig. 3.1 Specimen geometry used for Tension tests

3.7 Fractography

Fracture surfaces of tensile specimens fractured at various cryogenic temperature ranging from room temperature at a constant strain rate were examined using Scanning Electron Microscope (FEI, QUANTA 450) to observe the nature of failure of the tensile specimens. The machine was operated at 20KV.

CHAPTER-4

RESULT AND DISCUSSION

4.1 Optical Micro-structure.

Comprehensive optical microscopy was performed on AISI 304 the received sample and also on the strained specimens, deformed at room temperature. Figure 4.1(a) and 4.1(b) shows the micrographs of received AISI 304 austenitic stainless steel as received condition and in deformed condition after deformation at a strain rate of 0.001 s^{-1} at room temperature.

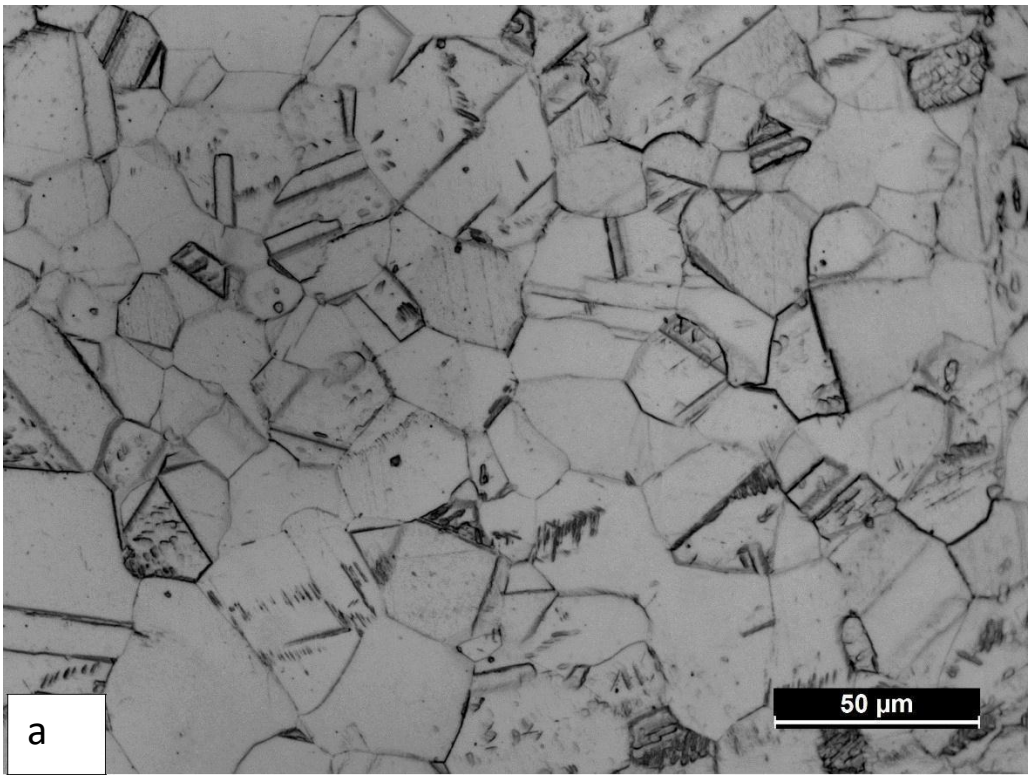

Figure -4.1(a)Micro-structure of 304 AISI stainless steel as received condition.

From the micro-graphs it can be seen that 304 austenitic stainless steel shows highest austenitic stability. In fig -4.1(a) we can see the majority of grain are austenitic (fcc).

The grain sizes were measured by mean linear intercept method . Table 4.1 shows the number of intercepts counted per millimetre, average intercept distance, and the calculated grain size number according to ASTM standard.

Table – 4.1 Grain size of the received 304 AISI stainless Steel.

Grade	Average Intercept count. n/l (mm-1)	Average intercept distance (μm)	ASTM grain size number G	Average Grain Size, d(in mm)
AISI 304	5025	633	21	0.0255266

4.2 Monotonic deformation behaviour of AISI 304 stainless steel

Engineering stress-strain curve fig 4.3(a) and true stress-strain curve fig-4.3(b) of the AISI 304 stainless steel tested at six cryogenic temperature ranging from -4 ^{o} C to -100 ^{o}C in addition to that also a room temperature tensile test performed. All the above mentioned test are done in a constant strain rate of 0.001 s^{-1}. The results are tabulated in table 4.2.

Table-4.2 Tensile properties of 304 AISI stainless Steel at various cryogenic temperature at constant strain rate of 0.001 s^{-1}.

Temperature	**UTS (MPa)**	**0.2% offset Yield stress (MPa)**	**Elastic Modulas(GPa)**	**% Total Elongation**	**% Uniform ELongation**
Room Temperature	667.016	338	186	72.38	59.75
-4 ^{o} C	789.49	360	169	76.45	68.52
-20 ^{o} C	848.89	369	162	78.04	61.53
-40 ^{o} C	948.658	394	155	59.78	49.69
-60^{o} C	1062.76	424	149	55.09	46.26
-80 ^{o} C	1165.54	449	142	51.20	41.42
-100 ^{o} C	1229.887	474	138	49.22	40.20

From the table 4.2 it can be seen that as temperature decreased %elongation increased which can be due to the TRIP effect and then it decreased due to the formation of α' martensite which result in reduce ductility.

From the engineering stress-strain stress and from the true stress-true strain graph it can be seen that both the yield stress and the ultimate tensile stress increases with decreasing temperature. This can be seen in fig 4.4 (a) and fig-4.4(b).

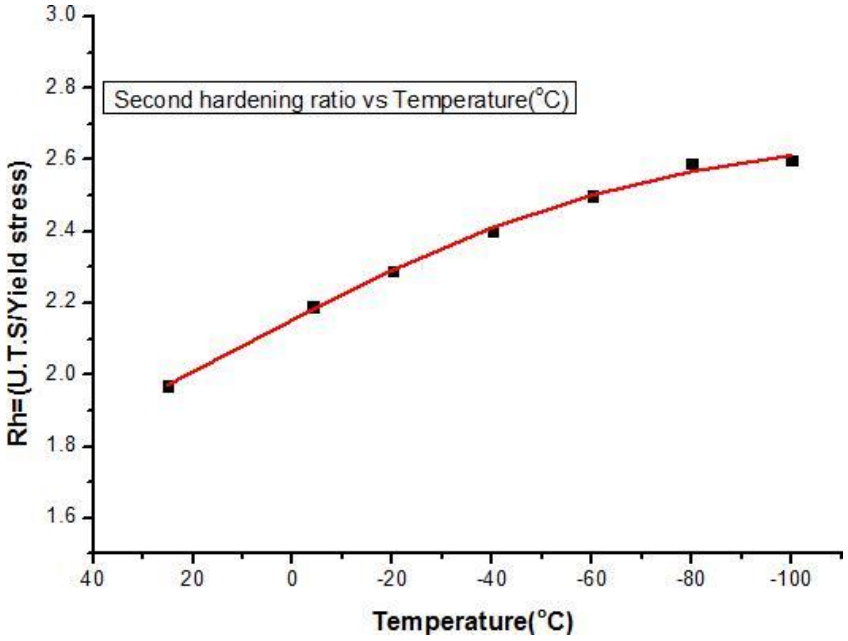

Figure-4.2 Second hardening ratio at various cryogenic temperature.

As seen in the figure4.2 the second hardening ratio Rh=UTS/Y.S increases almost linearly with decreasing temperature. This is directly related to the formation of α'-martensite.

As seen in the figure 4.4(b) the UTS increases linearly with decreasing temperature. From figure 4.4(a) the yield stress also increase slowly with decreasing temperature up to -20 ^{o}C . After that in increases linearly from -20 to -100^{o}C. This is because as the temperature decreases the strain-hardening increases due to the formation of α' martensite and this formation becomes predominant below -20 ^{o}C.

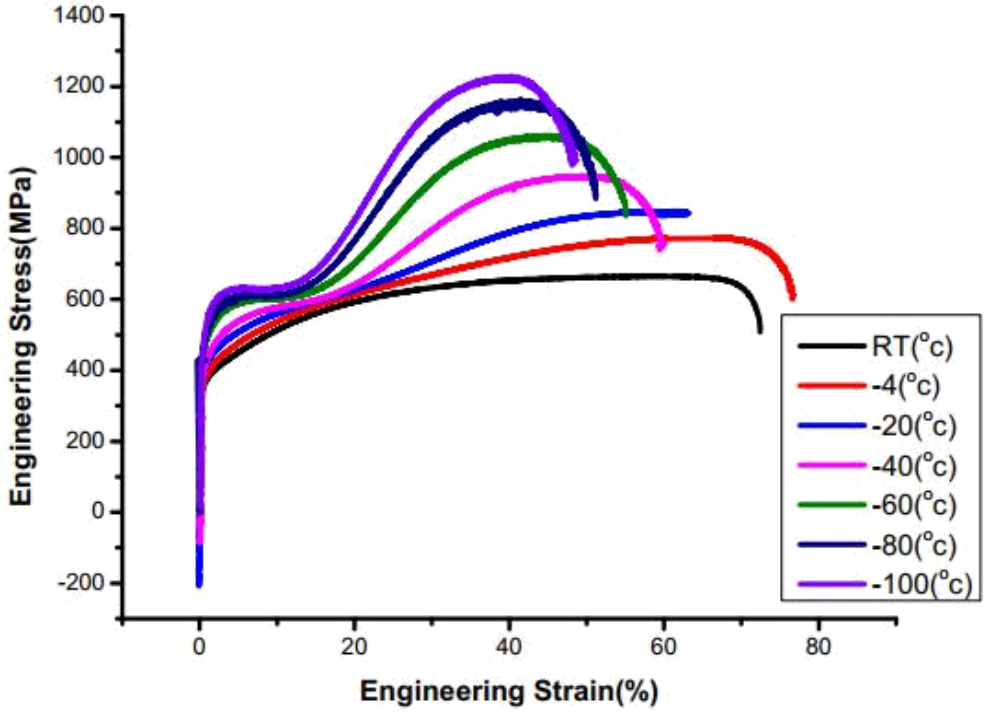

Fig 4.3- Engineering stress strain curve of AISI 304 Stainless steel at various cryogenic Temperature at a constant stain rate of 0.001 s^{-1}.

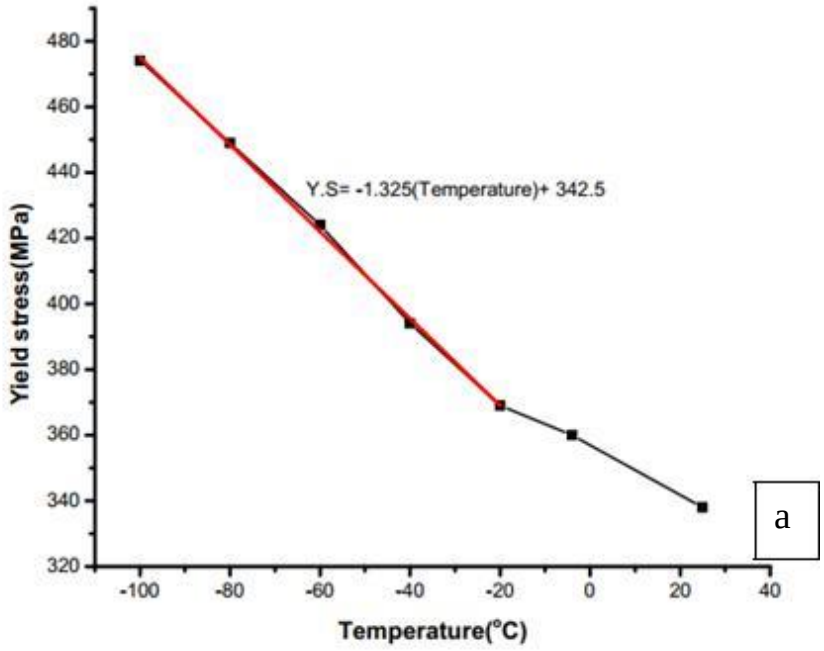

Figure-4.4(a) variation of yield stress(MPa) with temperature(oC) of AISI 304 stainless steel .

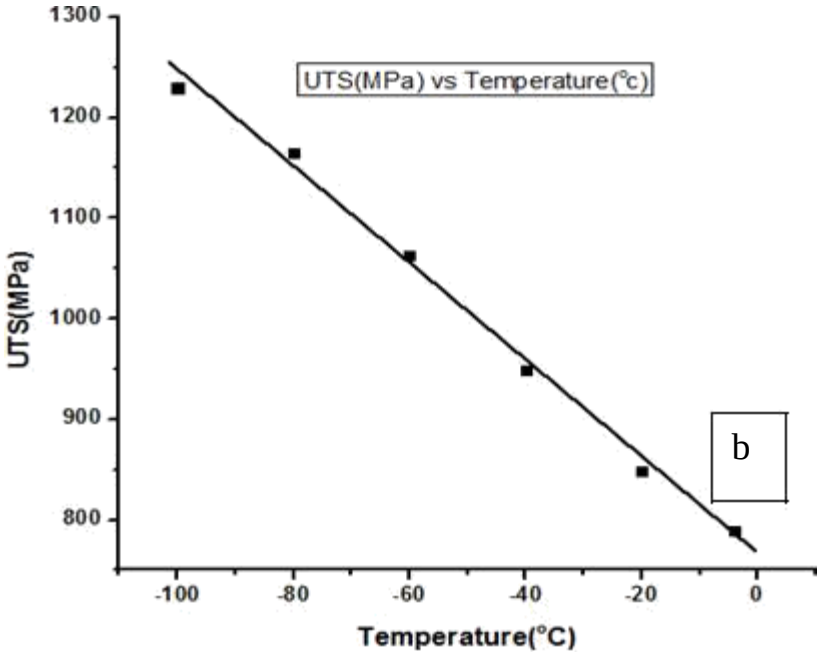

Fig- 4.4(b)- variation of UTS(MPa) with temperature(oC) of AISI 304 stainless steel.

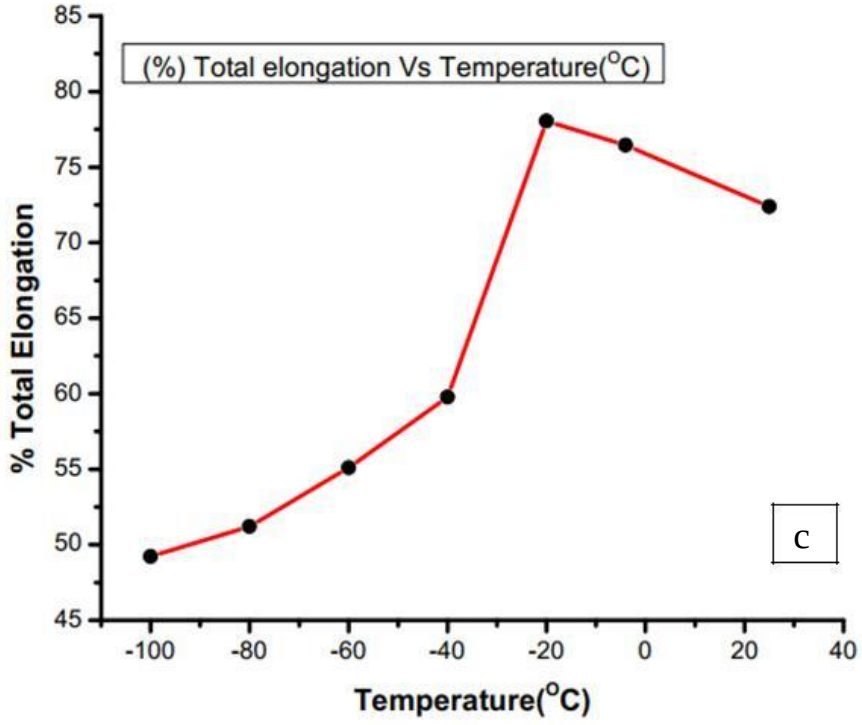

Figure-4.4(c) variation of Total elongation with temperature(oC) of AISI 304.

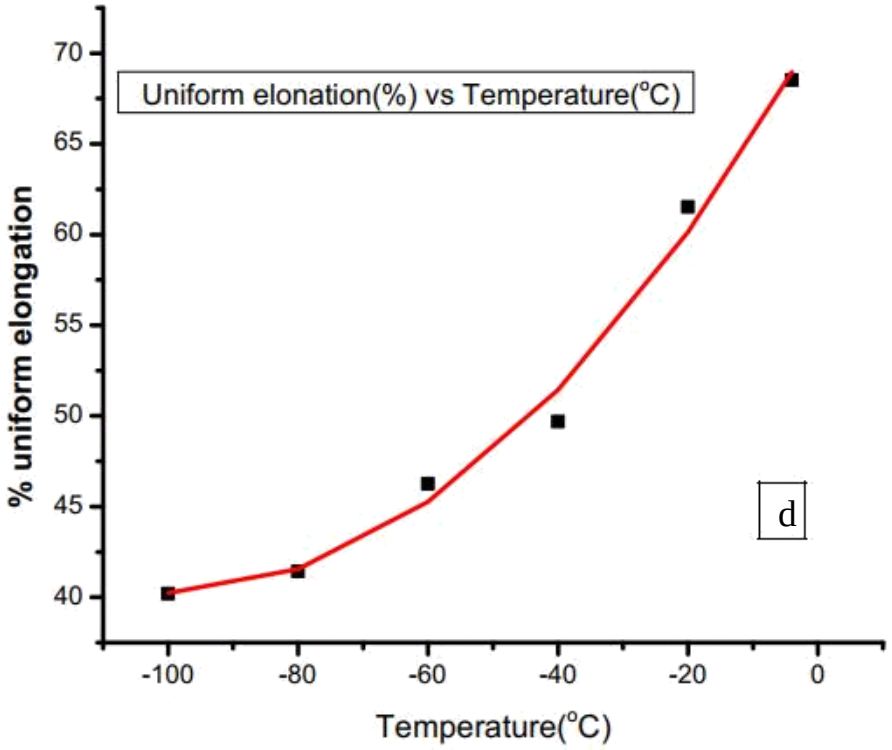

Figure-4.4(d) variation of Uniform elongation with temperature(^{o}C) of AISI 304 stainless steel.

From the graph 4.4(c) it can be seen that the total elongation first increases upto point -20 ^{o}C , this is due to the transformation induced plasticity effect initially. At -20^{o}C the α'-martensite formation becomes predominant that's why the total elongations falls rapidly after that as the strain hardening increases the elongation further decreases and also the ductility.

From fig-4.4(d) it can be seen that the uniform elongation decreases gradually as the temperature falls causing the ductility to decreases which is aslo due to the formation of α'-martensite at cryogenic temperature range.

4.3 Work hardening behaviours

4.3.1 Hollomon analysis

Woong Sup Park, Seong Won Yoo, Myung Hyun Kim, Jae Myung Lee [193] has shown in Fig.2.8, at below 223 K temperatures, the austenitic stainless steel shows two-stage sigmoidal deformation which is non-linear hardening behavior that is dependent on temperature. This phenomenon can also be seen in figure 4.5(a) ,4.5(b),

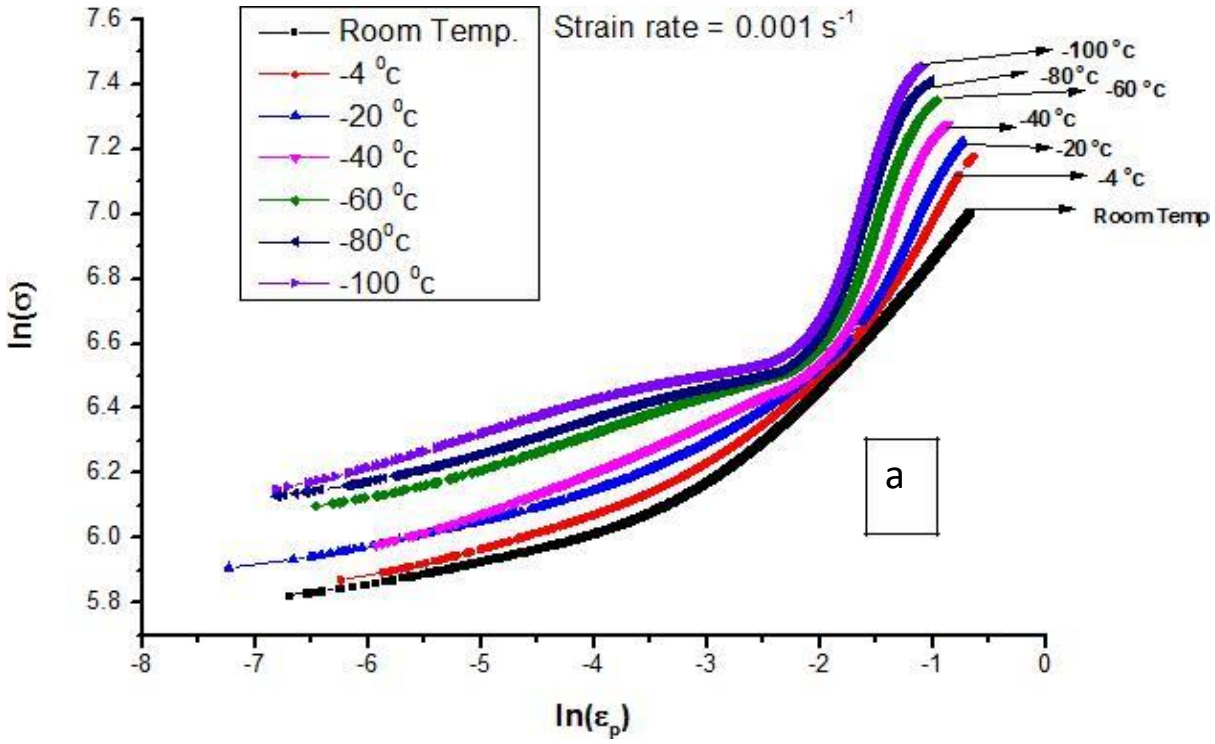

Figure -4.5(a) hollomon curve of AISI 304 stainless steel at various temperature ranging from room to cryogenic temperature at constant strain rate of 0.001s^{-1}.

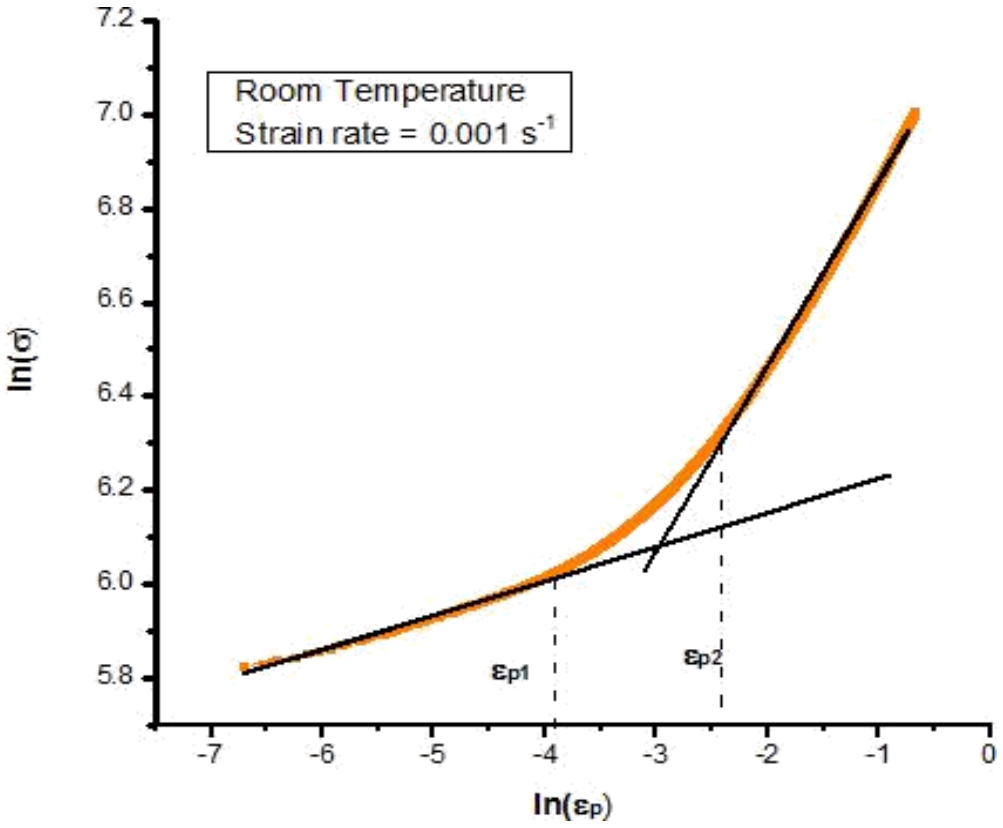

Figure -4.5 (b) The two stage strain hardening of 304 AIAI ss at room temperature deformation.

From the figure 4.5(a), it can be observed that the as the temperature increases there is rapid increase in the strain hardening rate as the temperature decrease compared to the room temperature.

Table 4.3 shows the he strain hardening exponents (n), strength co-efficient (K) for stage I and stage II and plastic strain at which transition occurs, have been calculated from the figure (4.5) by using the hollomon equation.

Table -4.3 Results of Hollomon analysis of 304 ss at various cryogenic temperature at constant strain rate of 0.001 s^{-1}.

TEMPERATURE(^{O}C)	Hardening exponent stage-1(n1)	Hardening exponent stage-2(n2)	Hardening co-effient(K1)	Hardening co-ffient(K2)	End of stage -1 hardening ε_{p1}(%)	Starts of stage-2 hardening ε_{p2}(%)
Room Temp.	0.0724	0.39	539	1408	1.9	6.8
-4	0.1128	0.503	678	1754	3.1	11.15
-20	0.0807	0.637	632	2230	1.8	15.28
-40	0.1465	0.814	888	3121	10.9	6.95
-60	0.1107	0.902	862	4188	9.0	7.41
-80	0.1067	0.99	888	5218	4.9	9.96
-100	0.1024	1.076	925	6438	3.1	11.17

It has been found that strain hardening exponents of stage I is very low as compared to stage II, irrespective of the temperature. The stage-2 work hardening exponent is much higher than stage-1. It was observed that the work hardening parameter (n_1) in stage I deformation is higher in case of cryogenic temperature compared to room temperature. Also in cryogenic temperature the strain hardening exponent is almost similar in stage I. At room temperature, it might be expected that the slip occurs on only one slip system and the dislocations are able to move over relatively large distance without encountering the barriers, in stage I. In case of cryogenic temperature, the stage -1 work-hardening exponent is high may be due to fact of formation of α'-martensite.

In stage II strain hardening increases rapidly as the temperature decrease more and this is due to the formation of α'-martensite.

4.3.2 Ludwik Analysis

The strain hardening behavior of the present material has been analyzed according to the relationship purposed by Ludwik[62]. Figure 4.6 shows the variation of $\ln(\sigma - \sigma_0)$ as a function of $\ln(\varepsilon_p)$ at different cryogenic temperature for 304 AISI stainless steel.

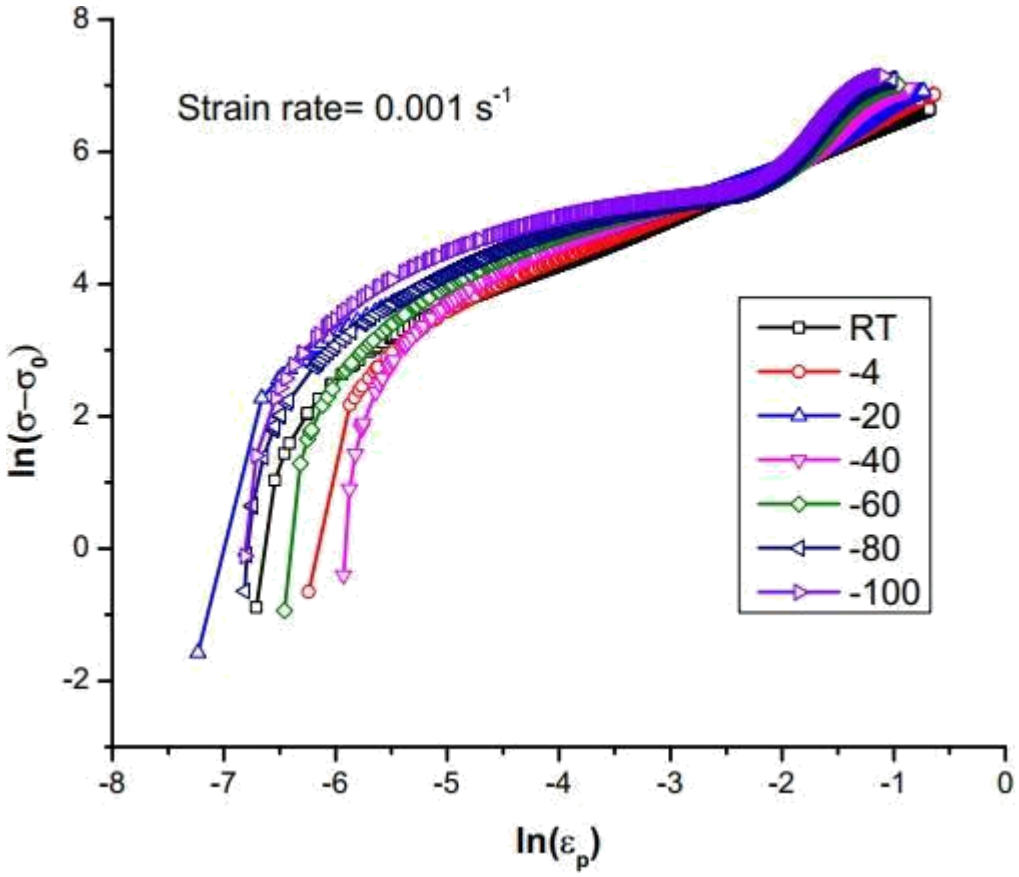

Figure- 4.6 Variation of ln(σ - σ0) as a function of ln(εp) at different cryogenic temperature at constant strain rate of 0.001 s^{-1} for 304 AISI ASS.

Figure 4.6, 4.6(a) revealed that the plot of ln(σ - σ0) vs. ln(εp) yield a straight line with regression coefficient (R^2) value greater than 0.99 for room temperature deformation.

But in case of in case of cryogenic deformation plot of ln(σ - σ0) vs. ln(εp) fig 4.6(b) does not follow a straight line . In case of cryogenic deformation we can observe two region the first one is parabolic and then there is a certain decrease and the again a parabolic increase. This can be illustrated from the fact that may be in first stage the TRIP effect is predominate and after that the α' –martensite formation becomes predominate.

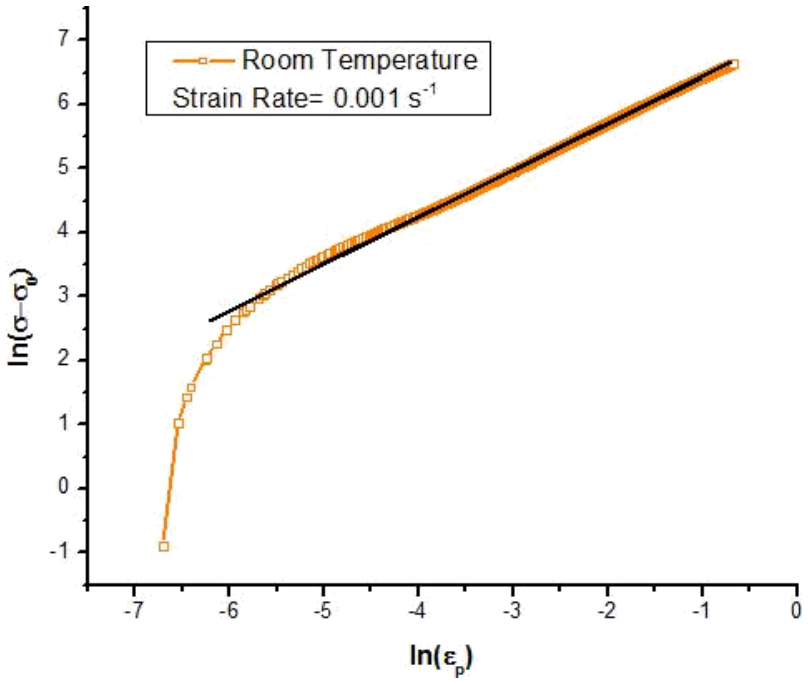

Figure -4.6(a) Variation of ln(σ - σ0) as a function of ln(εp) at room temperature at constant strain rate of 0.001 s^{-1} for 304 AISI ASS

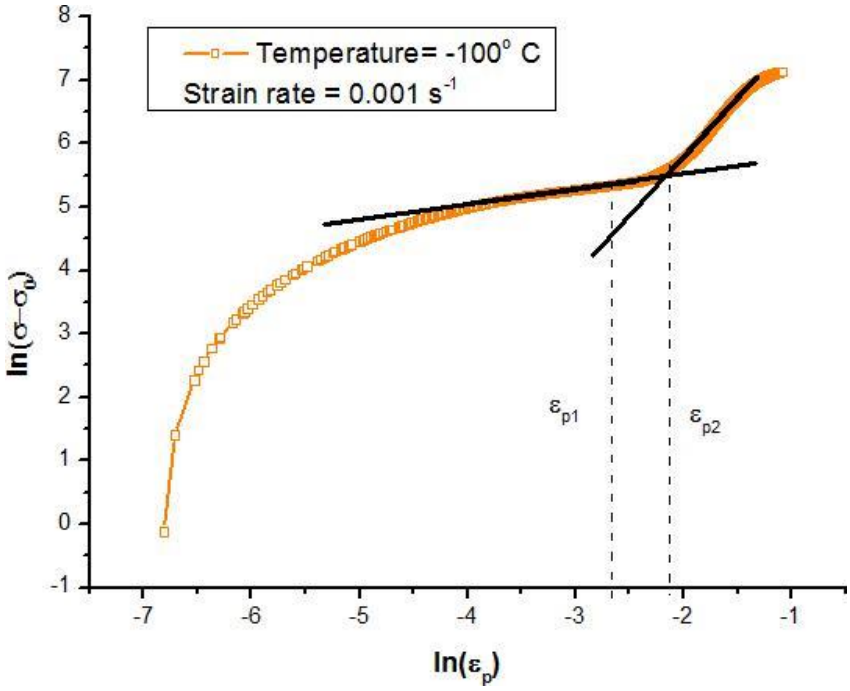

Figure -4.6(b) Variation of ln(σ - σ0) as a function of ln(εp) at -100^{o} C temperature at constant strain rate of 0.001 s^{-1} for 304 AISI ASS

The Ḱ, ń values are calculated from the figure 4.6, 4.6(a), 4.6(b) by using the ludwik equation and represented in table 4.4.

TEMPERATURE (^{O} C)	STAGE-1			STAGE-2			ε_{p1}-ε_{p2}(%)
	Hardening exponent ($n_{1)}$	Hardening co-efficient (k1)	End of satge-1 hardening ε_{p1}(%)	Hardening exponent (n2)	Hardening co-efficient (k2)	Starts of satge-2 hardening ε_{p2}(%)	
Room Temperature.	0.73	1299					
-4	0.69	1260	18.1	0.91	1790		
-20	0.58	1004	17.18	0.97	2109	19.9	2.7
-40	0.51	818	12.17	1.36	4044	16.6	4.2
-60	0.38	552	9.0	1.66	7259	15.5	6.3
-80	0.29	432	7.7	1.78	10198	13.3	5.6
-100	0.23	391	6.96	1.86	13359	11.8	4.9

From table-4.4 it is observed that that there is only stage one stage hardening for room temperature in ludwik analysis.

The second stage hardening for ludwik analysis start at -4 ^{o} c. In first stage the strain hardening exponent decrease with decreasing temperature. In the second stage the strain hardening exponent increases with decreasing temperature.

The transition zone from stage -1 to stage -2 first increases with decreasing temperature up to -60^{o} c . Then decreases with decreases with decreasing temperature. This also conclude the fact that as temperature decrease the α’ martensite formation becomes severe and cause the TRIP effect.

4.3.3 Kocks-Mecking (K-M) Analysis

Kocks and Mecking [61] pointed out that the different work hardening stages can be better understood, when work hardening rate (θ) is multiplied with true flow stress(σ) and plotted against flow stress. Work hardening rate (θ) is represented as:$\theta = d\sigma/d\varepsilon_p$. Figure 4.7 shows the variation of work hardening rate as a function of flow stress of 304 SS at different cryogenic temperature ranging from room temperature.

From the figure 4.7 it is observed that the work hardening rate initially decreases rapidly followed by gradual decrease with the true flow stress and the reaches a minimum and increase and again decrease. As temperature decreases it is seen that the first stage decrease become more rapid and after strain hardening rate is also increase with decrease temperature.

From figure 4.7 and 4.8 it can be said that the non-linear behavior is because of non-linear the TRIP effect. The peaks in the graph is related to the formation of α' martensite. Because of the athermal effect below Ms according to Koistinen and Marburger equation [142];martensite formation is more causing the sharp increase in the second stage of the strain hardening rate.

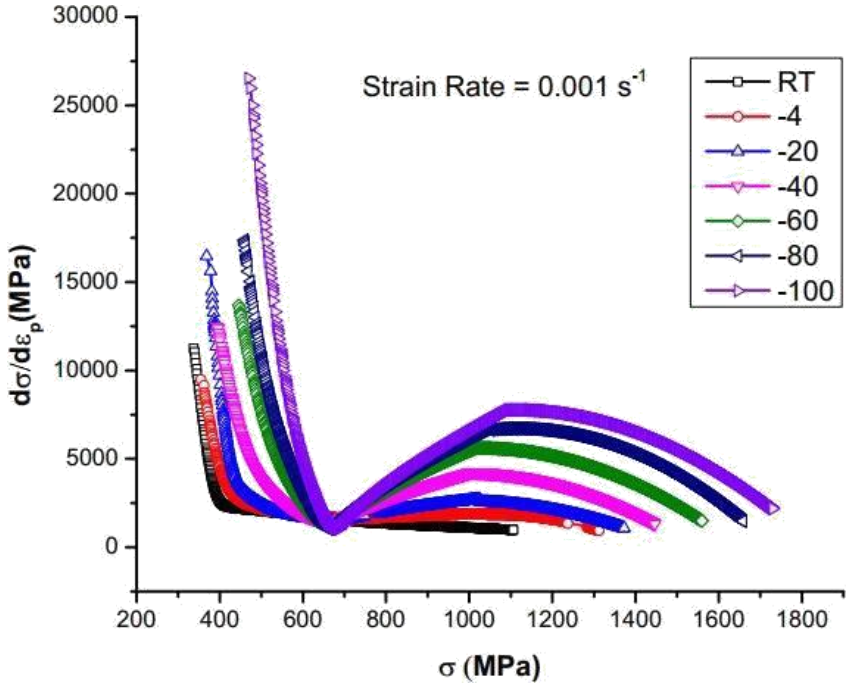

Figure 4.7: Variation of work hardening rate (θ) with true flow stress (σ) at different cryogenic temperature ranging from room temperature at constant strain rate.

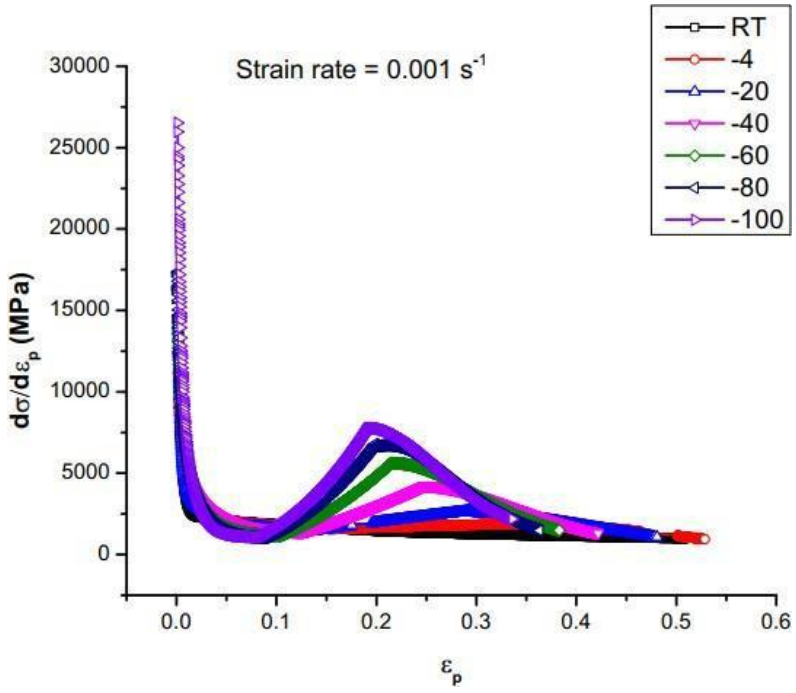

Figure 4.8- : Variation of work hardening rate (θ) with true plastic strain(ε_p) at different cryogenic temperature ranging from room temperature at constant strain rate.

When the work hardening rate (θ) is multiplied by flow stress three distinct stages of work hardening behaviour have been observed, as seen from figure 4.9.

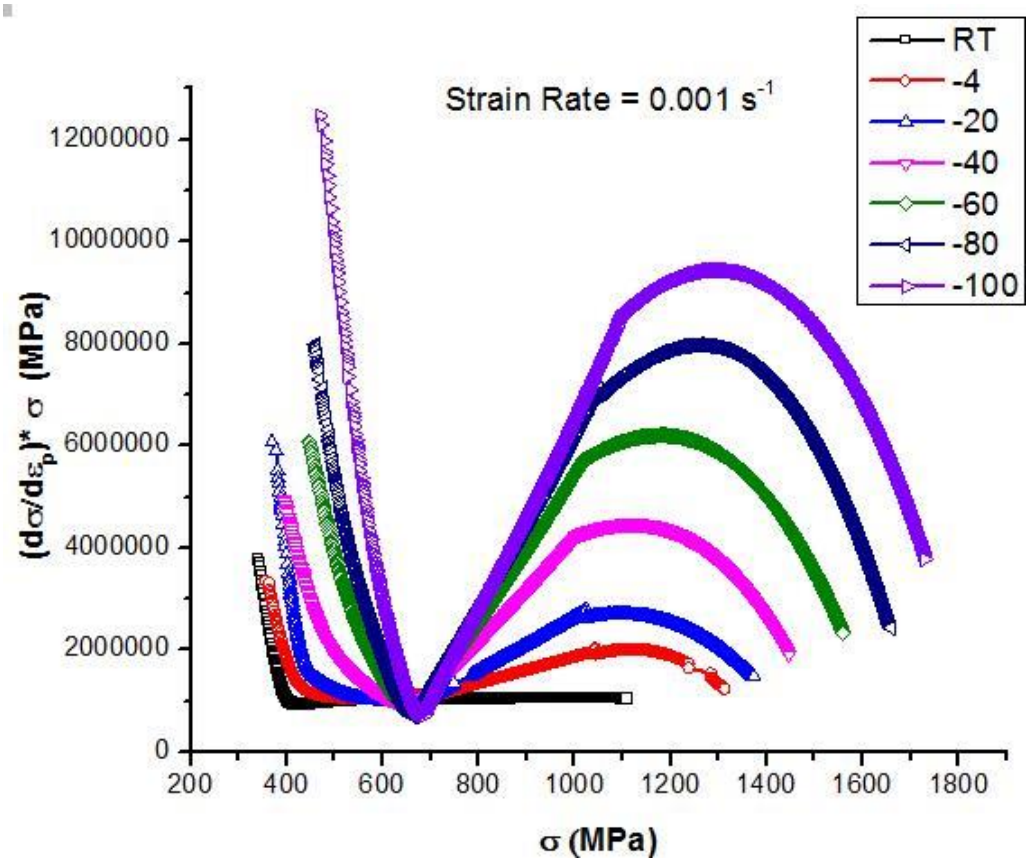

Figure 4.9: Variation of (θ×σ) with true flow stress (σ) at different cryogenic temperature ranging from room temperature at constant strain rate.

In the first stage, (θ × σ) value decreases rapidly with increase in the flow stress. This is the transition stage for material. Then it gradually increases and reaches maximum value (stage II) followed by gradual decrease i.e. stage III.

In stage II athermal hardening is the dominant mechanism. It is expected that, in stage II, the formation of α' martensite promoted the work hardening rate. Stage III is characterized by the decrease in (θ × σ) value with increase in flow stress. This may be due to dynamic recovery at from room to low temperature.

4.4 Fractography

The SEM micgraphs of fractured specimen at constant strain rate of 0.001 s^{-1} ranging from room temperature to -100 ^{O}C are shown from figure-4.10 to figure -4.16.

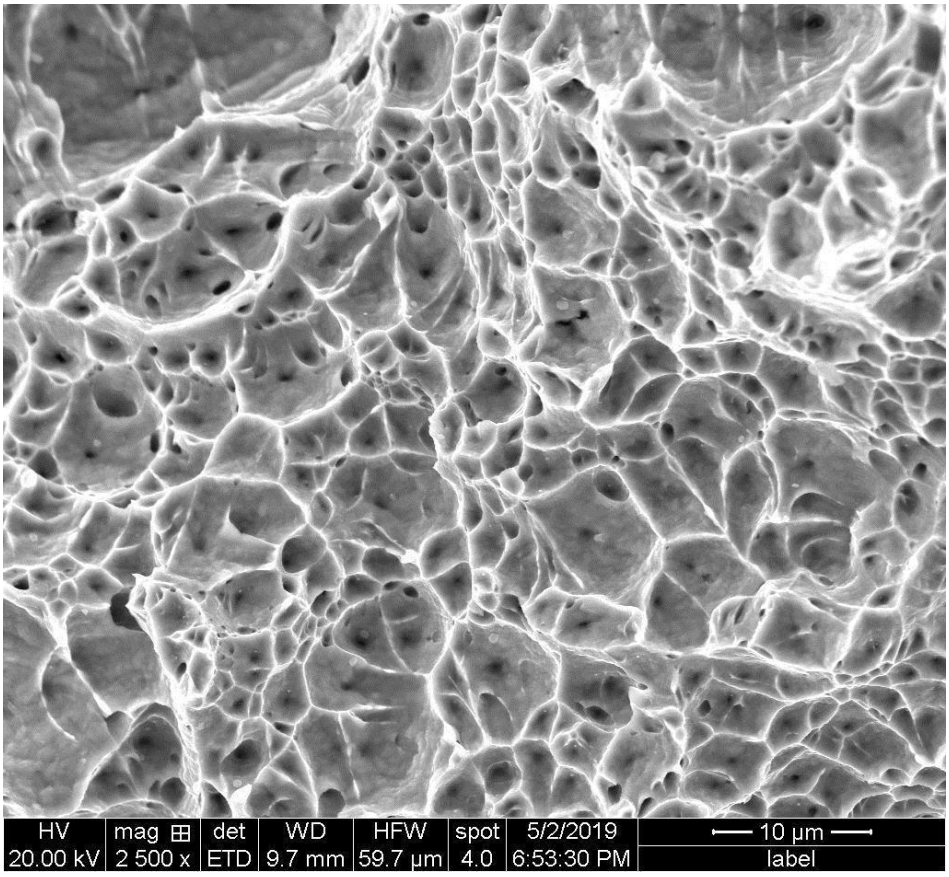

Figure-4.10 SEM image at room temperature of fracture surface at constant strain rate of 0.001 s^{-1} .

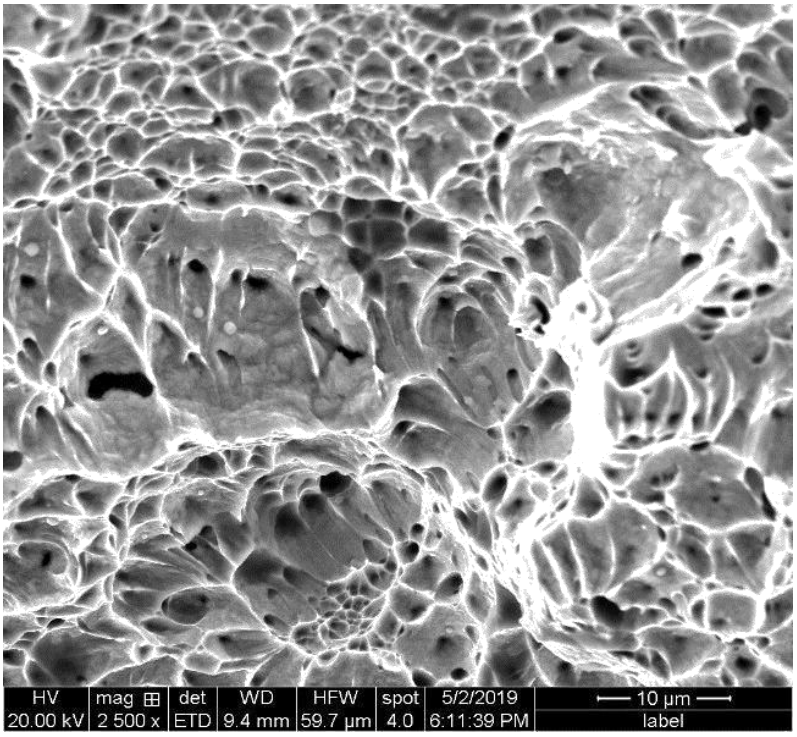

Figure-4.11 SEM image at -4 ^{o}c temperature of fracture surface at constant strain rate of 0.001 s-1 .

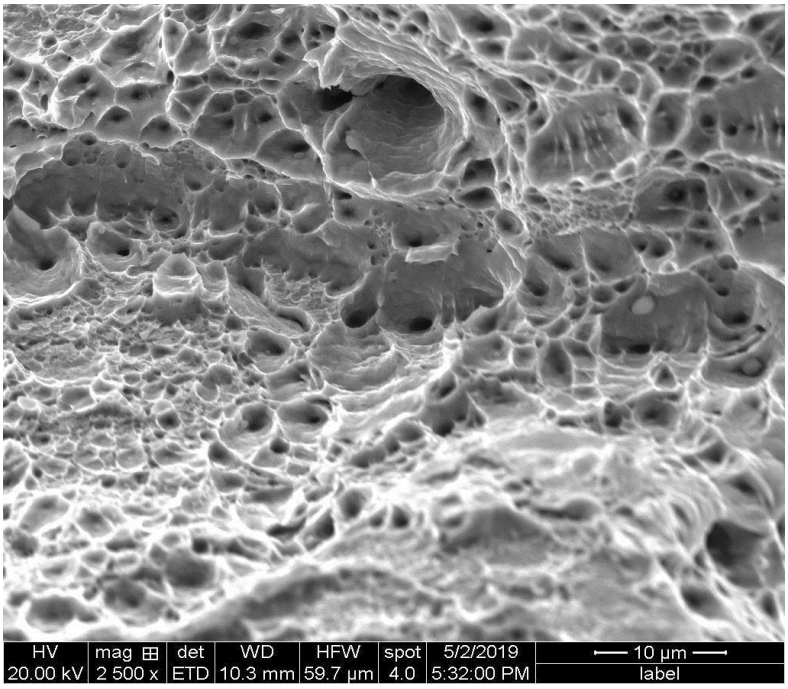

Figure-4.12 SEM image at -20 ^{o}c temperature of fracture surface at constant strain rate of 0.001 s-1 .

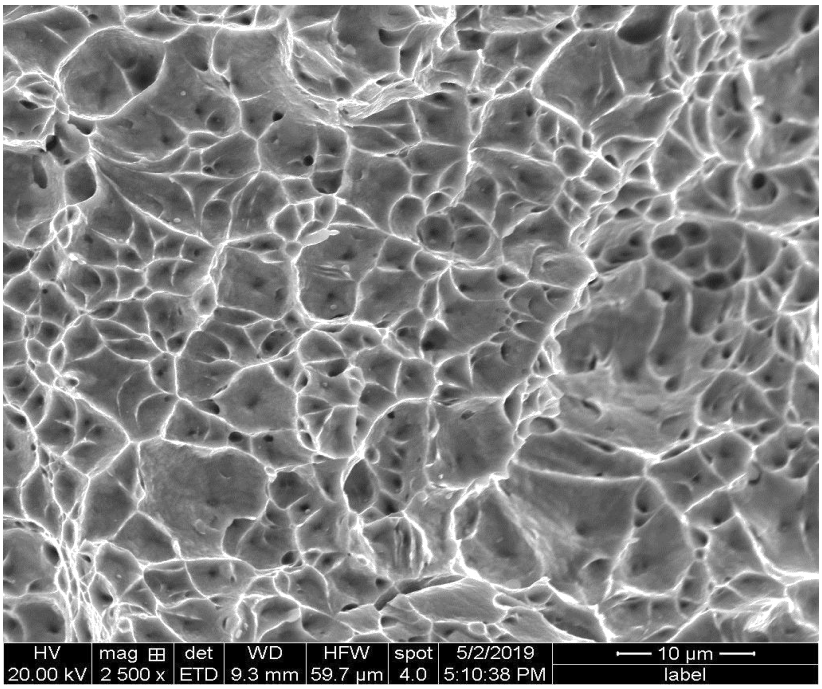

Figure-4.13 SEM image at -40 ^{o}c temperature of fracture surface at constant strain rate of 0.001 s-1 .

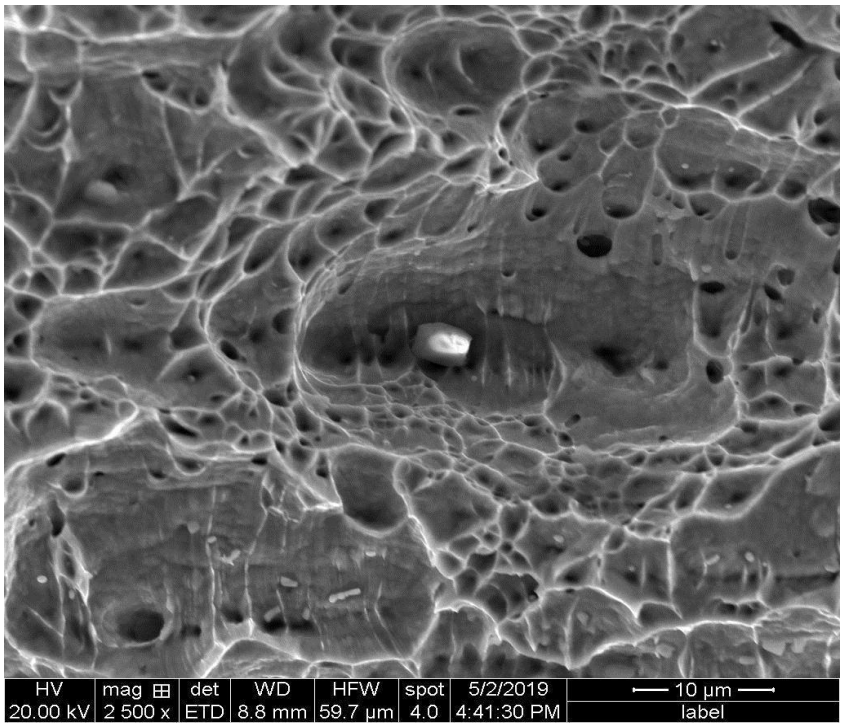

Figure-4.14 SEM image at -60 ^{o}c temperature of fracture surface at constant strain rate of 0.001 s-1 .

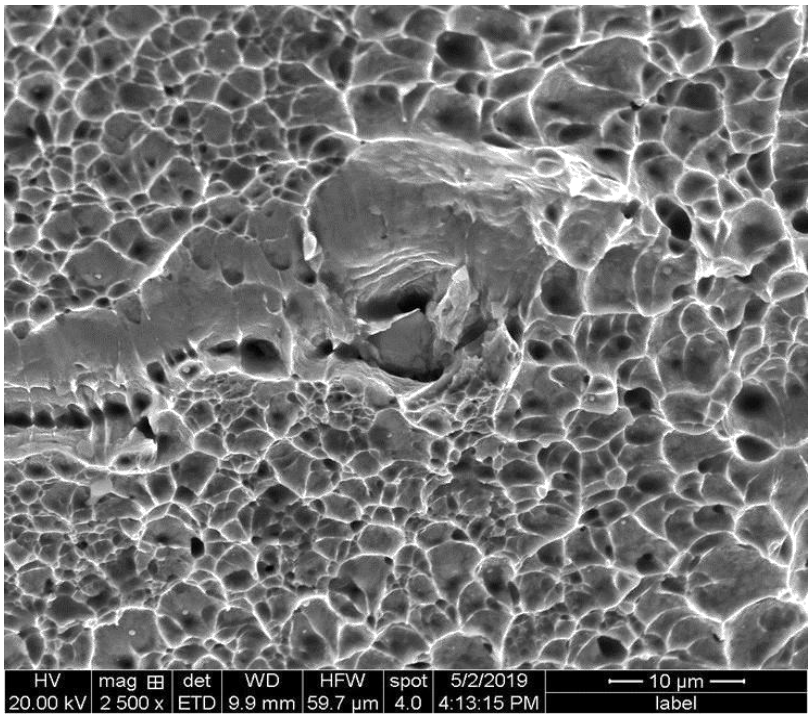

Figure-4.15 SEM image at -80 ^{o}c temperature of fracture surface at constant strain rate of 0.001 s-1 .

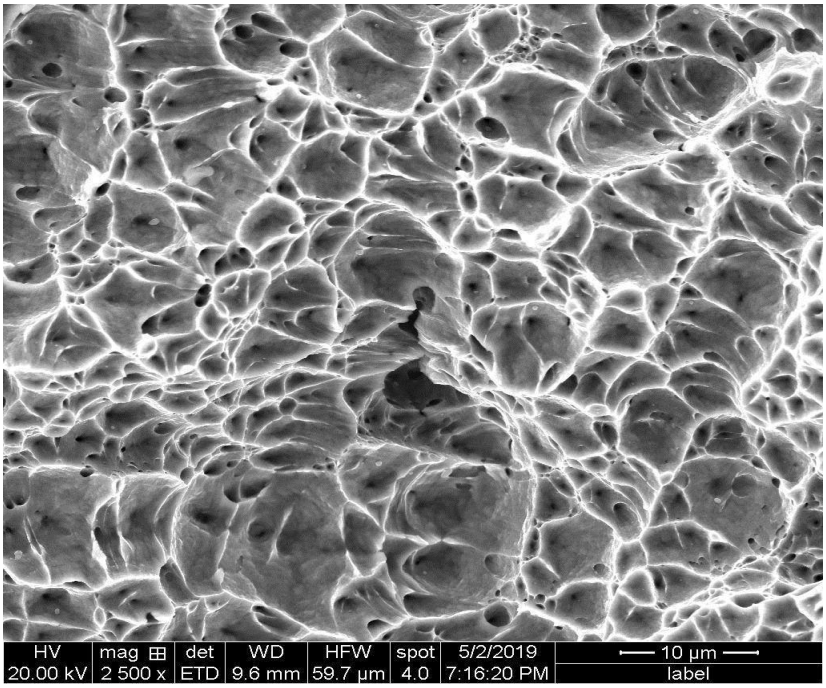

Figure-4.16 SEM image at -100 ^{o}c temperature of fracture surface at constant strain rate of 0.001 s-1 .

From the above SEM image from fig 4.10 to 4.16 it can be seen that the , all test specimens have shown local necking and the cup and cone form of ductility fracture. At the fracture section, fibrous zones and shear lips, which are typical forms of ductility fracture, were found. In general, ductile fracture occurs following three successive events, e.g. void nucleation, void growth and their coalescence. Figure 4.10-4.15 shows that the fracture surface consists of more number of voids and inclusions. This inclusion generates the crack initiation and void growth. Similarly all fracture surfaces in figure 4.10-4.15represent the void growth and nucleation and inclusion. It is also seen as the temperature decrease the flat region fig-4.14 to fig-4.16 surrounded by ductile dimple region increase this is may be due to ductile-brittle transition at very low temperature.

4.5 XRD analysis

The XRD graphs of the tensile specimen deform upto 30% true strain are shown below.

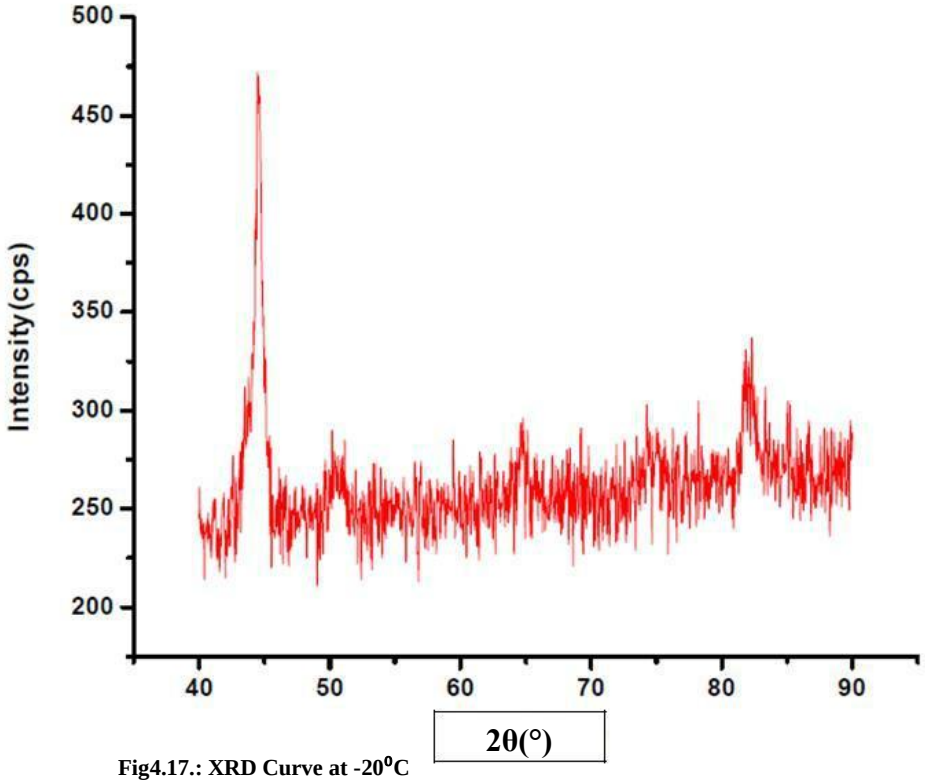

Fig4.17.: XRD Curve at -20^{0}C

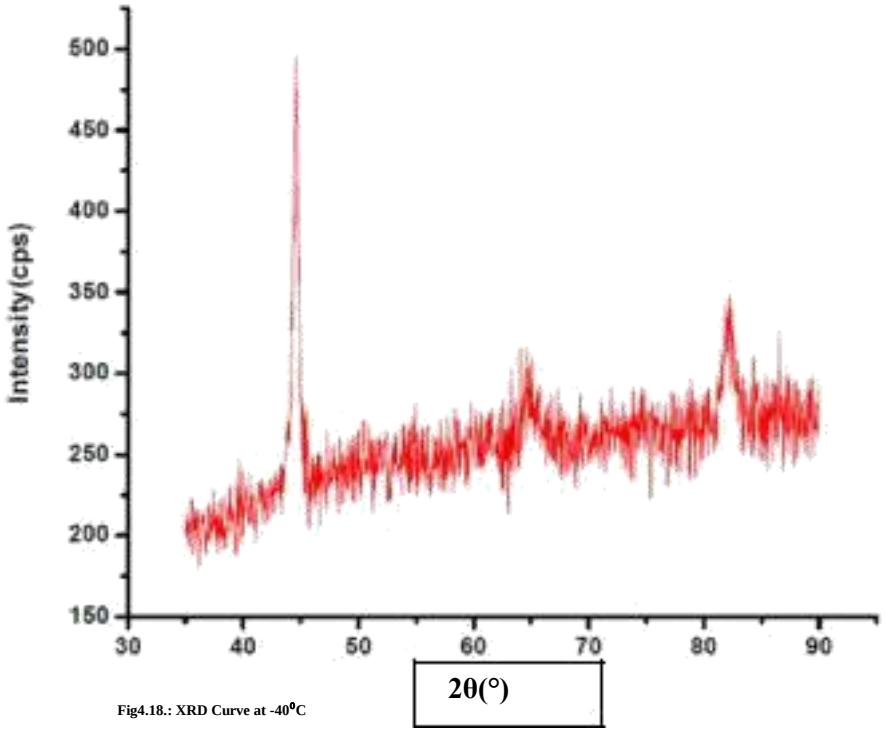

Fig4.18.: XRD Curve at -40^{o}C

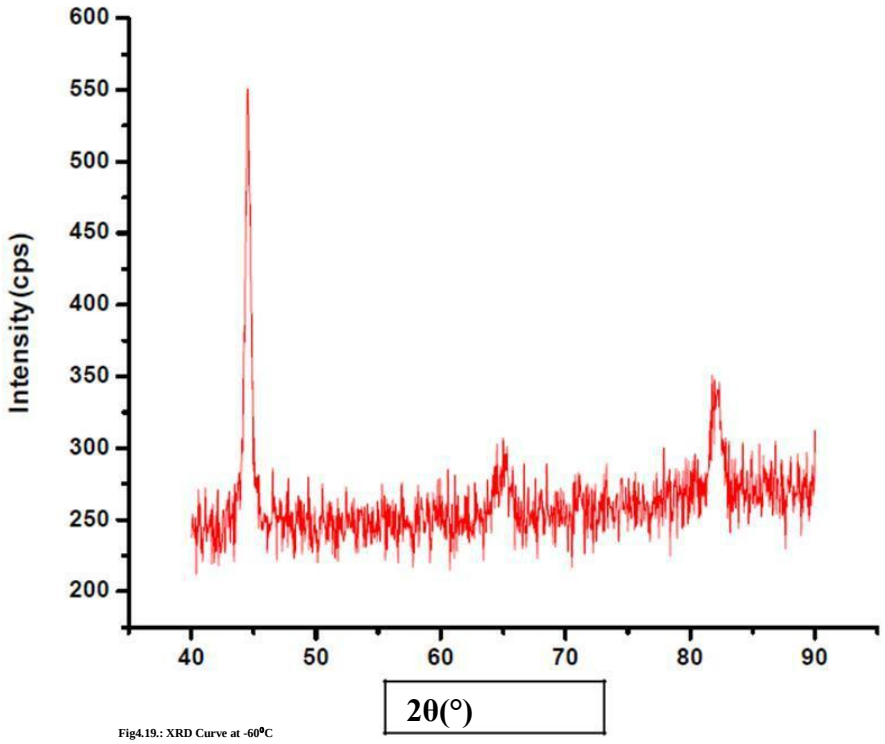

Fig4.19.: XRD Curve at -60^{o}C

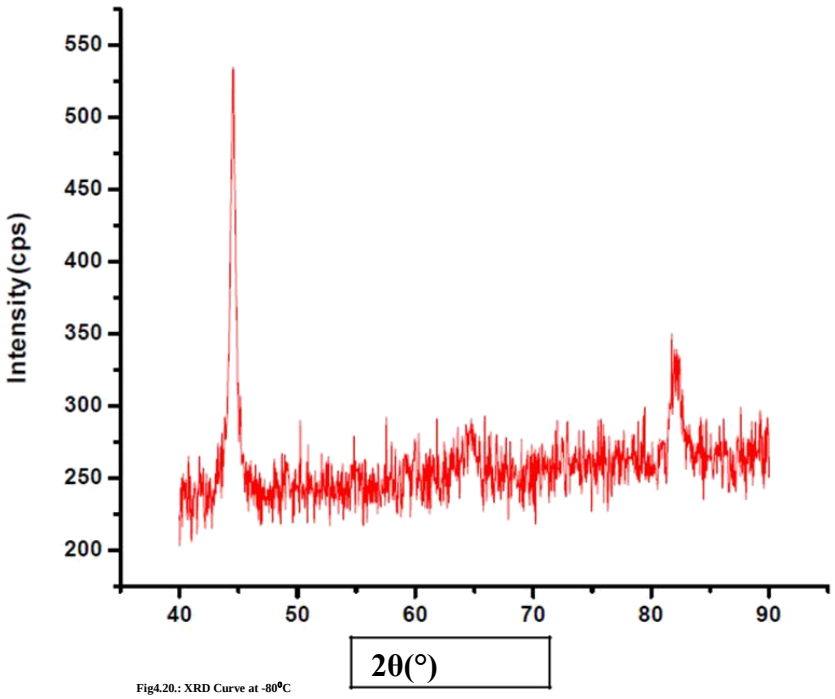

Fig4.20.: XRD Curve at -80^{o}C

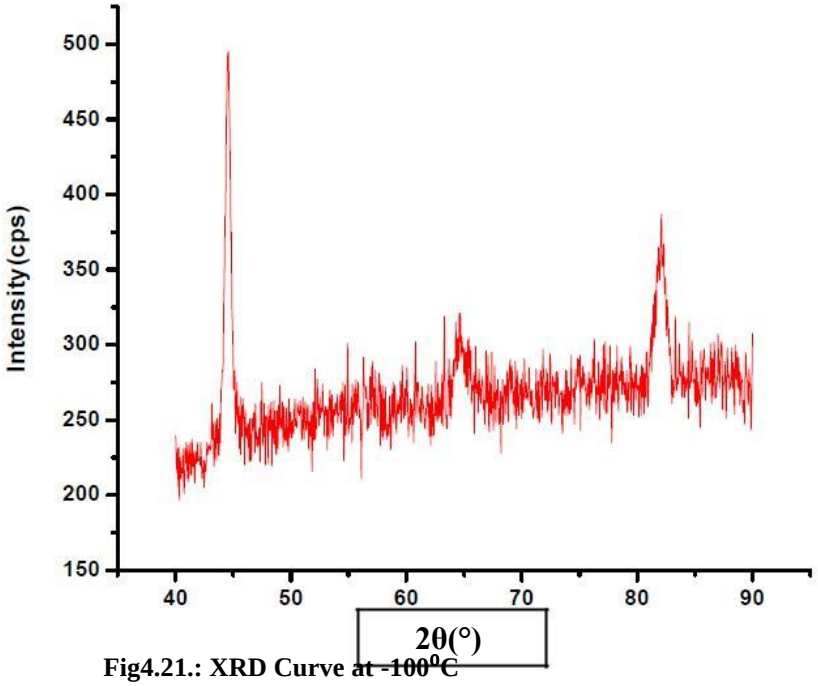

Fig4.21.: XRD Curve at -100^{o}C

From the xrd micrographs it can be seen that there is intensity peaks for austenite as well as Martensite at different cryogenic temperature.

The parameters table are listed below in table 4.5.

Table 4.5-The parameters for XRD analysis.

PARAMETERS	-20(^{o}C)	-40(^{o}C)	-60(^{o}C)	-80(^{o}C)	-100(^{o}C)
	825	1367	1387	1395	1891
	3586	4153	4023	3820	4059
	12	12	12	12	12
	8	8	8	8	8
	24.72	24.72	24.72	24.72	24.72
	23.78	23.78	23.78	23.78	23.78
	1.1748	1.1748	1.1748	1.1748	1.1748
	2.035	2.035	2.035	2.035	2.035
	98.33291877	98.35084667	98.39207687	98.43330099	98.37056617
	209.0435991	206.1190441	206.0649008	206.0943057	206.115953
	0.5	0.5	0.5	0.5	0.5
	0.5	0.5	0.5	0.5	0.5
	1.0192349	1.0197243	1.0208721	1.0220507	1.0202694
	1.62636937	1.37049903	1.36681384	1.63881158	1.37028784

From the table after calculating the volume percentage of α' martensite it is listed below.

Table-4.6 Valome fraction of martensite and austenite at different cryogenic temperature.

PARAM-ETERS	-20(^{o}C)	-40(^{o}C)	-60(^{o}C)	-80(^{o}C)	-100(^{o}C)
	825	1367	1387	1395	1891
	3586	4153	4023	3820	4059
	0.728941	0.75900	0.76645	0.80623	0.81660
	0.271058	0.24099	0.23354	0.19376	0.18339

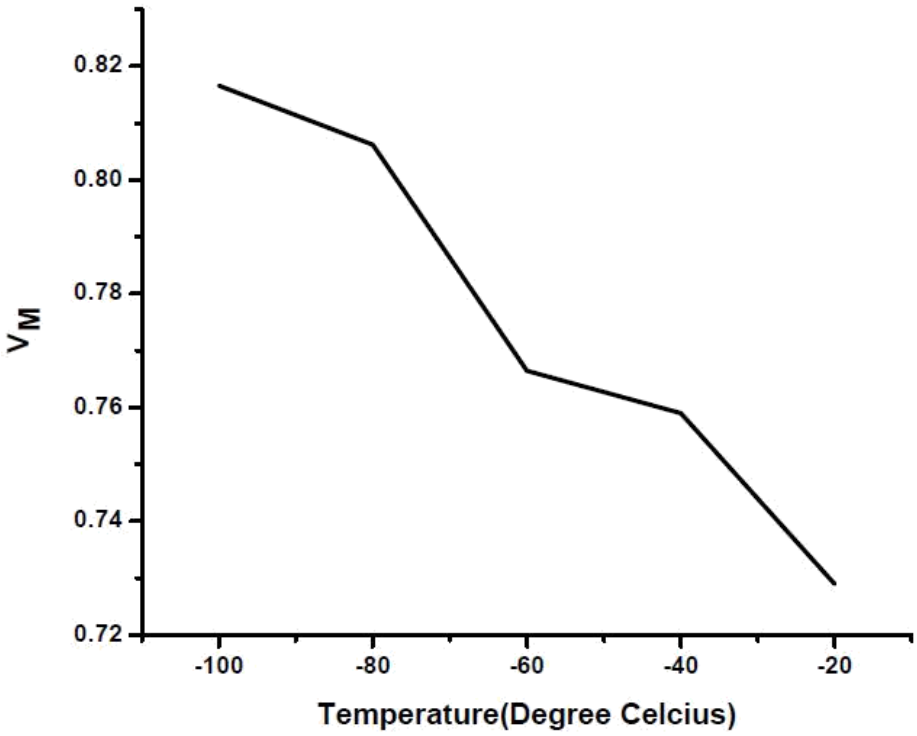

Fig4.22.: Volume fraction of martensite vs Temperature

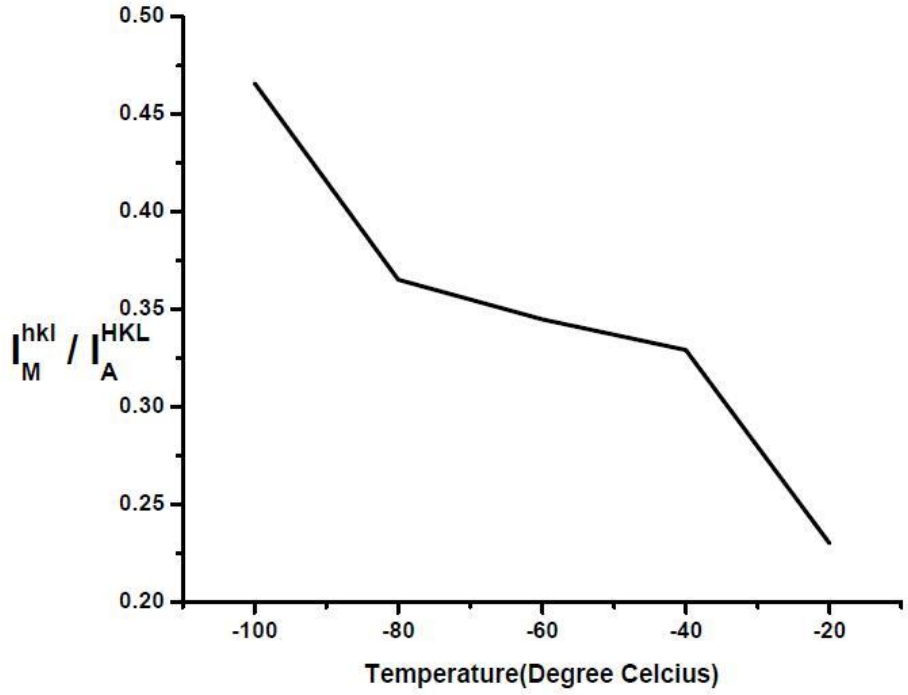

Fig.: 4.23(Integrated intensities of martensite) / (Integrated intensities of austenite) vs Temperature

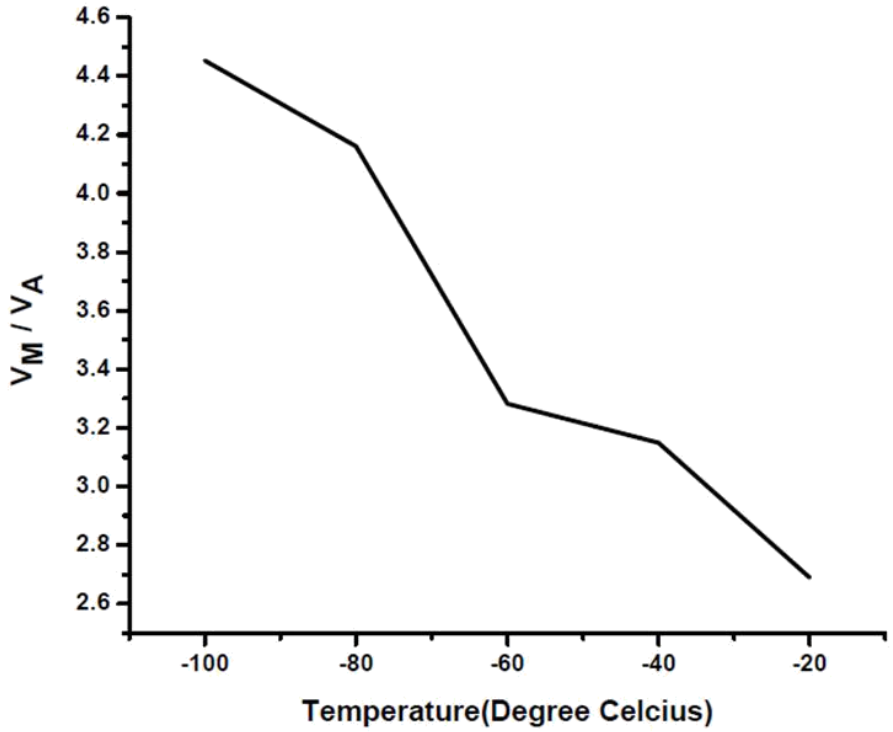

Fig.4.24: (Volume Fraction of Martensite) / (Volume Fraction of Austenite) vs Temperature

From the table 4.6 it is clearly visible that the as the temperature decreasing the volume fraction of martensite increasing.

Graph 4.22, 4.23 and 4.24 confirms the fact that as the temperature decreasing the volume fraction of martensite increases.

CONCLUSION

1. UTS increases linearly with decreasing temperature. The yield stress also increase with decreasing temperature. This is because as the temperature decreases the strain-hardening increases due to the formation of α' martensite martensite

2. the total % elongation and uniform elongation both initially sharply increases with decreasing temperature this may be due to the transformation induced plasticity effect which improve ductility. Then as the temperature decrease more and more the α'-martensite form and formation of martensite becomes predominant, due to this ductility decreases gradually. The peak indicate the starting of the α'-martensite formation

3. In case of cryogenic deformation plot of $\ln(\sigma - \sigma 0)$ vs. $\ln(\varepsilon p)$ does not follow a straight line . In case of cryogenic deformation we can observe two region the first one is parabolic and then there is a certain decrease and the again a parabolic increase. This can be illustrated from the fact that may be in first stage the TRIP effect is predominate and after that the α' –martensite formation becomes predominate.

4. The non-linear behavior ofwork-hardening is because of non-linear the TRIP effect. The peaks in the graph is related to the formation of α' martensite. Because of the athermal effect below Ms according to Koistinen and Marburger equation [95];martensite formation is more causing the sharp increase in the second stage of the strain hardening rate.

5. $(\theta \times \sigma)$ vs σ happens in three stages.

6. SEM image reveal , all test specimens have shown local necking and the cup and cone form of ductility fracture and as the temperature decrease the flat regsurrounded by ductile dimple region increase this is may be due to ductile-brittle transition at very low temperature.

7. From the XRD analysis it can be concluded that the as the temperature decreases the volume fraction of martensite increases.

REFERENCE

[1] P. Hedstrom. Deformation induced martensitic transformation of metastable stainless steel AISI 301. PhD thesis, Division of Engineering Materials Department of Applied Physics and Mechanical Engineering, Lulea University of Technology, SE-971 87 Lulea Sweden, 2005. 11, 12, 125, 126, 133.

[2]. D. Sastry, Y. Prasad, and S. Deevi, "Influence of temperature and strain rate on the flow stress of an FeAl alloy," Materials Science and Engineering: A, vol. 299, pp. 157-163, 2001.

[3]. U. Lindholm, "Some experiments with the split hopkinson pressure bar∗," Journal of the Mechanics and Physics of Solids, vol. 12, pp. 317-335, 1964.

[4] G. E. Dieter and D. J. Bacon, Mechanical metallurgy vol. 3: McGraw-hill New York, 1986.

[5] A. Kundu and P. C. Chakraborti, "Effect of strain rate on quasistatic tensile flow behaviour of solution annealed 304 austenitic stainless steel at room temperature," Journal of materials science, vol. 45, pp. 5482-5489, 2010.

[6] M. Dao, L. Lu, Y. Shen, and S. Suresh, "Strength, strain-rate sensitivity and ductility of copper with nanoscale twins," Acta Materialia, vol. 54, pp. 5421-5432, 2006.

[7] A. Cottrell, "AH Cottrell, Philos. Mag. 44, 829 (1953)," Philos. Mag., vol. 44, p. 829, 1953.55.

[8] H. K. D. H. Bhadeshia, Geometry of Crystals, 2nd edition, 2001. ISBN 0–904357–94–5, p. 51-54.

[9] C. Crussard, "Relationship between exact form of tensile curves of metals and accompanying changes in their structure," Rev. Metall, vol. 50, pp. 697-710, 1953.

[10] J. H. Hollomon, "Tensile deformation," Aime Trans, vol. 12, pp. 1-22, 1945.

[11] U. Kocks and H. Mecking, "Physics and phenomenology of strain hardening: the FCC case," Progress in materials science, vol. 48, pp. 171-273, 2003.

[12] P. Ludwik, "Elemente der Technologischen Mechanik, Julius Springer, Berlin," CrossRef Google Scholar, p. 32, 1909.

[13] K. K. Chawla and M. Meyers, Mechanical behavior of materials: Prentice Hall, 1999.

[14] Y. Jiang and H. Sehitoglu, "Cyclic ratchetting of 1070 steel under multiaxial stress states," International journal of plasticity, vol. 10, pp. 579-608, 1994.

[15] X. Xie, D. Ning, and J. Sun, "Strain-controlled fatigue behavior of cold-drawn type 316 austenitic stainless steel at room temperature," Materials Characterization, vol. 120, pp. 195-202, 2016.

[16] Wakasa K, Wayman CM, Kubo H, Shimizu K. Scripta Metall 1980;14:261

[17] B. Choudhary, J. Christopher, and E. I. Samuel, "Applicability of Kocks–Mecking approach for tensile work hardening in P9 steel," Materials Science and Technology, vol. 28, pp. 644-650, 2012.

[18] D. R. Palaparti, B. Choudhary, E. I. Samuel, V. Srinivasan, and M. Mathew, "Influence of strain rate and temperature on tensile stress–strain and work hardening behaviour of 9Cr–1Mo ferritic steel," Materials Science and Engineering: A, vol. 538, pp. 110-117, 2012.

[19] Thomas S. DeSisto and Frank L. Carr Research of Metals and Nonmetallic Materials for Ordnance Construction, December 1961, WATERTOIN ARSENAL.

[20] Eiji fukushima, akira goto, Mitsuzo fushimi, tensile properties of 18-8 stainless steel at cryogenic temperature, development center , Tokyo shibaura electric co-ltd , Kawasaki.

[21] Woong Sup Park, Seong Won Yoo, Myung Hyun Kim, Jae Myung Lee, Department of Naval Architecture and Ocean Engineering, Pusan National University, 30 Jangjeon-Dong, Geumjeong-Gu, Busan 609-735, Republic of Korea.

[22]) Jeong-Hyeon Kim a, Woong-Sup Park a, Min-Sung Chun b, Jong-Joo Kim b, Jun-Hong Bae b, Myung-Hyun Kim a, Jae-Myung Lee a, Effect of pre-straining on low-temperature mechanical behavior of AISI 304L.

[23] G. E. Dieter. Mechanical Metallurgy. McGraw Hill Book Company, UK, 1988. 12, 13, 17, 19, 58, 61.

[24] A. K. De, D. C. Murdock, M. C. Mataya, J. G. Speer, and D. K. Matlock. Quantitative measurement of deformation{induced martensite in 304 stainless steel by X{ray diffraction. Scripta Materialia, 50(12):1445{1449, 2004. 12, 57, 65, 125, 126, 133.

[25] S. F. Peterson, M. C. Mataya and D. K. Matlock: JOM, 49 (1997), No. 9, 54.

[26] Jr. William D. Callister. Materiials Science and Engineering: An Introduction{5th Edition. John Wiley & Sons. Inc., New York, 1999.
13, 14.

[27] . Latanision RM, Ruff AW. Metall Trans 1971;2:505.

[28] H. K. D. H. Bhadeshia. Geometry of Crystals{2nd edition. Institute of Materials, London, 2006. 24, 25, 34, 36, 158, 160

[29] G. H. Eichelman and F. C. Hull. The effect of composition on the temperature of spontaneous transformation of austenite to martensite in 18{8 type stainless steel. Transactions of ASM, 45:77{95, 1953. 26

[30] F. B. Pickering. Physical metallurgical development of stainless steels. In Stainless Steels. The Institute of Metals, London, UK, 1985. 26, 30, 126

[31] D. J. Dyson and B. Holmes. Effect of alloying additions on the lattice parameter austenite. Journal of the Iron and Steel Institute, 208:469{474, 1970. 26, 45

[32] A. F. Padilha and P. R. Rios. Decomposition of austenite in austenitic stainless steels. ISIJ International, 42(325):4, 2002. 26, 53.

[33] J. Talonen. Effect of strain-induced α'(bcc) martensite transformation on mechanical properties of metastable austenitic stainless steels. PhD thesis, Helsinki University of Technology (Espoo, Finland), 2007. 26, 28, 29, 41, 56, 65, 66, 125, 126, 133

[34] J.A. Venables. : Phil. Mag., 7 (1962), 35-44.

[35] H. Fujita and S. Ueda. Acta Metallurgica 20 (1972), p. 759

[36] J.W. Brooks, M.H. Loretto, R.E. Smallman, Acta Metallurgica 27. (1979) 1829–1838.

[37] H. K. D. H. Bhadeshia, Geometry of Crystals, 2nd edition, 2001. ISBN 0–904357–94–5, p. 51-54.

[38] P.L. Mangonon, JR. and G. Thomas, Metallurgical Transactions, Volume 1, June 1970, 1577 1587

[39]. G. Kurdjomov and G. Sachs: Z. Phys., 1930, vol. 64, pp. 325–43.

[40]. H. Kitahara, R. Ueji, Nobuhiro Tsuji, Y. Minamino: Acta Materialaia 54 (2006), 1279-1288.

[41]. Z. Nishiyama, Sci. Repts. Tohoku Imp. Univ. 23 (1934), p. 637.

[42]. S. Morito, X. Huang, T. Furuhara, T. Maki, N. Hansen: Acta Materialia 54 (2006),5323-5331.

[43]. Brandon DG. Acta Metall 1966; 14:1479.

[44]. S. F. Peterson, M. C. Mataya and D. K. Matlock: JOM, 49 (1997), No. 9, 54.

[45]. V. Taylan, R. H. Wagoner and J. K. Lee: Metall. Mater. Trans. A, 29A (1998),

2161.

[46]. Maki T. Mater. Sci. Forum 1990;56-8:157. References 64

[47]. Kelly PM. Nutting J Proc R Soc A 1960;259:45.

[48]. Krauss G, Marder AR. Metall Trans A 1971;2:2343.

[49]. Maki T, Tsuzaki K, Tamura I. Trans ISIJ 1980;20:207.

[50]. Kelly PM, Jostsons A, Blake RG. Acta Metall Mater 1990;38: 1075.

[51]. Morito S, Tanaka H, Konishi R, Furuhara T, Maki T. Acta Mater 2003;51:1789.

[52]. Matsuda S, Inoue T, Mimura H, Okamura Y. In: Proc. Of Int. Sympo. on Toward Improved Ductility and Toughness. Kyoto, Japan, 1971:47.

[53]. Marder JM, Marder AR. Trans. ASM 1969;62:1.

[54] J. F. Humphreys and M. Hatherly. Recrystallization and Related Annealing Phenomena.Pergamon Press, Kidlington, Oxford, OX5 1GB, UK, 1995. 15, 24, 112.

[55] G. Ghosh and G. B. Olson. Kinetics of FCC ! BCC heterogeneous martensitic nucleation - I. the critical driving force for athermal nucleation. Acta

Materialia, 42(10):3361{3370, 1994. 26

[56] G. Ghosh and G. B. Olson. Kinetics of FCC ! BCC heterogeneous martensitic nucleation - II thermal activation. Acta Materialia, 42(10):3371{3379,

1994.

[57] T. Cool and H. K. D. H. Bhadeshia. Prediction of martensite start temperature of power plant steels. Materials Science and Technology, 12(1):40{44,

1996

[58] G. Ghosh and G. B. Olson. Computational thermodynamics and the kinetics of martensitic transformation. Journal of Phase Equilibria, 22(3):199{

207, 2001.

[59] G. Ghosh and G. B. Olson. The isotropic shear modulus of multicomponent Fe{base solid solutions. Acta Materialia, 50(10):2655{2675, 2002. 26

[60] W. G. Vermeulen, P. F. Morris, A. P. de Weijer, and S. van der Zwaag. Prediction of martensite start temperature using artificial neural networks.

Ironmaking and Steelmaking, 23(5):433{437, 1996. 26

[61] C. Capdevilla, F. G. Caballero, and C. Garc`ia de Andres ´ . Determination of MS temperature in steels: A bayesian neural network model. ISIJ.

[62] T. Y. Hsu and X. Zuyao. Martensitic transformation in Fe-Mn-Si based alloys. Materials Science and Engineering A, 273-275:494{497, 1999. 27

[63] K. Datta, R. Delhez, P. M. Bronsveld, J. Beyer, H. J. M. Geijselaers, and J. Post. A low{temperature study to examine the role of martensite during strain{induced transformations in metastable austenitic stainless steels. Acta Materialia, 57(11):3321{3326, 2009. 27, 28, 39

[64] J. W. Brooks, M. H. Loretto, and R. E. Smallman. In situ observations of the formation of martensite in stainless steel. Acta Metallurgica, 27(12):1829{1838, 1979. 27, 30

[65] J. W. Brooks, M. H. Loretto, and R. E. Smallman. Direct observations of martensite nuclei in stainless steel. Acta Metallurgica, 27(12):1839{1847, 1979. 27, 28

[66] J. A. Venables. The martensite transformation in stainless steel. Philosophical Magazine, 7(73):35{44, 1962. 27, 28, 30, 32.

[67] Z. Z. Yuan, Q. X. Dai, Q. Zhang, X. N. Cheng, and K. M. Chen. Effects of temperature cycling and nitrogen on the stability of microstructures in austenitic stainless steels. Materials Characterisation, 59(1):18{22, 2008. 27

[68] B. Petit, N. Gey, M. Cherkaoui, B. Bolle, and M. Humbert. Deformation behaviour and microstructure/texture evolution of an annealed 304 AISI stainless steel sheet. International Journal of Plasticity, 23(2):323{341, 2007. 28, 66, 67, 104, 133

[69] J. H. Jun and C. S. Choi. Variation of stacking fault energy with austenite grain size and its effect on the MS temperature of martensitic transformation in Fe{Mn alloy. Materials Science and Engineering A, 257(2):353{356, 1998. 28

[70] J. H. Yang and C. M. Wayman. On secondary variants formed at intersection of martensite variants. Acta Metallurgica and Materialia, 40(8):2011{ 2023, 1992. 28

[71] J. H. Yang and C. M. Wayman. Intersecting shear mechanisms for the formation of secondary martensite variants. Acta Metallurgica and Materialia, 40(8):2025{2031, 1992. 28.

[72] B. E. Warren and E. P. Warekois. Stacking faults in cold worked alpha{ brass. Acta Metallurgica, 3(5):473{479, 1955. 28

[73] G. B. Olson and M. Cohen. Kinetics of strain{induced martensitic nucleation.

Metallurgical Transactions A, 6(4):791{795, 1975. 29, 49, 103, 124.

[74] T. S. Byun, N. Hashimoto, and K. Farrell. Temperature dependence of strain hardening and plastic instability behaviours in austenitic stainless steels. Acta Materialia, 52(13):3889{3899, 2004. 29, 51

[75] L. Remy and A. Pineau. Twinning and strain{induced F.C.C. ! H.C.P. transformation on the mechanical properties of Co-Ni-Cr-Mo alloys. Materials Science and Engineering, 26(1):123{132, 1976. 29.

[76] P. L. Mangonon and G. Thomas. The martensite phases in 304 stainless steel. Metallurgical Transactions A, 1(6):1577{1586, 1970. 28, 30, 53, 65, 67, 102.

[77] B. Bracke, L. Kestensa, and J. Penninga. Transformation mechanism of α; martensite in an austenitic Fe-Mn-C-N alloy. Scripta Materialia, 57(5):385 388, 2007. 28, 30

[78] W. S. Lee and C. F. Lin. The morphologies and characteristics of impact induced martensite in 304l stainless steel. Scripta Materialia, 43(8):777 782, 2000. 30, 65, 66, 103

[79] N. Gey, B. Petit, and M. Humbert. Electron backscatter diffraction study of α' martensitic variants induced by plastic deformation in 304 stainless steel. Metallurgical and Materials Transactions A, 36(12):3291{3299, 2005. 30, 103, 104, 159

[80] T. Narutani, G. B. Olson, and M. Cohen. Constitutive flow relations for austenitic steels during strain{induced martensitic transformation. Journal de Physique, 43(C4):429{434, 1982. 30, 50

[81] T. Narutani. Effect of deformation{induced martensitic transformation on the plastic behaviour of metastable austenitic stainless steel. Materials Transactions JIM, 30(1):33{45, 1989. 30.

[82] J. A. Lichtenfeld, M. C. Mataya, and C. J. Van Tyne. Effect of strain rate on stress{strain behaviour of alloy 309 and 304L austenitic stainless steel. Metallurgical and Materials Transactions A, 37(1):147{161, 2006. 30, 65, 66, 125, 126, 127, 133

[83] L. E. Murr, K. P. Staudhammer, and S. S. Hecker. Effects of strain state and strain rate on deformation{induced transformation in 304 Part stainless steel: II{microstructural study. Metallurgical Transactions A, 13(4):627{ 635, 1982. 3, 30, 43, 65, 66, 67, 103, 151.

[84] P. M. Kelly. The martensite transformation in steels with low stacking fault energy. Acta Metallurgica, 13(6):635{646, 1965. 30, 103

[85] Thomas S. DeSisto and Frank L. Carr Research of Metals and Nonmetallic Materials for Ordnance Construction, December 1961, WATERTOIN ARSENAL.

[86] A. J. Bogers and W. G. Burgers. Partial dislocations on the f110g planes in the B.C.C. lattice and the transition of the F.C.C. into the B.C.C. lattice. Acta Metallurgica, 12(2):255{261, 1964. 31

[87] G. B. Olson and M. Cohen. A general mechanism of martensitic nucleation: Part I general concepts and the FCC ! HCP transformation. Metallurgical Transactions A, 7(12):1897{1904, 1976. 31, 67, 103

[88] G. B. Olson and M. Cohen. A general mechanism of martensitic nucleation: Part II FCC ! BCC and other martensitic transformations. Metallurgical Transactions A, 7(12):1905{1914, 1976. 31, 67, 103, 152.

[89] F. Lecroisey and A. Pineau. Martensitic transformations induced by plastic deformation in the Fe-Ni-Cr-C system. Metallurgical Transactions, 3(2):387{396, 1972. 32, 51, 65, 67, 72, 103, 104

[90] W. S. Lee and C. F. Lin. Impact properties and microstructure evolution of 304L stainless steel. Materials Science and Engineering A, 308(1-2):124{ 135, 2001. 32, 50, 53

[91] N. Clement. L'Ordre et le Desordre dans les Materiaux. Les Editions de Physique, Ecole D'Hilver, Aussois, France, 1984. 23

[92] I. Karaman, Sehitoglu, H. J. Maier, and Y. I. Chumlyakov. Competing mechanisms and modelling of deformation in austenitic stainless steel single crystals with and without nitrogen. Acta Materialia, 49(19):3919{3933, 2001. 32

[93] P. J. Ferreira, J. B. Vander Sande, M. Amaral Fortes, and A. Kyrolainen. Microstructure development during high{velocity deformation. Metallurgical and Materials Transactions A, 35(10):3091{3101, 2004. 32, 112

[94] S. Mahajan and G. Y. Chin. Formation of deformation twins in fcc crystals. Acta Metallurgica, 21(10):1353{1363, 1973. 32

[95] D. P. Koistinen and R. E. Marburger. A general equation prescribing the extent of the austenite{martensite transformation in pure iron{carbon alloys and plain carbon steels. Acta Metallurgica, 7(1):59{60, 1959. 34, 127,130

[96] E.C. Bain. The nature of martensite. Transactions of American Institute of Mining and Metallurgical Engineers, 70:25,35, 1924. 35

[97]. E.P. Butter and M. G. Burke: Acta Metall., 34 (1986), 557.

[98]. Y. Kaieda and A. Oguchi: J. Mater. Sci., 20 (1985), 1847.

[99]. C.M. Wayman and H.K.D.H. Bhadeshia: Physical Metallurgy (Fourth Edition)

1996, Pages 1507-1554.

[100]. Patel, J. R., Cohen, M.: Criterion for the action of applied stress in the martensiticntransformation. Acta Metall.1, 531–538 (1953).

[101]. G.B. Olson, M. Cohen, J. Less-Common Met. 28 (1972) 107.

[102] R. Rosenfield, E. Votava, and G. T. Hahn. Ductility. Transactions of the American Society for Metals, Metals Park, Ohio, 1968. 17.

[103]. K. Nohara, Y. Ono and N. Ohashi, J. Iron Steel Inst. Jpn. 63 (1977), pp. 212 222.

[104]. Schramm RE, Reed RP. Metall Trans A 1975;6:1345.

[105]. Rhodes CG, Thompson AW. Metall Trans A 1977;8:1901.

[106]. Ferreira PJ, Mu¨ llner P. Acta Mater 1998;46:4479.

[107]. Lecroisey F, Pineau A. Metall Trans 1972;3:387

[108] Abrassart F. Metall Trans 1973;4:2205.

[109]. Latanision RM, Ruff AW. Metall Trans 1971;2:505.

[110]. L. Remy and A. Pineau. Mater. Sci. Eng. 28 (1977), p. 99.

[111]. V. Seetharaman and R. Krishnan: J. Mater. Sci., 16 (1981), 523.

[112]. L. F. M. Martins, R. L. Plaut and A. F. Padilha: ISIJ Int., 38 (1998), 572.

[113]. G. T. Burstein, I. M. Hutchings and K.Sasaki: Nature, 407 (2000),

885. Metallurgy. ASM, Cleveland, OH, 1950. 39

[114] T. Angel. Formation of martensite in austenitic stainless steels. Journal of the Iron and Steel Institute, 177(5):165{174, 1954. 41, 45, 47, 57, 125, 126, 133, 152

[115] K. Nohara, Y. Ono, and N. Ohashi. Composition and grain{size dependencies of strain{induced martensitic transformation in metastable austenitic stainless steels. Journal of Iron and Steel Institute of Japan, 63(5):212{222, 1977. 41, 43.

[116] G. N. Haidemenopoulos, G. B. Olson, and M. Cohen. Dispersed-phase transformation toughening in UHS steels in-sagamore army materials research conference proceedings. In Innovations in ultrahigh{strength steel technology, Washington DC, August-September 1990. 41, 43

[117] J. L. Gonzales, R. Aranda, and M. Jonap. The influence of grain size on the kinetics of strain induced martensite in type 304 stainless steel. In Applications of

Stainless Steel, The Institute of Metals, ASM International, Stockholm, Sweden, 1992. 43, 152

[118] T. Iwamoto, T. Tsuta, and Y. Tomita. Investigation on deformation mode dependence of strain-induced martensitic transformation in TRIP steels and modelling of transformation kinetics. International Journal of Mechanical Sciences, 40(2-3):173{182, 1998. 45, 50, 154

[119] S. K. Varma, J. Kalyanam, L. E. Murr, and V. Srinivas. Effect of grain size on deformation{induced martensite formation in 304 and 316 stainless steels during room temperature tensile testing. Journal of Materials Science Letters, 13(2):107{111, 1994. 45, 125, 126, 133, 152.

[120] V. Shrinivas, S. K. Varma, and L. E. Murr. Deformation{induced martensitic characteristics in 304 and 316 stainless steels during room temperature rolling. Metallurgical and Materials Transactions A, 26(3):661{671, 1995. 45, 152

[121] H. S. Yang and H. K. D. H. Bhadeshia. Austenite grain size and the martensite{start temperature. Scripta Materialia, 60:493{495, 2009. 43, 45, 130, 152

[122] E. H. Lee, M. H. Yoo, T. S. Byun, J. D. Hunn, K. Farrell, and L. K. Mansur. On the origin of deformation microstructures in austenitic stainless steel: Part II - mechanisms. Acta Materialia, 49(16):3277{3287, 2001. 43

[123] K. Spencer, J. D. Embury, K. T. Conlon, M. Vron, and Y. Brchet. Strengthening via the formation of strain-induced martensite in stainless steels. Materials Science and Engineering A, 387-389:873{881, 2004. 50, 133

[124] V. F. Zackay, E. R. Parker, D. Fahr, and R. Busch. The enhancement of ductility in high{strength steels. Transactions of the American Society for Metals, 60(2):252{259, 1967. 51

[125] R. P. Reed and C. J. Guntner. Stress{induced martensitic transformations in 18Cr- 8Ni steel. Transactions of the Metallurgical Society of AIME, 230(7):1713{1720, 1964. 51, 52, 103

[126] D. V. Neff, T. E. Mitchell, and A. R. Troiano. The influence of temperature, transformation, and strain rate on the ductility properties of austenitic stainless steels. Transactions of the American Society for Metals, 62(4):858{ 868, 1969. 52

[127] G. D. Huang, D. K. Matlock, and G. Krauss. Martensite formation, strain rate sensitivity, and deformation behaviour of type 304 stainless steel sheet. Metallurgical Transactions A, 20(7):1239{1246, 1989. 51, 52, 53, 63

[128] X. F. Fang and W. Dahl. Strain hardening and transformation mechanism of

deformation{induced martensite transformation in metastable austenitic stainless steels. Materials Science and Engineering A, 141(2):189{198, 1991. 51

[129] A. K. De, J. G. Speer, D. K. Matlock, D. C. Murdock, M. C. Mataya, and R. J. Comstock. Jr. Deformation{induced phase transformation and strain hardening in type 304 austenitic stainless steel. Metallurgical and Materials Transactions A, 37(6):1875{1885, 2006. 51, 52, 126.

[130] R. Lagneborg. The martensite transformation in 18% Cr - 8% Ni steels. Acta Metallurgica, 12(7):823{843, 1964. 30, 103

[131] G. W. Powell, E. R. Marshall, and W. A. Backofen. Strain hardening of austenitic stainless steel. Transactions of the ASM, 50(1):478{497, 1958. 43, 52

[132] J. P. Bressanelli and A. Moskowitz. Effects of strain rate, temperature and composition on tensile properties of metastable austenitic stainless steels. Transactions of the American Society for Metals, 59:223{239, 1966. 52, 53, 65

[133] G. P. Sanderson and D. T. Llewellyn. Mechanical properties of standard austenitic stainless steels in the temperature range -196 to 800◦C. Journal of the Iron and Steel Institute, 207(8):1129{1140, 1969. 52

[134] A. Rosen, R. Jago, and T. Kjer. Tensile properties of metastable stainless steels. Journal of Materials Science, 7(8):870{876, 1972.

[135] A. P. Livitsanos and P. F. Thomson. The effect of temperature and deformation rate on transformation-dependent ductility of a metastable austenitic stainless steel. Materials Science and Engineering, 30(2):93{98, 1977. 52

[136] N. Tsuchida and Y. Tomota. A micromechanical modelling for transformation induced plasticity in steels. Materials Science and Engineering A, 285(1-2):345{352, 2000. 53.

[137] G. B. Olson and M. Cohen. Martensitic transformation as a deformation process. In Proceedings of Earl R. Parker symposium on structure/property relationships, TMS-AIME, Warrendale, PA, USA, 1986. 53

[138] T. Iwamoto and T. Tsuta. Computational simulation of the dependence of the austenitic grain size on the deformation behaviour of T98 steels. International Journal of Plasticity, 16(7-8):791{804, 2000.

[139] Y. Tomota, H. Tokuda, Y. Adachi, M. Wakita, N. Minakawa, A. Moriai, and Y. Morii. Tensile behaviour of TRIP{aided multi{phase steels studied by in situ neutron diffraction. Acta Materialia, 52(20):5737{5745, 2004. 53

[140] H. K. D. H. Bhadeshia. TRIP-assisted steels? ISIJ International,

42(9):1059{1060, 2002. 53

[141]. G. W. Powell, E. R. Marshall and W. A. Backofen: ASM Trans., 1958, 50, 478-497.

[142]. R. D. Arnell: J. Iron Steel Inst., 1968, 206, 1035-1036.

[143]. Quantitative phase analysis by X-ray diffraction of martensite and austenite in strongly oriented orthodontic stainless steel wires R. W. CHEARY Department of Applied Physics, University of Technology Sydney, NSW 2007, Australia.

[144]. Quantitative measurement of deformation-induced martensite in 304 stainless steel by X-ray diffraction Amar K. De a, David C. Murdock b, Martin C. Mataya c, John G. Speer a, David K. Matlock.